Doctoral Dissertation
Doctoral Program in Material Science and Technology (36th Cycle)

Cellulose rich Composite materials from layer by layer coated fibers

Massimo Marcioni

* * * * * *

Supervisor
Prof. Federico Carosio, Politecnico di Torino

Doctoral Examination Committee:

Dr. Alexander B. Morgan, University of Dayton, referee

Prof. Andre Dorigato, University of Trento, referee

Prof, Alberto Frache, Politecnico di Torino, member

Prof. Alberto Fina, Politecnico di Torino, member

Prof. Orietta Monticelli, Università di Genova, member

Politecnico di Torino
2024

Declaration

I hereby declare that the contents and organisation of this dissertation constitute my own original work and does not compromise in any way the rights of third parties, including those relating to the security of personal data.

Massimo Marcioni
Torino, 2024

* This dissertation is presented in partial fulfillment of the requirements for Ph.D. degree in the Graduate School of Politecnico di Torino (ScuDo).

Acknowledgments

I would like to begin by expressing my deepest gratitude to my supervisor, Professor Federico Carosio, for guiding me throughout this path, and for all the advice and help he has given me during these years. I would like to thanks also Professor Alberto Fina for the interesting exchange of opinions and advice during these years.

I extend my gratitude to Professor Lars Wagber, thank you for having welcomed in your group during my visiting period at KTH, for all the knowledge shared and all the hospitality.

A PhD teaches you not to work alone, but to be part of a team, and I was lucky to have found fantastic colleagues with whom to share everyday life, both in the lab and outside. Thank you, Lorenza, Chiara, Lorenza, Marta, Fulvia, Giulia, Chiara, Elisa, and Emir, for being part of this journey. And, of course, a big thank you to all the people with whom I've worked in Alessandria.

It's not easy to be alone in a new country, but thanks to you, it was much easier. Thank you, Mengxiao, Johanna, and Jowan, for all the help during my stay in Stockholm and for welcoming an Italian into your office. And, a big thank you to Maria and Hasse, I would have been lost without you.

I can safely say that many friends have accompanied me over the years, and it would take several pages to thank you all personally. But I am grateful to all of you for being part of this journey, for listening to all the strange anecdotes and facts I told you, and for believing in me.

I believe the biggest thanks should go to those who encouraged me from a young age to study, grow, and be curious about the world. Mom, Dad, it is thanks to you that I have come this far. Thank you for always supporting me and pushing me to give my best. A big thanks also goes to my little brother, and favorite engineer, Alessio.

And thank you for always being there throughout this journey, in both the good the difficult times, whether we were close or separated by thousands of kilometers. Thank you, Marta, for always encouraging me and believing in me.

To my family.

Index

List of acronyms 3
List of tables....4
List of figures....5
1. Introduction....9
1.1 Natural fibers in material science....10
1.1.2 Cellulose fibers....11
1.1.2 Cellulose nanofibers....14
1.2 Natural fibers composites....15
1.2.1 High density bio-polymers composites....15
1.2.2 Polyurethane foam composites....18
1.2.3 Cellulose fibers light-weight materials....21
1.2.4 State of art challenges and limitations....23
1.3 Flame retardant properties....24
1.3.1 Fire mechanism....24
1.3.2 Flame retardancy of cellulose based materials....25
1.3.1 Layer-by-layer approach....28
2. Polybutylene succinate composites....32
2.1 Materials and methods....32
2.1.1 Materials....32
2.1.2 Layer by layer assembly....33
2.1.3 Composites preparation by melt blending....34
2.1.4 Characterizations....34
2.2 Results and discussion....35
2.2.1 Layer-by-layer assembly....35
2.2.2 Thermal stability....40
2.2.3 PBS morphology and mechanical properties....42
2.2.4 Flame-retardant properties....46
2.3 Conclusion....51
3. Rigid polyurethane foam composites....52
3.1 Material and methods....53
3.1.1 Materials....53
3.1.2 Layer-by-layer assembly....54

3.1.3 Polyurethane foam forming 55
3.1.4 Characterization 55
3.2 Results and discussion 57
3.2.1 Layer-by-layer assembly on cellulose fibers 57
3.2.2 Coated fibers characterization 58
3.2.3 Thermal stability 61
3.2.4 Polyurethane foaming and physical properties 65
3.2.5 PU foam flame retardancy 68
3.3 Conclusions 71
4. Cellulose fibers lightweight materials 72
4.1 Materials and methods 74
4.1.1 Materials 74
4.1.2 Layer by layer assembly 74
4.1.3 Porous fiber network preparation 75
4.1.4 Characterization 75
4.2 SHMP-CH assembly results and discussion 77
4.2.1 Coating growth and assembly on fibers 77
4.2.2 Low density fiber network forming and characterization 79
4.2.3 Thermal stability 82
4.2.4 Flammability and combustion properties 83
4.2.5 Post combustion residue analysis 87
4.3 Phy-CNF-Ch assemblies results and discussion 90
4.3.1 Coating growth and assembly on fibers 90
4.3.2 Low density fiber network morphology and mechanical properties 92
4.3.3 Fire-retardant properties 93
4.4 Conclusions 95
5. General conclusions and future perspectives 97
6. References 100

List of acronyms

APP: ammonium polyphosphate

ATR: attenuated total reflectance

BC: bacterial cellulose

BL: bi-layer

BM: ballmilled

BPEI: branched polyethyleneimine

CH: chitosan

CNC: cellulose nanocrystals

CNF: cellulose nanofibers

EHC: effective heat of combustion

FRs: flame retardants

FT-IR: Fourier transformat infrared

Hal: halloysite nanotubes

HRR: heat release rate

LbL: layer-by-layer

PBS: polybutylene succinate

Phr: parts per hundred rubber

Phy: phytic acid

PLA: polylactic acid

PU: polyurethane

PUF: polyurethane foam

SEM: scanning electron microscopy

SHMP: sodium hexametaphosphate

SPR: smoke production rate

QL: quad-layer

THR: total heat released

TSR: total smoke released

TTI: time to ignition

List of tables

Table 1: composites formulations.....34
Table 2: TGA values for pure cellulose and lbl coated fibers and.....41
Table 3: Mechanical properties of PBS composites 44
Table 4: HRR, THR and TSR of PBS composites.....50
Table 5: TGA data for PUF composites.....63
Table 6: data from compression tests and thermal conductivity for PUF previously studied by SEM.....68
Table 7: data from cone calorimetry for all PUF samples 70
Table 8: deposition solution concentration for the 3 assemblies proposed.....75
Table 9: data from thermogravimetric analysis of neat and coated fibers 82
Table 10: Flammability test data.....83
Table 11: Time to ignition (TTI), heat release rate (HRR), total heat release (THR) and total smoke production (TSR) from cone calorimetry 85
Table 12: cone calorimetry data.....95

List of figures

Figure 1: procedure followed for fiber-composites materials of this thesis 9
Figure 2: Hierarchical structure of cellulose. Figure reprinted with the permission of Elsevier from ref (10) 12
Figure 3: TEM images of CNC and CNF. This figure is adapted from (24) with permission from Royal Society of Chemistry and adapted with permission from (25).Copyright 2007 American Chemical Society. 14
Figure 4: SEM micrographs of fracture surface of a) PLA - kenaf and b) PLA - rice husk composites. Figure reprinted with the permission of Springer Nature from ref (43).....16
Figure 5: SEM micrograph of fracture surface of neat PBS (A, B), PBS with kenaf fibers (C, D), PBS with cellulose fibers extracted from kenaf (E, F) and PBS with commercial cellulose (G, H). Figure reprinted with the permission of John Wiley and Sons from ref (59).....17
Figure 6: bio-derived feedstock for biopolyols production. Figure reprinted with the permission of Elsevier from ref (71).....19
Figure 7: SEM micrographs for the (a) matrix foam and the composite foams containing respectively, (b) 1%, (c) 3%, (d) 4%, (e) 8%, (f) 12%, and (g) 16% w/w respect to polyols (the scale bar is 500 μm). Figure reprinted with the permission of John Wiley and Sons from ref (77).....20
Figure 8: Terminology and processes for nanocellulose foams manufacturing. Figure reprinted with the permission Royal Society of Chemistry from ref (82)..21
Figure 9: (a) Scheme illustration of crystal growth under different temperatures. SEM images of nanocellulose aerogel with various freezing temperatures. (b) Refrigerator (− 20 ◦C). (c) Cold trap (− 80 ◦C). (d) Liquid nitrogen (− 196 ◦C). Figure adapted from (88) with permission of Elsevier 22
Figure 10: Combustion cycle representing common processes involved in flame propagation. Reproduced with permission from (101).....24
Figure 11: cone calorimetry curves for PBS composites. 50kW/m^2 heating flux. Where, PBS: polybutylene succinate, LSA: PBS + 6.6% sepiolite + 6.6% APP + 6.6% Lignin, L5A15: PBS + 15APP + 5% lignin, L10: PBS + lignin and L5S5A10: PBS + 5% sepiolite + 10% APP + 5% Lignin. Figure reprinted with the permission John Wiley and Sons from ref (118) 26
Figure 12: representation of an LbL assembly with A) the sequence commonly used in a deposition, B) surface Bi-layer build-up and C) two common polyelectrolytes, sodium salt of poly (styrene sulfonate) and poly (allylamine hydrochloride).....28
Figure 13: graphs representing the dependence of A) coating thickness vs salt concentration for 10BL of PDDA/PSS coating and B) coating thickness vs deposition temperature for 10BL of PDDS/PSS. Figure adapted from (153) and (154). Copyright 2001 American Chemical Society 29
Figure 14: graphical depiction of an intumescent flame retardant 30
Figure 15: deposition scheme for cellulose fibers and layer-by-layer.....33
Figure 16: IR-spectra of pure chemicals.....36
Figure 17: FT-IR spectra plot showing the LbL growth for a) Phy-Hal/CH on a silicon wafer substrate and the correlated BL number vs intensity plot, b)

magnification of the portion between 1300 and 800 cm^{-1} ir spectra of Phy-CH/Hal growth and c) APP-Hal/CH on a silicon wafer substrate and the correlated BL number vs intensity plot....37
Figure 18: IR spectra of Phy – CH/Hal coated fibers (magnified)....38
Figure 19: IR spectra of APP – CH/Hal coated fibers (magnified)....39
Figure 20: SEM images of treated fibers....40
Figure 21: TGA thermograms of treated fibers in nitrogen on the left and in air on the right....40
Figure 22: SEM images of PBS composites after brittle fracture....42
Figure 23: SEM micrographs of PBS composites with Phy-CH/Hal coated fibers after brittle fracture....43
Figure 24: SEM micrographs of PBS composites with APP-CH/Hal coated fibers after brittle fracture....43
Figure 25: SEM micrographs of PBS composites with APP-CH/Hal coated fibers after brittle fracture....44
Figure 26: SEM micrographs of tensile-fractured surface....46
Figure 27: snapshot at various time of flammability test....47
Figure 28: Cone calorimetry results of PBS composites with heat release rate (HRR)and total heat release rate (THR)....49
Figure 29: PUF from lbl coated cellulose....53
Figure 30: deposition scheme for coated cellulose....55
Figure 31: IR spectra of Sodium hexametaphosphate, ammonium phosphate and chitosan....57
Figure 32: (a) FT-IR spectra plot showing the LbL growth for SHMP-CH on a silicon wafer substrate and the correlated BL number vs intensity, (b) FT-IR spectra plot showing the LbL growth for APP-CH on a silicon wafer substrate and the correlated BL number vs intensity....58
Figure 33: SEM micrographs of long cellulose fibers and ballmilled fibers....59
Figure 34: ATR-IR spectra of LbL coating on long cellulose fibers of a) SHMP-CH and b) APP-CH system....60
Figure 35: SEM micrographs of a) coated fibers with the two systems, b) BM fibers coated with 1 to 3 BLs of SHMP-CH LbL assembly....61
Figure 36: TG plots of C700 and BM fibers (in Nitrogen and Air) for both LbL systems....62
Figure 37: a) untreated cellulose fibers flammability test and b) C700 samples after flammability test....64
Figure 38: Flammability test for BM fibers coated with SHMP-CH assembly ...65
Figure 39: a) neat PU reference with digital photo and SEM micrograph and b) digital images of PUF samples prepared with untreated cellulose and coated cellulose....66
Figure 40: digital images of PUF samples prepared with untreated BM cellulose and lbl coated BM cellulose....66
Figure 41: SEM images of PUF with 7.5 and 15 phr of C700 or BM cellulose, uncoated or coated....67
Figure 42: Heat release rate (HRR), total heat release rate (THR), smoke production rate (SPR) and total smoke release (TSR) for PUF made with untreated and coated BM cellulose....69

Figure 43: lightweight fiber-networks from lbl coated cellulose fibers 73
Figure 44: a) FT-IR spectra showing the LbL growth on a silicon wafer substrate, SEM images of b) neat cellulose fibers, c) 1BL, d) 2BL, e) 3BL coated fibers....77
Figure 45: ATR-IR of 1,2 and 3BL coated cellulose fibers vs neat un-coated cellulose 78
Figure 46: a) Total adsorbed mass for cellulose-rich fibers as evaluated with charge titration for each individual adsorption step including rinsing during the build-up of 3BL, b) composition of dry fibers in %wt., calculated from the charge titration measurement 79
Figure 47: scheme of fiber network preparation.....79
Figure 48: Fiber network morphological and mechanical characterization, a) digital images of the as prepared fiber networks, b) SEM images at different magnification of a 3BL sample in which is visible the coating interconnection between fibers, c) compression stress/strain plots for 1, 2 and3BL samples with an insert showing higher magnification of the compression range 0 to 30%.....80
Figure 49: untreated fibers after freeze-drying.....80
Figure 50: TG plots of neat cellulose and 1, 2 and 3 BL fiber networks in a) nitrogen and b) air.....82
Figure 51: Flammability test snapshots of a) horizontal flame test of freeze-dried neat cellulose, b) horizontal and vertical flame test snapshot of a commercial PU foams, c) horizontal and vertical flame test for 1BL, 2BL, and 3BL foams (from left to right) with the flame and after the flame was removed.....84
Figure 52: Heat release rate (HRR), total heat release rate (THR), smoke production rate (SPR) and total smoke release (TSR) for porous fibers network and PUF 85
Figure 53: Comparison of cone calorimetry results of different rigid FR foams from the literature background. PET: polyethylene terephthalate, PS: polystyrene, DOPO: 9, 10-dihydro-9-oxa-10-phosphaphenanthrene-10-oxide, ATH: aluminumtrihydroxide 86
Figure 54: SEM micrographs of porous fibers network from LbL coated fibers.87
Figure 55: Raman spectra of fiber network residues with deconvoluted fittings of peak D and G 88
Figure 56: Schematic representation of the fiber network flame-retardant mechanism upon exposure to a flame or heat flux 89
Figure 57: IR spectra of Phy-CH-CNF assembly on Si-wafer, with magnification of portion between 1800 and 850 cm^{1} 90
Figure 58: polyelectrolytes titration results with total adsorbed mass after each deposited layer, coated fibers composition and coating composition 91
Figure 59: SEM micrographs of coated fibers.....91
Figure 60: SEM micrographs of lightweight fiber-networks obtained from freeze drying.....92
Figure 61: Compression stress test for cellulose lightweight materials and comparison with previously obtained one 92
Figure 62: thermal conductivity of lightweight materials from this work compared to a pulp foam made by borate crosslinking and a water-blown PUF of similar density. (134, 243) 93
Figure 63: Smoldering during flammability test of Phy1CNF0.2 94

Figure 64: cone calorimetry data for cellulose based porous lightweight materials 94

1. Introduction

This thesis investigates the Layer-by-Layer (LbL) approach as surface nanostructuring tool capable of enhancing the flame retardant and mechanical properties of fiber-polymer composites. The hypothesis is that the high tunability of the LbL technique can effectively improve fiber-matrix interactions, thereby enhancing final properties such as flame retardancy and mechanical strength. This study evaluates three different scenarios: bulk composites, foam composites, and all-fiber materials, as shown in **Figure1.**

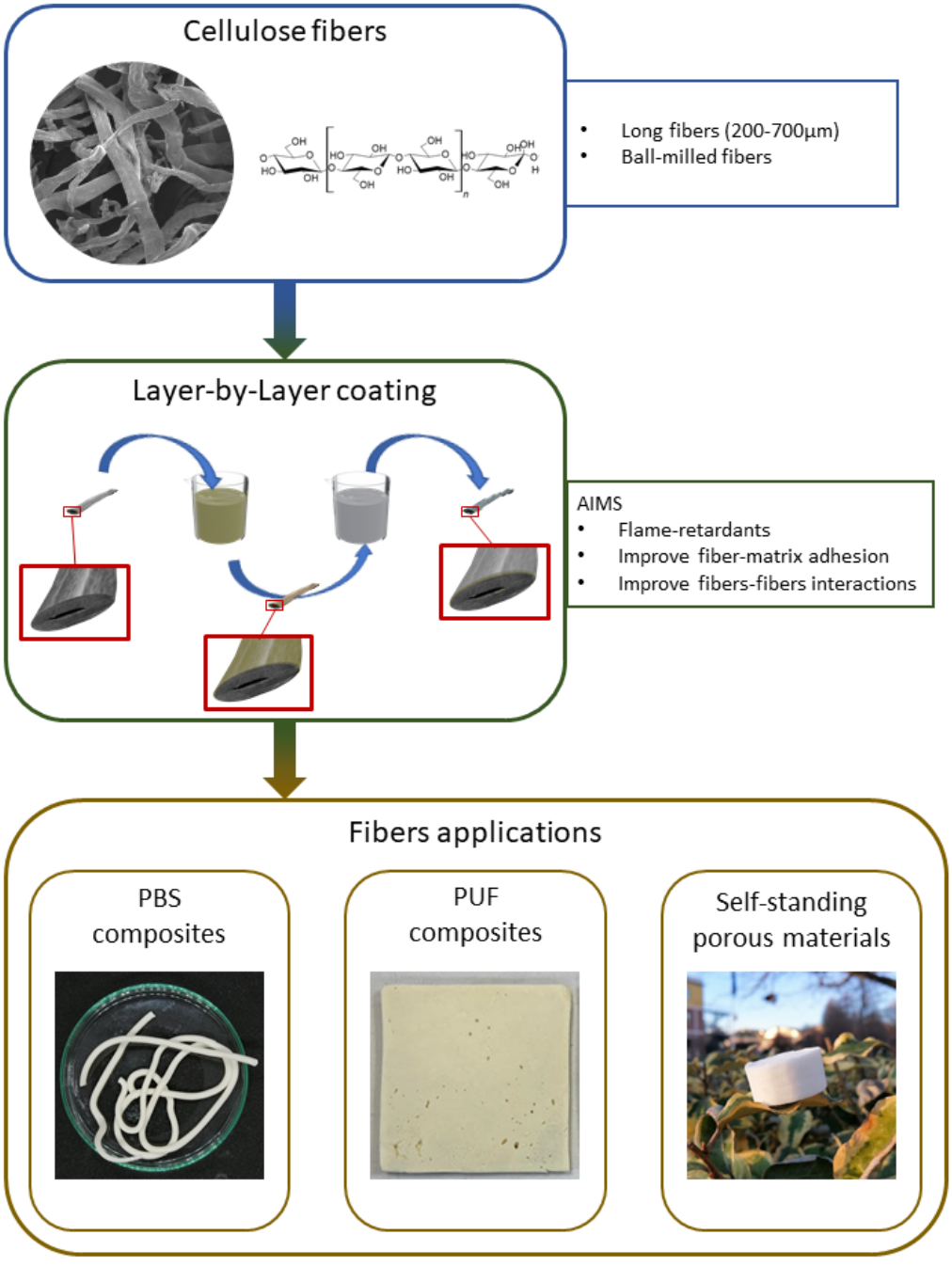


Figure 1: procedure followed for fiber-composites materials of this thesis

Specific requirements for each scenario must be met to support the proposed hypothesis, which are individually described in this thesis.

In **this chapter**, the state of the art regarding cellulose fiber composites and their application in material science is presented. Flame-retardancy issues are addressed, and the layer-by-layer (LbL) technique is proposed as a viable strategy to impart flame-retardant properties to cellulose fibers

In **chapter 2,** cellulose fibers are coated with two flame-retardant assemblies and used to prepare composites with polybutylene succinate. The hypothesis is that the flame-retardant assemblies on the cellulose fibers will be successfully integrated into the PBS matrix, thereby imparting significant fire resistance to the final composite. At the same time the incorporation of coated cellulose fibers will maintain or enhance the mechanical strength of the PBS composites compared to those without flame-retardant coatings.

In **chapter 3**, cellulose fibers are coated with a LbL assembly comprising a flame-retardant agent and a compatibilizer. Long fibers and ball-milled fibers are evaluated and coated, with a major focus on flame retardant properties, and then used as filler for rigid polyurethane foams. The main hypothesis for this section is that LbL coating with a flame-retardant agent and a compatibilizer will significantly improve the flame-retardant properties of both long and ball-milled cellulose fibers.

In **chapter 4**, cellulose fibers are coated with an LbL assembly and used to obtain a 3D lightweight stable material by freeze-drying. The main hypothesis is that coating cellulose fibers with the LbL assembly before freeze-drying will significantly improve fiber-fiber interactions, leading to a stable 3D structure. Moreover, the use of a flame retardant LbL will supposedly impart flame-retardant properties to the cellulose fibers, contributing to the overall fire safety of the final material.

1.1 Natural fibers in material science

The necessity of more environmental-friendly processes and materials is a major subject in the scientific research world in the last decade. Concept like circular economy and waste recovery are part of everyday life, in particular in the material science field. Indeed, many common materials used nowadays are the same as years ago, especially when we are talking about polymers.(1) While so-called bioplastics are becoming more and more present in everyday life, thanks also to directives from major institutions, like the European Union, in many cases they are not at the same properties level of already established plastics.(2) This lead scientist to find solutions in order to make them more competitive and at least mitigate problems related to fossil source depletion, used to produce common polymers, and pollution, mainly due to mismanage of wastes. Regarding this, one of the approaches commonly used to reduce the amount of polymer, and at the same time have better properties, is the addition of natural based fillers to obtain a composite. Nowadays,

natural fibers are widely used in material science, both alone and in combination with a matrix, to make composite.(3) They have replaced synthetic fibers in many fields thank to their properties. Thanks to their environmentally-friendly/biodegradability character, interesting physical and mechanical properties and low cost attracted many researchers, leading to an extensive research. This phenomenon is accentuated from the possible gains in term of circular economy. Indeed, this route opens the road to the exploitation of wastes coming from agriculture, food and goods production.(4, 5) Natural fibers can be divided in categories based on their origins: plant, mineral and animal derived fibers. Among them, plant-based fibers, thanks to their low cost and abundancy, attract a lot of attention in many fields.(6)

1.1.2 Cellulose fibers

Wood is one of the major sources of fibers and it's commonly classified in softwood (pine, spruce, etc.…) and hardwood (birch, aspen, etc.…)(7) and its main components are carbohydrates, like cellulose and hemicellulose, and lignin. Cellulose and hemicellulose commonly represent 65/70% of total dry weight of wood and together are referred as holocellulose.(8) Cellulose, being the most abundant organic polymer in nature, attracted scientific community attention since its isolation and together with lignin and hemicellulose is a major component of plants and its content vary with species, climate and growing conditions. (9) Cellulose molecular structure is made by the repetition of a β-D-glucopyranose unit linked to another by the acetal function between the equatorial OH group of C4 and the C1 carbon atom. The result is a long and linear chain with plenty hydroxy groups along the chain which form hydrogen bonds with nearby fibers, aggregating the single chains in structures called fibrils that further aggregates to make fibers and form a hierarchical structure, as displayed in **Figure 2.**(10)

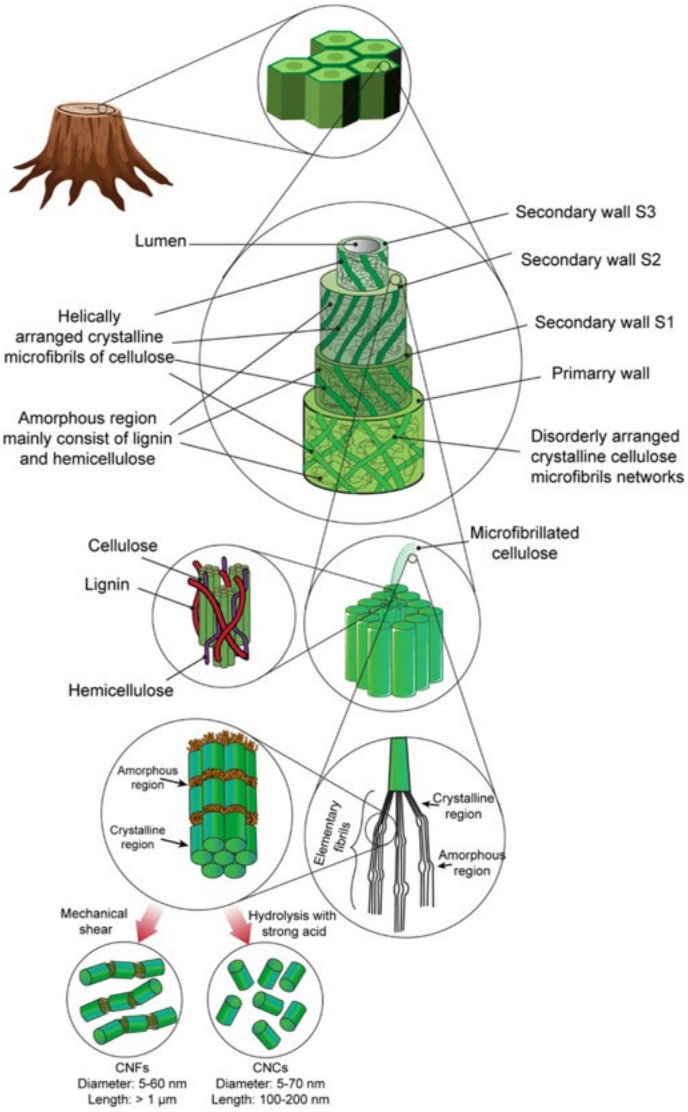


Figure 2: Hierarchical structure of cellulose. Figure reprinted with the permission of Elsevier from ref (10)

Hemicelluloses are polysaccharide with different structure depending on the plant species from which they are extracted. They show branched, amorphous structure, generally made by different combinations of hexoses and pentoses, like galactoglucomannans and glucuronoxylans. Several studies have reported the substantial influence of hemicelluloses on the characteristics exhibited by cellulose fibers. Firstly, they effectively enhance pulp fibrillation by reducing the occurrence of coalescence between fibers.(11) Secondly, they contribute to the improvement of colloidal stability within suspensions by increasing the repulsive forces among the fibers due to their higher charge.(12) The inclusion of hemicelluloses significantly enhances the characteristics of the fibers, particularly in terms of thermal stability and strength.(11) However, a substantial quantity of hemicellulose undergoes degradation during the pulping procedure.(13) Fibers, with different characteristic depending on the source, are extracted from wood and plants with a process called pulping, which is needed to remove the lignin contained in the feedstock without altering the fibrous structure. Moreover, cellulose is present

within the cell wall in two distinct forms denoted as crystalline and non-crystalline regions, alternatively referred to as amorphous or disordered regions. Crystalline regions present limited accessibility to water, chemicals, or microorganisms, whereas non-crystalline regions offer relatively greater accessibility.(8) Pulping process can be divided into three categories: mechanical, chemical and semi-mechanical. Each of them will produce a pulp with different properties and thus suitable for different applications.(14) Mechanical pulping converts wood chips in pulp using mechanical energy, this method conserve both cellulose and lignin producing a unrefined pulp used mainly for cardboard, newspaper and short-spawn products.(14) Chemical pulping can be divided in two main processes: kraft and sulfite pulping. The first one consists in using alkaline conditions, high temperature and mechanical stress to break the lignin structure, with the aid of the chemicals used, such as NaOH and Na_2S. The result are cellulose fibers with low contents of lignin and hemicellulose, that tends to aggregate.(15) Sulfite process use SO_2 for lignin modification and a cationic base. The variety of cationic base that can be used permit to have an higher range of working pH, from 1.5 (with drawbacks in fiber integrity) to pH5.(16) The semi-chemical pulping method comprises a dual-stage pulping process that incorporates both chemical and mechanical pulping techniques. The initial phase involves a process of controlled chemical treatment applied to wood chips, which results in the partial softening of the material. This treatment aims to weaken the inter-fiber bonding within the chips by selectively removing a portion of hemicellulose and lignin. Subsequently, the refined biomass undergoes a mechanical refining stage, wherein the chemically treated material is processed to separate individual fibers and fiber bundles.(17) Undesired reactions of the polysaccharides occurs during pulping, such as peeling and hydrolysis due to chemicals used. However, thanks to the compact structure and high crystallinity, cellulose suffer less than hemicellulose from these side-reactions. Indeed, it's estimated that approximately between 40 to 50% of hemicellulose is lost in the cooking process.(14) The outcome of the pulping process are slightly different between kraft process and sulfite, with fibers presenting an higher crystallinity coming from kraft pulping respect to sulfite.(18) Also, the surface chemistry of fibers produced vary with the method chosen. Sulfite pulp and fibers present a higher content of carboxylic acid groups on the fiber surface than kraft pulp, joined by the presence of sulphate groups thanks to the use of sulfuric acid and sulfite derivates.(19, 20) Despite the effectiveness of chemical pulping methods in enhancing the mechanical properties of cellulose fibers, it should be noted that lignin persists on these fibers. Therefore, it is essential to incorporate bleaching technology for the purpose of removing any remaining lignin without causing any adverse effects on the mechanical properties of the fibers. Bleaching typically consists of a sequential process consisting of four to six stages. Typically, this process starts with an oxidative phase, followed by an alkali rinse to improve solubility and remove lignin. The resulting lignin content of the fibers can vary depending on the selection of chemicals employed at each stage of the process.(21) The outcome are fibers with low lignin content and bright white color. However,

bleaching further modify the fibers structure and properties, like an increase in crystallinity due to further removal of amorphous lignin and hemicellulose.(22) To conclude, pulping processes and cellulose fibers production is a well-established industry, able to produce large volumes of this raw material. The exploitation of fibers coming from this route present the major advantage of being well characterized and economical. However, in order to avoid and reduce forest depletion, new feedstock source must be found or converted, such as agricultural waste and fast-growing plants.

1.1.2 Cellulose nanofibers

In last decades, studying the nanoscale has become easier and easier and researcher have noticed that the nanosized corresponding of a macroscale material has often properties that deviates from the original. In this ambit nanocellulose is a broad term used to define all those form of cellulose with nanometric dimension, from nanocrystals to nanofibers. Nanocellulose attracted the attention of the scientific community thanks to its interesting properties, like biodegradability, filmability and its outstanding mechanical properties.(23) Nanocellulose can be divided in three main categories: cellulose nanocrystals (CNC), cellulose nanofibers (CNF) and bacterial cellulose (BC). **Figure 3**

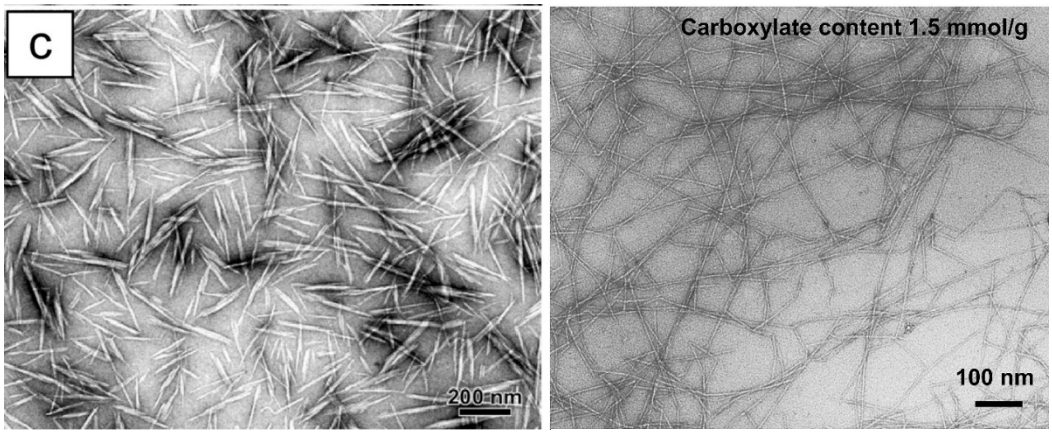


Figure 3: TEM images of CNC and CNF. This figure is adapted from (24) with permission from Royal Society of Chemistry and adapted with permission from (25).Copyright 2007 American Chemical Society.

Cellulose nanocrystals have a short rod like shape, with diameters of 2-20 nm and length of 100-500 nm(23, 26, 27) and they are commonly obtained from acid hydrolysis of cellulose fibrils, which remove the amorphous region of cellulose, maintaining intact the crystalline portion.(28) For this purpose, sulfuric acid is commonly used,(27, 28) although many other acids have been reported for CNCs preparation.(26, 29) If CNC presents a high crystallinity, CNF present both crystalline and amorphous phases in its structure and thus it can be seen as a nanometric version of a micrometric cellulose fibrils. Indeed, CNF is mainly produced by mechanical methods, such as homogenization, microfluidization or grinding, as long as other unconventional methods.(30-33) With diameters in the 5-50 nm order and length of few micrometers, CNF have an higher aspect ratio (length

to diameter) respect to CNC, which results in different characteristics and possible applications. Opposed to CNC and CNF, which are extracted from lignocellulosic biomass, BC is made starting from sugars by bacteria. This results in a pure cellulose form without lignin, hemicellulose and others components.(34). Nanocellulose and its composites have a great potential in the material science field. However, in order to produce nanosized fibers, or crystals, one or more steps have to be added to the already long process of pulp refining. This step is often high energy demanding, impacting on the final cost and environmental impact, counterbalancing the extraordinary properties that can arise from its use. (35) Cost is not the only drawback in nanocellulose production. Indeed, the production of nanocellulose requires more precise machines that lower the production output, resulting in a way lower amount of nanocellulose produced, compared to common pulp.(36, 37) A way to increase the sustainability of this class of materials is the exploitation of agricultural waste as feedstock, to respect a circular economy approach.(38) In conclusion, nanocellulose use must be evaluated considering also its limitations in order to better tailor the possible application fields.

1.2 Natural fibers composites

In recent years, there has been a growing interest in utilizing natural fibers as reinforcements in polymer composites due to their renewable nature, low cost, and potential for improving mechanical properties. This has led to extensive research and development efforts focused on understanding the properties and behavior of these materials, as well as exploring new manufacturing techniques to optimize their performance. In this chapter, three application fields are discussed: natural fibers-polymer composites, divided in high density polymer composites (e.g. poly lactic acid (PLA), poly butylene succinate (PBS) composites, Polyhydroxyalkanoates (PHA)) and low-density polymer composites, (e.g. Polyurethane foams (PUF) composites) and all fiber-based lightweight materials.

1.2.1 High density bio-polymers composites

The employment of natural fibers in composites with high density polymers has been studied since decades,(39, 40) with a developing trend in composites with bio-polymers. Indeed, the development of bio-polymers offered a good opportunity to detach from the conventional olefin-based polymers. Unfortunately, their properties (mechanical, thermal, permeability, etc…) cannot always compete with more common polymers like polyethylene, polypropylene or polyethylene terephthalate. The formulation of composites allows to obtain materials with comparable, or better, properties and applications. Regarding this, PLA, PHA and PBS are some of the most studied bio-polymers and their composites with natural fibers attracted the research community in the last years. Natural fibers polymer composites are normally produced exploiting procedures already established and used for conventional fiber reinforced polymer composites.(41) Among them melt blending and compression molding are the most prominent thanks to vast literature present, even if new techniques such as additive manufacturing (3D printing) are also

emerging.(42) Together with the processing method, the matrix chosen exert a fundamental role. Many studies focused their attention into bio-composites based on natural fibers and PLA, being the latter a polymer of major interest. Regarding this, the source of fibers has been found to have significant influence on the final composite properties. Hassan et al. compared the final properties of two composites obtained with the same procedure and similar filler dimensions, but with fibers coming from different sources: kenaf fibers and rice husk.(43) Overall, kenaf fibers performed better than rice husk, with a 32% increase in flexural modulus respect to the 15% of rice husk. This study evidenced also the limitations in PLA/natural fibers blending, like the decrease of thermal stability and poor interactions between fibers and matrix, as visible in **Figure 4.**

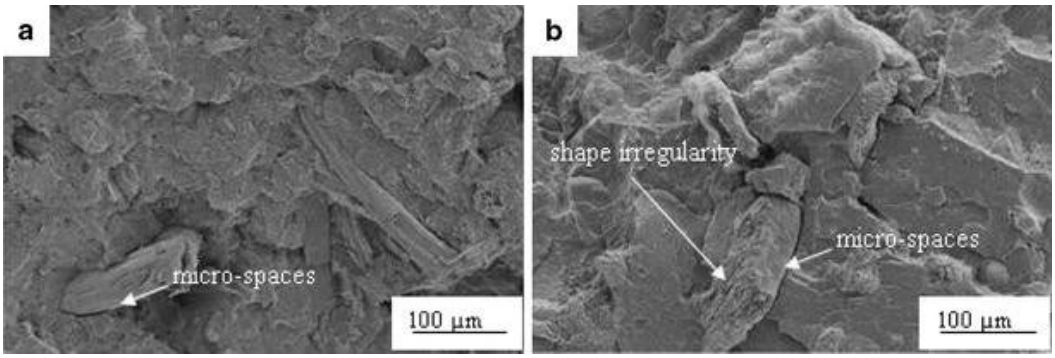


Figure 4: SEM micrographs of fracture surface of a) PLA - kenaf and b) PLA - rice husk composites. Figure reprinted with the permission of Springer Nature from ref (43)

Together with the poor affinity between fibers and matrixes, thermal stability of natural fibers is also an issue. Indeed, plant-based fibers present thermal decomposition path which can influence the processing step, resulting in either loss of mechanical performance or decrease in composite thermal stability. To confirm this effect, Filippone et al. studied the fiber-induced degradation of PLA in the molten state, finding that a low amount of hemp fibers (3%wt) was enough to induce PLA degradation.(44) The observed phenomenon can primarily be ascribed to the existence of water molecules bound to the fiber, highlighting the imperative requirement of an optimized drying process, which can pose a challenge for fibers derived from plant sources.(45, 46) The release of water bound to cellulose fibers present a threat during processing, especially for hydrolysable matrix like PLA, but it has to be noticed that it is not the only phenomena that occurs at high processing temperatures.(47) Plant-based fibers can contain low molecular weight components, in particular when not refined, which can start to degrade at temperature below 200°C, this effect can accelerate the further degradation of the rest of the fibers, leading to defects in the final composite.(48, 49) Working with lower melting point polymers can solve, or at least mitigate, this problem. PBS is a polymer obtained from the polycondensation of succinic acid (or dimethyl succinate) with 1,4-butanediol. (50) The monomers are commonly obtained from fossil-based resource, but routes for their production using bio-based feedstock are also available and under study,(51-53) giving to it good chance to overcome the use

of petrochemical raw materials in the future. Together with this, PBS present good bio-degradability,(54) becoming thus of interest in the nowadays market.(50) Aiming at improve its properties and broaden its field of application, several studies focused their attention in making composites with natural fibers and PBS. (54-58) Yang et al. showed how the addition of jute fibers with different surface treatment affect the biodegradability of PBS and how it can be linked with the adhesion between the two phases.(54) Indeed, as happens for matrixes like PLA, when untreated fibers are used, the poor interfacial strength cause a decrease in mechanical properties, as demonstrated by Srikulkit et al.(59) and visible in **Figure 5,** which show the fracture surface of PBS composite obtained from different source of fibers. The void between fibers and matrix is clearly visible, evidencing poor interactions between the two phases.

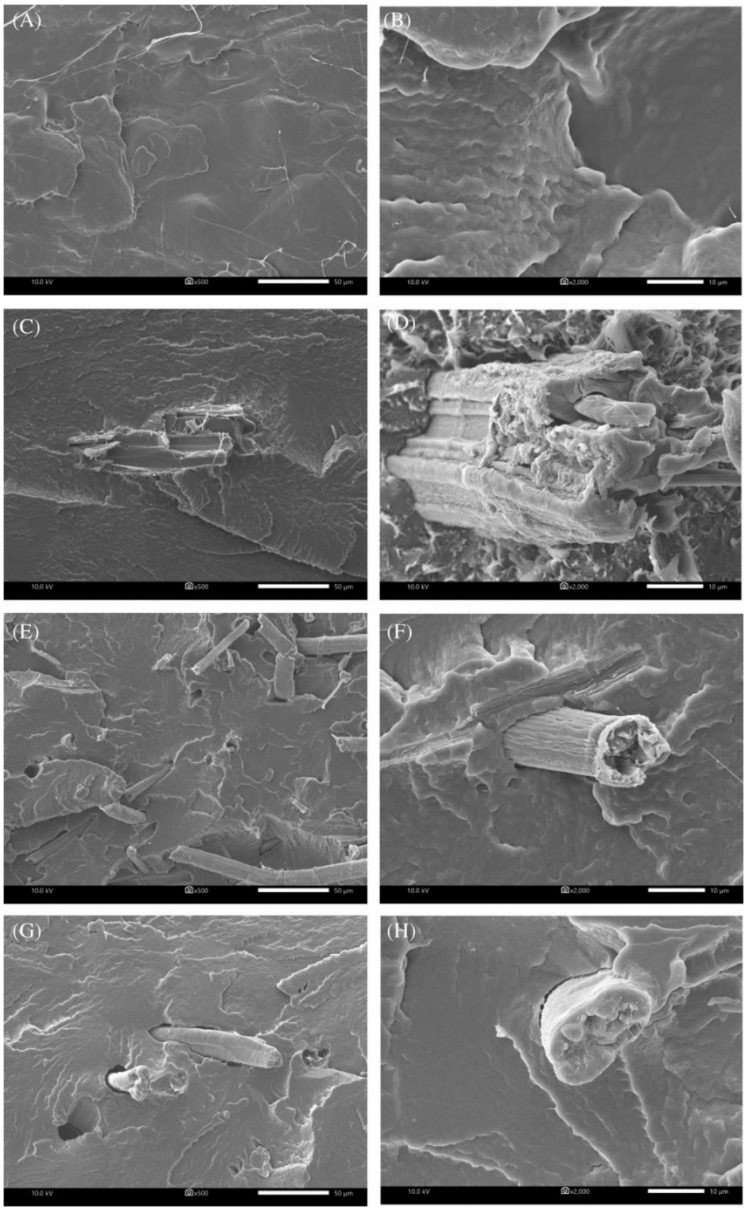


Figure 5: SEM micrograph of fracture surface of neat PBS (A, B), PBS with kenaf fibers (C, D), PBS with cellulose fibers extracted from kenaf (E, F) and PBS with commercial cellulose (G, H). Figure reprinted with the permission of John Wiley and Sons from ref (59)

Several approaches were studied to overcome this problem. Zhang et al. showed as the adsorption of silane coupling agent on rice straw fibers improve the adhesion between the two phases, resulting in higher tensile strength.(60) This approach was successfully used also on cotton fibers, demonstrating to be a versatile way to improve interfacial properties in fibers-PBS composites.(61) Fiber surface can be also treated with sodium hydroxide to alter the morphology and obtain a rougher surface, which can be useful to improve the adhesion with the matrix, as showed by Qu et al.(62)

1.2.2 Polyurethane foam composites

Many industries, including buildings and transportation, utilize lightweight and insulating materials, making them essential for creating a sustainable future. In 2019, the energy usage related to heating or cooling in residential buildings accounted for 11% of all global energy production. Clearly, the use of insulating materials is necessary in order to improve energy efficiency and reduce energy wastage within buildings.(63) When discussing about using natural fibers for low density materials, two possible route have to be taken into account: composites with common polymers (PUF, PET-Foam, etc…) or as self-standing natural fibers foam. In this chapter, the use of fibers for lightweight composites with common foams (e.g. Polyurethane foams) are discussed, while self-standing natural fibers foam will be discussed in the next chapter. Because of their light weight, low thermal conductivity, and simplicity of processing, polyurethane foams (PUF) are frequently employed as insulating materials. However, one of the primary problems of polyurethane is its environmental effect during manufacturing and disposal.(64, 65) Strategies for overcoming or at least mitigating this issue include the use of sustainable raw materials such as bio-based polyols(66) or recycled polyols(67), as well as the use of bio-sourced fillers(66), which can reduce the total ecological impact of foam. In the recent decade, researchers have extensively examined the substitution of typical petroleum-based polyols with bio-based polyols derived from various sources such as nut shell(68), soybean, linseed(69), and lignin(70). **Figure 6** depict the four generation of biomass feedstock for the production of bio-polyols.

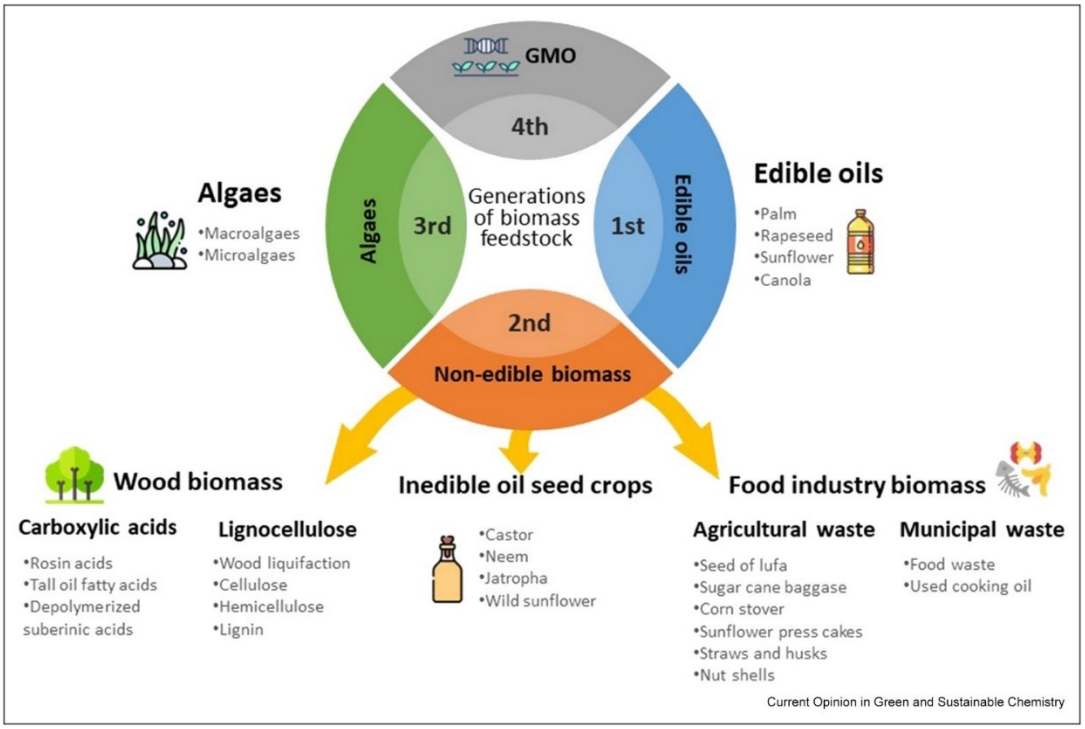


Figure 6: bio-derived feedstock for biopolyols production. Figure reprinted with the permission of Elsevier from ref (71)

The use of alternative source for polyols production has evolved during the years, starting from using vegetable edible oils, like palm(72) and canola(73), reaching the last stage of GMO employment. Edible oils were the first source of feedstock for bio-polyols extraction thanks to their already established agriculture and availability. However, the extraction of bio-polyols from this source is in competition with their use as food source, going against the common directives for a sustainable future. Second generation of biomass feedstock partially solve this issue by using vegetable oils coming from food waste or from inedible crops. However, oils as themselves do not have enough hydroxyl groups to be used for polyurethane manufacturing without prior modification, requiring thus some chemical modifications. During the years different routes were explored, such as the double bond epoxidation followed by hydroxylation, as shown by Wool et al, which produce polyols that can be used to prepare bio-based polyurethane foams.(74) One of the main advantage of this route is the flexibility in the oxirane ring opening, with properties which depend on the chemicals selected for this, as demonstrated by Shi et al.(75) Other routes like ozonolysis of vegetable oil were also studied.(76) The employment of renewable vegetable oils has a positive environmental effect onto the final foam. However, the chemical modification steps required to introduce hydroxy groups can present critical issues, like a big amount of solvents required or process safety. Another possible feedstock in the second generation are the wood biomass.(66) Having natural hydroxyl groups on their chains, lignocellulosic fibers are a good candidate in polyurethane foaming. Silva et al. prepared rigid PUF substituting part of the commercial polyols with cellulose fiber residue from pulp production. Composites were obtained using conventional

foaming process and fibers were added to polyols prior foaming (77) Up to 16% w/w, respect to polyols, were used in the formulation, resulting in foams with unaltered thermo-oxidative stability and mechanical properties, even though a cell size decrease was observed, as visible in **Figure 7**. Moreover, fungal growth was observed, indicating a higher susceptibility to biological attach.

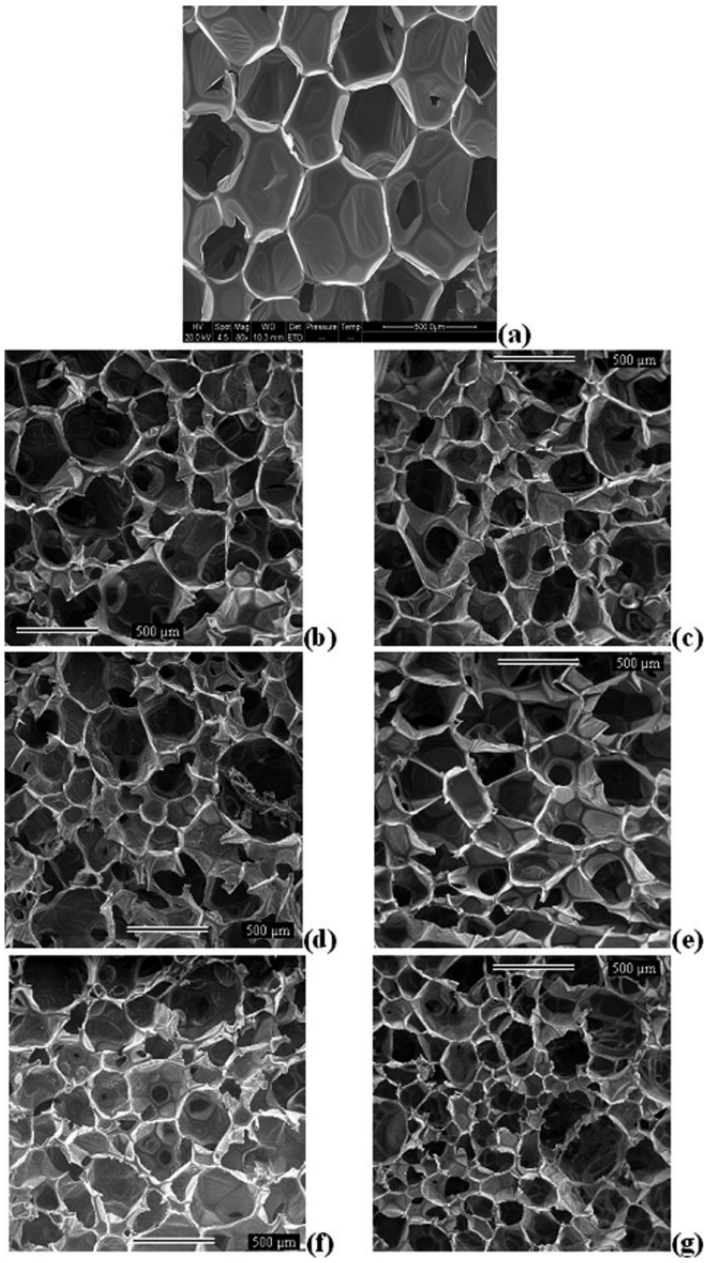


Figure 7: SEM micrographs for the (a) matrix foam and the composite foams containing respectively, (b) 1%, (c) 3%, (d) 4%, (e) 8%, (f) 12%, and (g) 16% w/w respect to polyols (the scale bar is 500 µm). Figure reprinted with the permission of John Wiley and Sons from ref (77)

The presence of fibers alters size and shape of PU cells. This phenomenon was observed also by Verdolotti et al. which developed a PUF comprising ball-milled cellulose with a 20% of loading. Both crystalline and amorphous cellulose were used resulting in a 30% reduction of the thermal conductivity, mainly thanks the smaller cell size.(78) The use of fibers present some limitations during foaming,

reducing the maximum amount that can be incorporated.(79) To try to solve or limit this effect, attempts in using microcellulose or nanocellulose have been made. Among them, Ragauskas et al. tried to incorporate cellulose nano whiskers into rigid PUF. The team demonstrated that whiskers take part in the PUF crosslinking step, being incorporated into the final properties. This permit the formation of a nanocomposite in which the mechanical properties of nanocellulose are imparted to final composite, improving both mechanical and thermal properties.(80)

1.2.3 Cellulose fibers light-weight materials

Creating stable and lightweight 3D structures that resemble polystyrene and polyurethane foams is one of the major challenges when utilizing cellulose for manufacturing purposes. To achieve this goal, various types of cellulose of different sizes, comprising both larger fibers and smaller particles, commonly referred to as nanocellulose, have been explored in recent years.(81) The use of nanocellulose, in form of fibers or crystals, in foams and aerogel manufacturing has grown rapidly in the last years, attracting the interest of the scientific community. The integration of an exceptionally low density, adjustable porous structure alongside remarkable mechanical properties makes nanocellulose base foams highly intriguing for a diverse array of applications in various fields. Commonly, the process to prepare nanocellulose-based foams can be divided in two steps: gel or wet foam formation and solvent removal. **Figure 8** shows examples of possible routes and processing methods, as long as correct terminology.

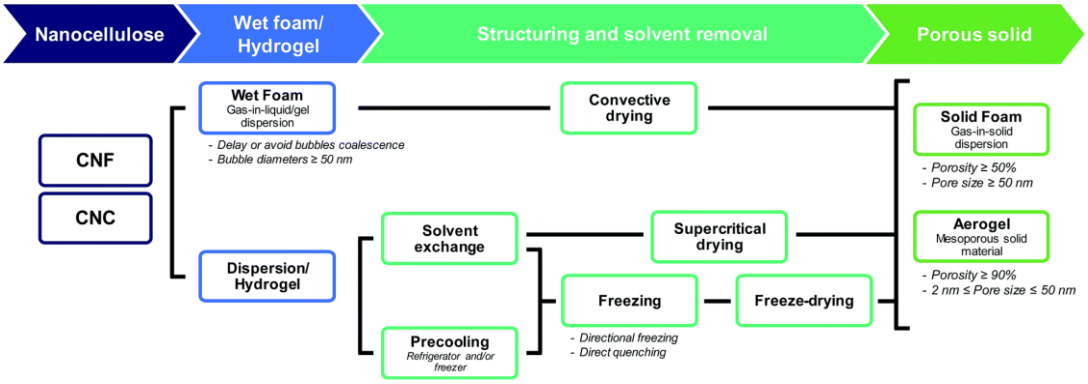


Figure 8: Terminology and processes for nanocellulose foams manufacturing. Figure reprinted with the permission Royal Society of Chemistry from ref (82)

One of the primary obstacles in the manufacturing process of nanocellulose-derived porous materials is the preservation of their porous structure throughout the solvent removal stage. The phenomenon of water evaporation from a porous material gives rise to capillary pressure-induced stress, which has the potential to cause deformation of the material's pores, leading to warping, collapse, or cracking.(83) A possible route is based on the concept of solvent exchange, which is commonly used to substitute water with solvents like acetone or ethanol. This substitution is usually made to remove a solvent which present high capillary force, like water, with solvents with lower capillary force. Moreover, when techniques as supercritical drying are used it is necessary to have solvents that are soluble in

supercritical carbon dioxide.(84) Such approach has proven to be effective in making aerogels from cellulose nanowhiskers by Thielemans et al., which proposed a process involving the solvent exchange of CNW suspension with ethanol, followed by CO_2 supercritical drying.(85) Similar approach was used also for other forms of nanocellulose. Another approach uses freeze-drying to obtain aerogels starting from nanocellulose suspensions. This allows to avoid the use of water as solvent, increasing the overall process safety. A typical procedure consist in freezing a nanocellulose dispersion and sublimate the frozen solvent with a freeze-dryer.(86) Freezing conditions have been shown to assert a role in pores dimension and orientation. Wågberg et al. showed that is possible to obtain anisotropic aerogels by forcing ice crystals growth in one direction, obtaining after freeze-drying an aerogel with oriented cavities.(87) In parallel, Liu et al. extensively studied the influence of freezing temperature in the final aerogels, as visible in **Figure 9**. Higher freezing temperature lead to bigger ice crystals and then higher pores, on the contrary, extremely low temperature induce the formation of small crystals.(88)

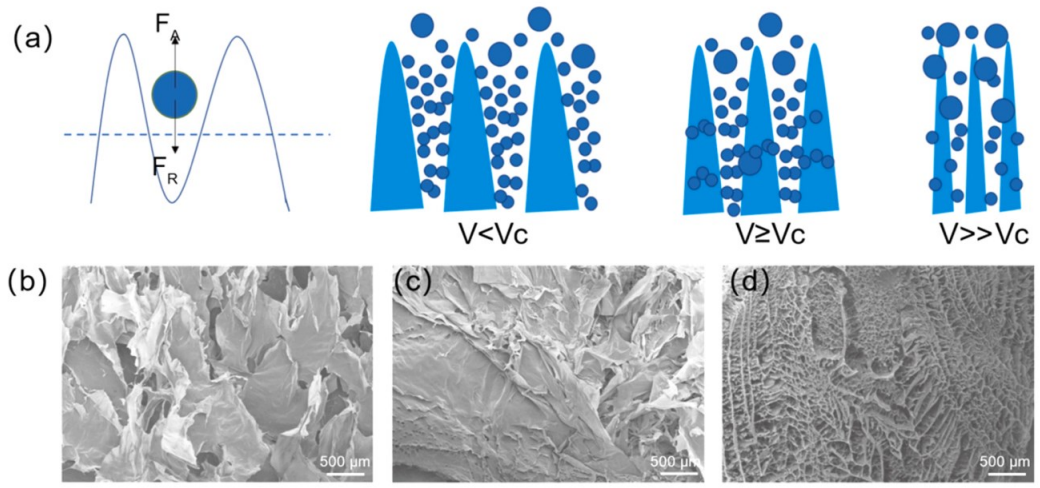


Figure 9: (a) Scheme illustration of crystal growth under different temperatures. SEM images of nanocellulose aerogel with various freezing temperatures. (b) Refrigerator (− 20 ◦C). (c) Cold trap (− 80 ◦C). (d) Liquid nitrogen (− 196 ◦C). Figure adapted from (88) with permission of Elsevier

These strategies provided to be effective in aerogel manufacturing, however they all require a heavy energy consumption step, like freezing, and/or non-aqueous solvent, with all the related dangers. For this reason, scientist focused their attention in searching solutions more industrially friendly. Indeed, Wågberg et al. showed as it is possible to obtain a cellulose based porous materials from the air drying of a stable wet-foams obtained by using octylamine as surfactant. Octylamine bearing CNF accumulate around air bubbles made by stirring, preventing their collapse and stabilizing them.(89) However, although nanocellulose is extensively utilized in various forms and with several manufacturing process, it appears that using pulp fibers is a more feasible option due to their simplified handling, cost-effectiveness, and environmentally friendly production.(90) However, pulp-like fibers are micrometric sized fibers, which provide a challenge in maintaining a stable 3D

structure. Structure collapsing is common when micrometric size fibers are used and it can result in foams with high density.(91) Choosing the right surfactant and foaming conditions can improve the final result, indeed, Hutzler et al. showed the possibility to prepare a lightweight material by using macroscopic cellulose fibers and surfactants, the result is a 3D network in which fibers are held together by only physical forces. (92) Common foaming method produce materials held together only by the interlocking of fibers, which do not interact with each other. To improve the adhesion between fibers, and thus the strength of final material, Larsson et al. demonstrated the possibility of making a lightweight material by cross-linking kraft pulp fibers and exploiting solvent exchange to obtain a 3D structure.(93) A similar principle was also exploited by Xiong et al. which optimized a crosslinking process involving polyamide epichlorohydrin and surfactant foaming.(94)

1.2.4 State of art challenges and limitations

From the previous chapters appears evident the interest of the scientific community in the employment of cellulose fibers either in composites and as self-standing lightweight materials. However, some challenges are still present and they are the main focus of researcher in the last years. Cellulose natural hydrophilicity works against its use in bulk polymer composites, leading to bad interface properties that do not allow the full exploitation of natural fibers. Moreover, natural fibers are extracted from many different sources and in different shape, with chemical composition that with season, species and world region. This leads to necessity to study each of them separately for each application desired. On contrary, the hydrophilicity of cellulose came in our help when designing self-standing materials all-natural fibers-based or when used for PUF composites. The hydrophilic nature of fibers can be used to introduce functional groups or for interaction with surfactants. In this field, the major challenge is the formation of a stable structure with micrometric, or even millimetric, fibers. Among the mentioned processes there can be find some critical aspects regarding cost, energy consumption and safety. Indeed, freezing has been found to be an effective method to form a stable structure, however, the energy consumption related to such low temperature must be considered. Similar consideration must be done also in choosing between nanocellulose and macroscopic fibers. Nanocellulose gave outstanding results in obtaining extremely low-density materials and it is well known for its promisingly good mechanical properties, however at the moment the energy consumption required for its production, from fiber refining to nanofiber production, is high if compared to macroscopic fibers. Last, cellulose rich materials can face limitations in many fields due to their high flammability.(95) Indeed, for applications in transportation, constructions and automotive (and others), fire retardancy is required to prevent loss of lives and expensive damage caused by fires.(96) This is especially true in the construction field, which saw an intensive spread of polymeric materials thanks to their lightness and insulation properties, where flame retardancy is a must to prevent damage and loss of lives.(97) This means that in order to use cellulose in materials employed in these fields, its inherently high flammability

must be mitigated with the addition of additives able to prevent its flaming and non-flaming combustion such as smoldering.(98, 99)

1.3 Flame retardant properties

1.3.1 Fire mechanism

Polymeric materials are well known for being lightweight and versatile, finding several applications (e.g. Insulation, Structural, Packaging, etc…). However, polymers are well known also for being extremely flammable. In a typical scenario, when a polymeric material is exposed to a heat flux, like a small flame or a faulty electrical appliance, the surface undergoes a thermal decomposition and release unstable volatiles, such as radicals. If they are above the ignition temperature and if the oxygen is enough, a fire starts. This generate more heat, that will be transferred to the material, which will further decompose liberating flammable volatiles, creating thus a self-sustained mechanism that will consume all the material remained.(100) A representation of this process is visible in **Figure 10.**

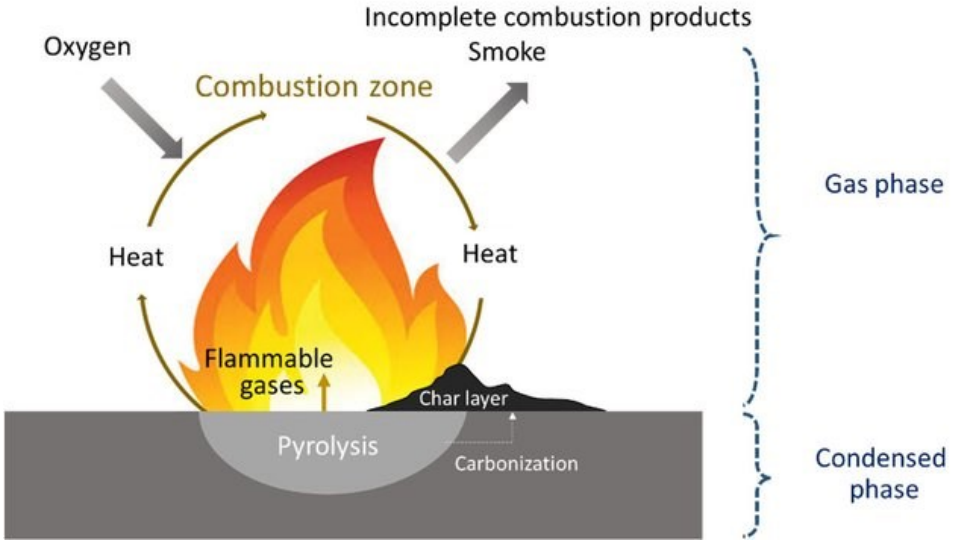


Figure 10: Combustion cycle representing common processes involved in flame propagation. Reproduced with permission from (101)

To achieve flame retardancy, the cycle of fuel, heat, and oxygen must be disrupted during combustion. Flame retardant agents are used to decrease the flammability of materials and block this cycle. Several mechanisms can be exploited to obtain this effect and they can fall in one of these categories: physical, chemical or both. Examples of physical effects are the endothermic effect, the formation of a protective layer and volatiles dilution. Endothermic effect is one of the most exploited mechanism of action of flame-retardants. Briefly, combustion happens when a heated combustible substance reaches its ignition point, resulting in the production of flue gas. In a short amount of time, the flame-retardant substance can absorb some of the heat emitted by the burning material, resulting in a powerful endothermic reaction. This can lower the surface temperature of the burning material, thus reducing smoke formation, and preventing the fire from

spreading.(102) The formation of a protective layer instead prevents the gas exchange with air and thus reduce the amounts of volatiles that can burn, reducing the overall flammability.(103) Lastly, volatiles reduction works by releasing inert, non-flammable, gases that dilute the flammable one coming from the material. The concentration of flammable gas progressively decreases as the volume of non-combustible gas increases, preventing continuous burning. (104, 105) Chemical action can work in the solid state or in gas phase. In the first case, a layer of carbon is formed on the surface of the material, preventing and limiting the exchange of heat and materials between the environment and matrix, slowing the thermal decomposition of it. In gas phase, flame retardants act as radical scavenger, which decrease their density in combustion zone, decreasing the burning rate of the material, until the flame is eventually extinguished.(104, 106)

1.3.2 Flame retardancy of cellulose based materials

Flammability is one of the main concerns when cellulose-rich materials are involved, limiting their possible fields of application. Indeed, a high concentration of cellulose lead to an increase of burnable materials in composites and in all-cellulose materials. In order to tackle this issue, flame-retardants (FR) have to be incorporated in the final materials with strategies that differs depending on the materials that has to be treated. For polymer commonly used as bulk materials, like PBS or PLA, the most common approach is the incorporation of flame retardants as filler during processing. Many flame-retardants have been studied along the years, but focusing on a green chemistry approach, conventional chemicals used, mostly halogen-based, do not represent a viable strategy having toxicological and environmental problems.(107, 108) A promising class of chemicals is represented by phosphate bearing FR. Indeed, phosphate bearing FRs are deemed to be safer from both an environmental and health point of view with the exception of the limited class of organophosphates(109, 110). Among phosphorous based compounds present on the market, ammonium polyphosphate (APP) has proven to be an effective chemical in the flame-retardant field.(111) Indeed, it is widely studied in PBS flame retardancy although not alone. It has been proved that its flame-retardant effect can greatly benefit from the combination with synergistic components than when used alone.(112) In the early years, Chen et al. studied the effect of a coupling agent and water crosslinking in APP added PBS. Tetraethoxysilane (TEOS) was used as coupling agent and composites were treated with water at 70°C. Composite with 15% of APP with and without TEOS coupling agent were compared in flammability test, obtaining a V-2 classification for APP alone and a V-0 when used in combination with TEOS. Evidencing that benefits obtained from the incorporation of synergistic component.(113) From this evidence, many strategies were developed, such as the inclusion of synergistic agents, char-forming agents, blowing agents or the combination of those three. (114-116) Together with phosphate-based flame-retardants, nanoparticles are nowadays widely applied in this field thanks to the low loading usually required, catalytic charring performance, physical barrier effect and high dispersibility. (117)

Flame-retardant nanocomposites with natural clay have been extensively studied by Lopez-Cuesta et al. comparing the effect alone and in combination with phosphate flame-retardant.(118) Nanoclays as sepiolite and halloysite demonstrated to improve the PBS fire behavior, even though a detrimental effect was observed in its thermal stability, mainly caused by water release, which lead to PBS hydrolysis. The best results were observed when clays were used in combination with APP and lignin, as visible in **Figure 11** evidencing one more time the importance of a joint effect of FR chemicals.

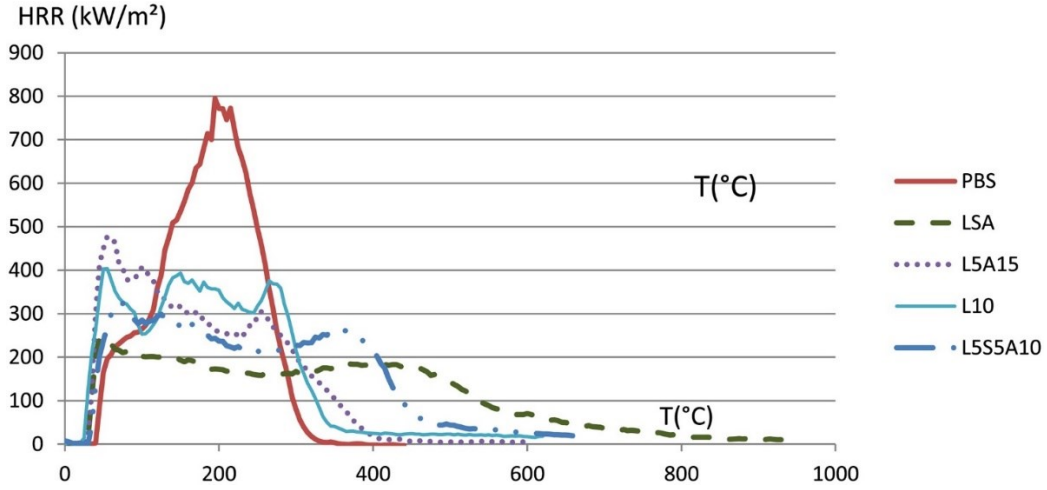


Figure 11: cone calorimetry curves for PBS composites. 50kW/m^2 heating flux. Where, PBS: polybutylene succinate, LSA: PBS + 6.6% sepiolite + 6.6% APP + 6.6% Lignin, L5A15: PBS + 15APP + 5% lignin, L10: PBS + lignin and L5S5A10: PBS + 5% sepiolite + 10% APP + 5% Lignin. Figure reprinted with the permission John Wiley and Sons from ref (118)

The addition of lignocellulosic fibers to polymer composites can be detrimental to their flammability, being cellulose extremely flammable. Kandola et al. explored investigated the effect of different woven non-woven textile made from different source in combination with PLA. A decrease in the peak associate at the heat release rate (pkHRR) was observed for composites with jute and sisal fibers, however, THR increased for all samples indicating a less intense, but longer burning behavior for all composites.(119) However, the addition of common flame-retardants to the textiles before compounding have been found to be detrimental to mechanical properties of final composites.(120) To limit this phenomena, alternative approach have been explored in the last years, such as the use of new flame-retardant agents, like phytic acid (121)or the exploitation of techniques like layer-by-layer.(122) Lopez-Cuesta et al. investigated the effect of flax fibers on flame properties of PBS, alone and in presence of phosphate groups. The presence of a lignocellulosic material, coupled with a phosphorous-based flame retardant, allow the formation of an extensive char which assert a major fire retardant effect in the composites, obtaining a visible pkHRR reduction(123). Similar results were obtained by Suppakarn er al., the addition of APP to a natural fibers-PBS composite was able to reduce its flammability, reaching the V-0 classification and a 53% reduction in pkHRR respect to neat PBS. Charring ability of cellulose rich materials showed to be effective in improving flame-retardant properties when combined with

phosphorous agent.(124) In particular, as studied by Hu et al., an increase in the concentration of fibers can assert a beneficial role in the amount of char formed and thus in a flammability decrease.(125) Similar approaches can be applied also on porous materials, like PUF. Indeed, many phosphorous based flame-retardant can be added during foaming, resulting in their incorporation in the final foams. Among them, APP showed to be effective in increase the Limiting Oxygen Index (LOI) and decrease flammability for water blown PUF.(126, 127) Other phosphorous based flame-retardants have been studied in the last years, like phytic acid(128), 9,10-dihydro-9-oxa-10- phosphaphenanthrene10-oxide (DOPO)(129) and phosphorylated polyols.(130) However, the addition of lignocellulosic fibers to PUF increase their flammability and alter cells dimensions, making it necessary to study viable strategies which take into consideration the effect of fibers. One of the main strategies is the prior modification of cellulosic fibers to impart them flame-retardant properties, followed by blending with polyols and foam them, to obtain a PUF composite.(131-133)

Cellulose-based lightweight materials are inherently flammable, limiting their possible application in contexts requiring fire safety, like transportation and buildings. Some studies evidenced the possibility of follow similar pathways as PUF, for example by adding flame-retardants during foam formation. In this context, Xing et al. prepared a foam comprised of CNF and phosphorous-hybridized graphene nanosheets by freeze-drying. A 94% reduction in pkHRR was obtained thanks to the high char forming capability of the system.(134) Another possibility is the insertion of phosphate groups directly into the CNF backbones to provide it of an inherently flame-retardancy. Wågberg et al. tried this approach and combined the resulting CNF with sepiolite. Phosphate groups are well-known for their flame-retardant properties and can catalyze the dehydration of carbohydrates at high temperature.(135) This effect leads to the formation of a thermal stable char structure which limit the release of volatiles. Phosphorylated fibrils have thus an intrinsic good char forming ability and when combined with the protection effect given by sepiolite, which act as a ceramic shield on fibers surface, lead to a foam with exceptional flame-retardant properties. Indeed, flame penetration test showed the ability of the obtained foam to withstand flame and protect the unexposed side, moreover a pkHRR of 34kW/m^2 was reported.(136) Meanwhile, Ek et al. demonstrated the possibility to impart flame retardancy to foams from non-nanometric cellulose fibers. Expandable graphite and commercial synergetic fire retardant were used in a formulation with more than 70% of pulp content, showing up to a 63% decrease in pkHRR as result of the formation of a protective char layer upon flame exposure.(137) The same group explored also the effect asserted by other flame-retardants, such as sulfonated or non-sulfonated kraft lignin and nanoclay, on foams obtained from recycled textile fibers and also in this case the formation of a protective layer on fibers surface asserted a fundamental role. Indeed, the best results were obtained with samples containing nanoclay, which was able to form a protective layer on fibers which prevented the underlying substrate further decomposition and thus avoided the ignition of the sample.(138) Peng et al.

followed a different route, obtaining pulp foams by borate crosslinking, which was seen to impart flame-retardant properties to the final foam. Indeed, samples with a borate concentration higher than 3% gave self-extinguishing behavior, with a 22% reduction in pkHRR. These results were mainly attributed to the borate groups, which improved the char formed after flame exposure.(139) Together with direct addition of flame-retardants, in which the flame retardant is incorporated during foaming, other routes are also possible. These methods mainly involve changing the surface of materials, either using plasma or sol-gel techniques, or using a water-based process to form a coating comprised by nanoparticles or natural substances, like polyelectrolytes.(140-143) Among these methods, Layer-by-Layer (LbL) technique emerge as a versatile candidate to impart flame retardant properties to materials and has found application with several substrates, such as textiles, (144) polyurethane foams(145) and composites(122, 146). Layer-by-layer application in flame retardancy will be further discussed in the next sections.

1.3.1 Layer-by-layer approach

The aim of Layer-by-layer is the deposition of a self-assembled coating using a water-based approach.(147) The Layer-by-Layer is based on the alternatively adsorption of opposite charge polyelectrolyte onto a substrate.(148) Typically, a LbL assembly proceeds with the following steps: (A) immersion of a charged substrate in an oppositely-charged polyelectrolyte (or particle) solution, charge reversal of the surface occurs. (B) unbound material is removed with a washing step. (C) immersion of the substrate in a second solution with opposite charge polyelectrolyte, which lead to the multilayer formation. This process is repeated up to the desired number of layers.(149, 150) **Figure 12** graphically represent this process.

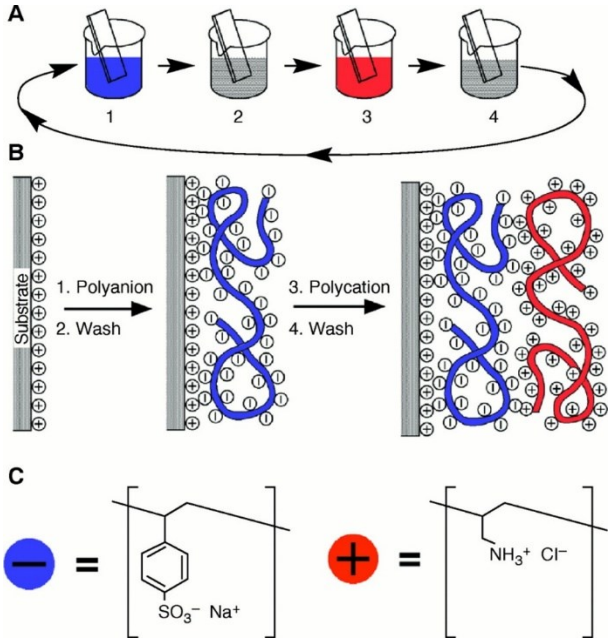


Figure 12: representation of an LbL assembly with A) the sequence commonly used in a deposition, B) surface Bi-layer build-up and C) two common polyelectrolytes, sodium salt of poly (styrene sulfonate) and poly (allylamine hydrochloride).

This leads to the formation of an interpenetrated and homogeneous coating. Electrostatic interactions are the most prominent forces involved in the formation of the multilayer, although weaker interaction (e.g. hydrogen bonding) have been demonstrated to take part in the coating formation .(151, 152) Apart from the polyelectrolytes involved, several parameters affect the deposition and the coating thickness. Temperature assert a visible influence on the deposition, with thickness that generally increase at the increase of deposition temperature.(153) Also, being electrostatic interaction one of the main force governing LbL assembly, polyelectrolyte charge and thus deposition pH assert an important role in the assembly. (154) Moreover, this effect can be exploited to build pH-responsive coating or Nano capsules for biomedical applications.(155, 156) Counterions presence and ionic strength are also parameters that influence the coating growth in LbL assembly. (157, 158) **Figure 13** show examples of correlations between these parameters and coating thickness.

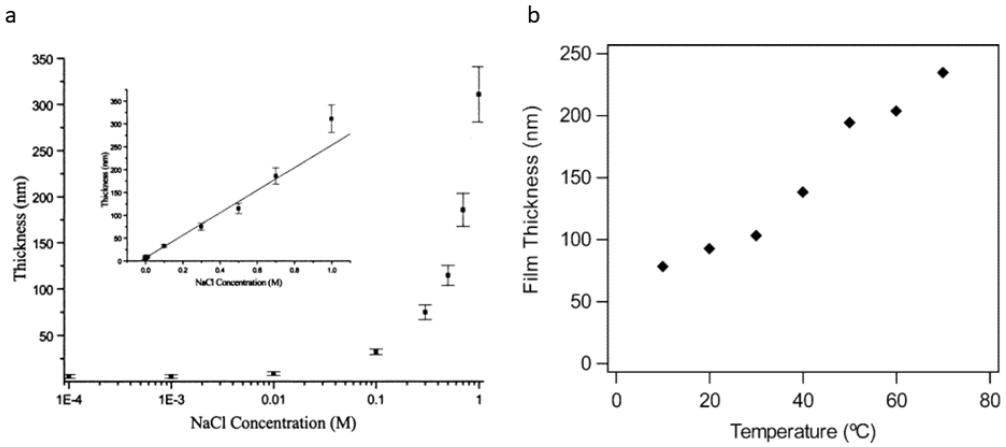


Figure 13: graphs representing the dependence of A) coating thickness vs salt concentration for 10BL of PDDA/PSS coating and B) coating thickness vs deposition temperature for 10BL of PDDS/PSS. Figure adapted from (153) and (154). Copyright 2001 American Chemical Society

LbL can be applied to many substrates thank to its tunability and properties, resulting in a flexible approach to impart properties like gas barrier, flame retardancy, chemical encapsulation and others. Among all possible substrates, lignocellulosic materials due to their natural hydrophilicity are an optimum substrate for LbL assembly(159). Indeed, Wågberg et al. compared paper sheets made by LbL coated fibers with sheets made from uncoated fibers. A coating comprising 5BL of polyallylamine hydrochloride (PAH) and Hyaluronic acid (HA) are able to increase the strain at break and the tensile strength of a factor three for both.(160) Also, Lu et al. showed how is it possible to exploit LbL coating to improve the outcome of recycled fibers use in papermaking. A coating comprised of HA and poly(styrene-sulfonate) (PSS) was assembled on broken fibers and later mixed with virgin pulp to simulate a recycling process, the coating was able to act as a glue between fibers in the mixture, avoiding loss of mechanical strength.(161) LbL has proven to be an effective way to introduce functionalities on the surface of many substrates, in particular in lignocellulosic-based ones. This can also come in

handy for the introduction of flame-retardant components that can address the issue of the high flammability of these materials. Indeed, LbL have been extensively used to impart flame-retardant properties to many kinds of substrates and its mechanism of action can most of the times fall into two major categories: the deposition of an inorganic coating or the deposition of intumescent coatings. The deposition of inorganic components aims at the formation of a sort of non-burnable shield, which can slow down matter and energy exchange between the condensed and gas phase, thus protecting the substrate. Many studies have been published regarding flame retardancy of cotton fabric, a common lignocellulosic material.(162) Indeed, in one of the first study on flame-retardancy of cotton fabric via LbL application, Grunlan et al. treated cotton fabrics with up to 20 BLs of an assembly comprising BPEI and montmorillonite (MMT). (163) This resulted in the reducing of afterglow time in vertical testing and put first basis for further development. (164)

Other studies focused their attention to nanofibrils aerogels, which can greatly suffer from high flammability of cellulose, which limits their possible exploitation in many fields. Koklukaya et al. presented how LbL coating on a nanofibrils aerogel with an assembly comprising 4QL of Ch/PVPA/Ch/MMT can produce a non-ignitable aerogel, able to prevent the flame penetration of a torch focused on its surface.(165) Intumescence, a process characterized by the formation of a carbon shield resulting from elevated temperatures or fire, stands as a viable alternative to fire protection using inorganic barrier creation. Intumescent coatings assert their effect in the condensed-phase, indeed, the formation of a carbon char shield interrupt the substrate combustion and thus the fuel generation necessary to sustain the burning of the material. This involves the conversion of the decomposing material in a graphitic or glassy char instead of fuel, char that will act as a physical barrier slowing down heat and mass transfer.(111, 166) Traditional intumescent flame retardant requires three components: a carbon source, an acid donor and a blowing agent.(167) During combustion, the presence of an acid source favors the formation of a more or less ordered carbon layer which is then blown by the blowing agent, expanding. In this way a more stable residue is formed which is able to protect the underneath material from further decompose, as depicted in **Figure 14**.(163)

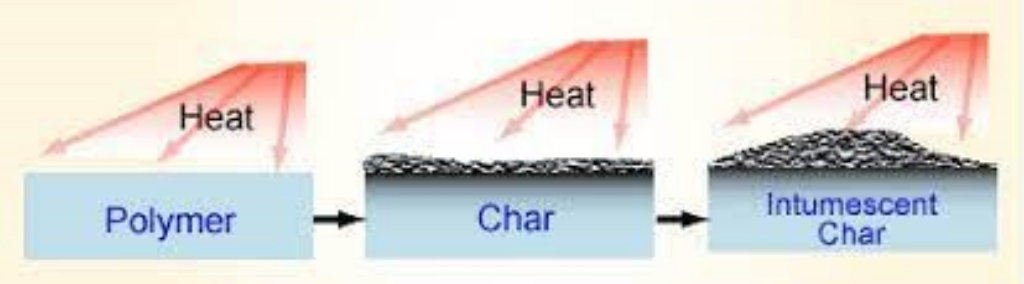


Figure 14: graphical depiction of an intumescent flame retardant

This effect was exploited by Grunlan et al. to coat a cotton fabric with an intumescent coating through layer-by-layer deposition. Poly (sodium phosphate)

was used as acid source and poly(allylamine) as blowing agent. Being cotton made majorly by cellulose, it was possible to use it as carbon source. The result was a coating that can withstand a vertical flame after 20BL and greatly reduce pk of HRR cotton fabric.(168) From that point, many researchers focused their attention in the application of LbL for intumescent flame-retardant coating for cotton fabrics. (169-172) However, fabrics are not the only substrate that can benefit from this method.

A clear example of LbL use for flame retardant in cellulose based materials came from Wågberg et al. where pulp fibers were coated with a LbL assembly comprised of chitosan (CH) and poly (vinyl phosphonic acid) (PVPA) and used for paper sheets forming. The coating was able to extinguish the flame after ignition, leaving intact part of the sheet, on the contrary untreated pulp burned completely.(173) Following a similar approach, Zhao et al. tested a system comprised by phytic acid (PA), polyethylenimine (PEI) and melamine on fibers coming from a simulated recycling process. The authors showed also the correlation bi-layer numbers/properties, indeed, 8 BL were necessary to obtain flame-retardant properties acceptable, while at 4 BL the improvement were not so relevant.(174)

2. Polybutylene succinate composites

As previously discussed in chapter 1.2, cellulose fibers incorporation in bio-polymers is a matter of interest in the composites field. Indeed, cellulose incorporation can increase the sustainability of bio-based polymers and increase mechanical properties, which are a well-known limitation in bio-polymers exploitation. Among bio-polymers, PBS composites are becoming more and more popular. PBS can be obtained from both from petrochemical monomers and renewable resources, providing a great manufacturing flexibility. Moreover, the addition of lignocellulosic fillers can broaden its fields of application, impacting positively its sustainability.(54-58) The major concerns about cellulose based materials in PBS composites production are related to the poor fiber-matrix adhesion, which has shown to be weak, and flammability of the final composite. The majority of state-of-art studies focused their attention to the first issue, the fiber-matrix adhesion, obtaining the successful incorporation of various source of fibers into the PBS matrix. However, each natural fiber source is different, due to the many natural parameters that regulate the fibers growth, and thus the final fibers properties, resulting in studies that are not universal applicable to all fibers. For what regards flammability of PBS-natural fibers composites, common approaches have been attempted, leading to promising results that can be further explored. However, many of them required the use of massive amount of flame-retardant, impacting thus both mechanical properties and sustainability of the process.

In this study a different approach is explored. Cellulose fibers are used as model natural fibers and a coating able to improve adhesion properties and with flame-retardant properties was developed. Briefly, layer-by-layer assemblies comprising flame-retardant agents, namely APP and phytic acid, and chitosan as have been developed and used to coat cellulose fibers. Then, fibers where used to make composites with up to 30% loading. Mechanical and thermal properties were then studied. The proposed approach differs from literature, trying to improve both properties at the same time and proving a possible solution that can hypothetically be applied to all lignocellulosic natural fibers.

2.1 Materials and methods

2.1.1 Materials

Commercial cellulose fibers (ARBOCEL BWW40) with an average length of 200 µm was kindly provided by J. Rettenmaier & Sohne GmbH (Rosenberg, Germany). Branched poly (ethylene imine) (BPEI, Mw ~25000 Da by light scattering, Mn ~10000 by gel permeation chromatography, according to the material datasheet), chitosan (low molecular weight, < 20000 Da and 75-85% deacetylated chitin, according to the material datasheet), acetic acid, ammonium polyphosphate (PHOS-CHEK® P30) was purchased from ICL Performance Products, Inc. phytic acid

(50% wt. solution) were purchased from Sigma Aldrich (St- Louis, USA). Suspensions and solutions were prepared using ultrapure water (18.2 MΩ deionized water supplied by a Q20 Millipore system, Italy). Phytic acid was diluted to 2% solution with ultrapure water and ammonium polyphosphate was used as 1% dispersion in ultrapure water. Halloysite suspensions were prepared at a concentration of 0.5% wt. in chitosan 0.5% wt., by mechanical stirring for 24h, to achieve a stable suspension.(175)

2.1.2 Layer by layer assembly

Two layer-by-layer assemblies were evaluated: first one comprised halloysite nanotubes and chitosan as positive layer and ammonium polyphosphate as negative layer, the second comprised halloysite nanotubes and chitosan as positive layer and phytic acid as negative layer. Each assembly was preceded by cellulose fibers activation with branched poly(ethylenimine) 0.5% wt. Briefly, cellulose fibers were rehydrated with ultrapure water, the excess of it was removed by filtration on a nylon filter (200 mesh). Fibers were then dispersed as 5% wt. in the BPEI solution, manually stirred for 10 min, filtrated on a nylon filter (200 mesh) and washed with water. The same procedure was repeated with the negative and the positive layer with the exception of contact time that was set at 5 min instead of 10. The deposition scheme is reported in **Figure 15.**

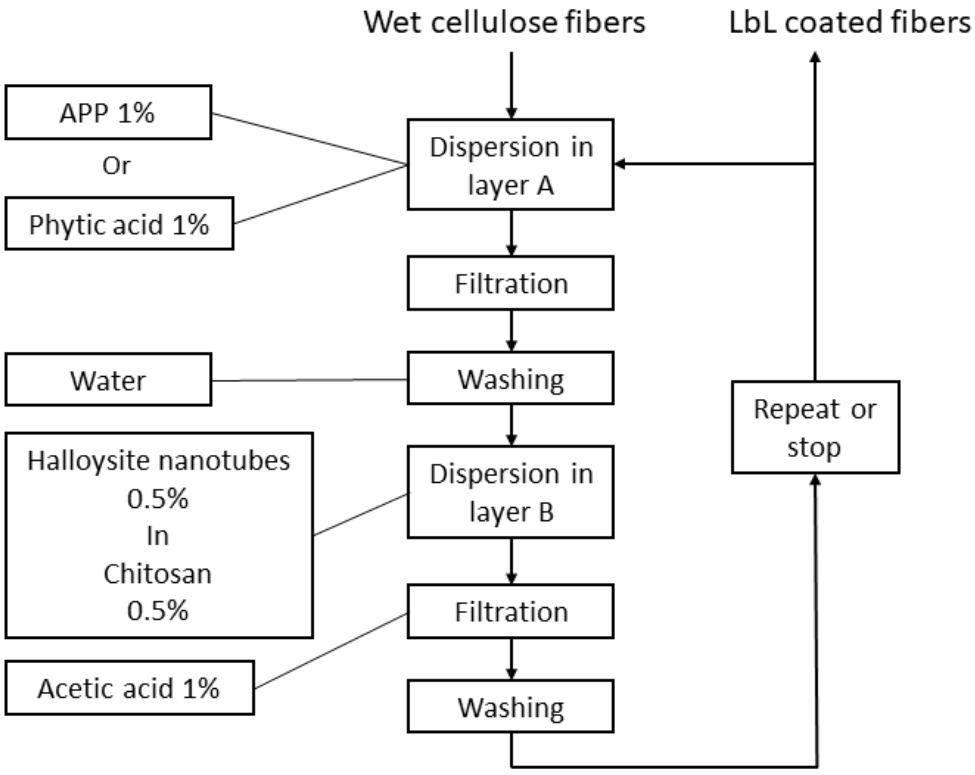


Figure 15: deposition scheme for cellulose fibers and layer-by-layer

Washing was performed with water for phytic acid and ammonium polyphosphate and 1% wt. acetic acid for the chitosan/halloysite suspension mixture. Coated fibers

were washed with water to remove any acetic acid excess and dried by freeze-drying for 48h (Toption TOPT-10A, vacuum freeze dryer).

2.1.3 Composites preparation by melt blending

Composites were prepared by melt-blending in a micro twin-screw compounder (Micro 15cc twin-screw compounder, DSM Xplore, Netherlands). Briefly, PBS and cellulose fibers were dried overnight and kept under vacuum until their use. PBS and fibers were then pre-mixed (**Table 1**) in an aluminum petri and charged in the extruder set at 130°C, melt blended for 5 minutes at 100 rpm and then collected as a filament. Composites filament were then manually cut and pressed at 130°C for 3 minutes with a 10x10x1 mm frame in a thermo-press (P200T, Collin) to obtain the final specimen.

Table 1: composites formulations

Name	Cellulose coating	Cellulose content (%)	PBS content (%)
PBS	/	0	100
PBS 15%	Untreated fibers	15	85
PBS 30%	Untreated fibers	30	70
PBS-APP15-3BL	CH/Hal-APP 3BL	15	85
PBS-APP15-6BL	CH/Hal-APP 6BL	15	85
PBS-APP30-3BL	CH/Hal-APP 3BL	30	70
PBS-APP30-6BL	CH/Hal-APP 6BL	30	70
PBS-Phy15-3BL	CH/Hal-Phy 3BL	15	85
PBS-Phy15-6BL	CH/Hal-Phy 6BL	15	85
PBS-Phy30-3BL	CH/Hal-Phy 3BL	30	70
PBS-Phy30-6BL	CH/Hal-Phy 6BL	30	70

2.1.4 Characterizations

Attenuated total reflectance (ATR) Fourier Transform infrared spectroscopy spectra for fibers and composites were collected using the same FT-IR spectroscope equipped with a diamond or germanium crystal. (16 scans, 4 cm^{-1} resolution). Surface morphology of fibers and composites was studied, after gold sputtering, using a LEO-1450VP Scanning Electron Microscope. Thermal stability of fibers was evaluated by TGA (Discovery, TA Analysis). Briefly, samples (approx. 10 ± 1mg) were placed into alumina pans and subjected to an isothermal treatment for 15 min at 100°C and then heated at 10°C min^{-1} up to 700°C. Samples were tested both in nitrogen and in air. T_{on} (temperature corresponding to 5 % weight loss), T_{max} (temperature at maximum rate of weight loss), and residue (%) were obtained by these measurements. Mechanical properties were evaluated using a dynamometer (Instrom 5966, 2kN cell, Canton, MA), specimens of 4 x 80 mm were tested at

traction for each formulation. Prior to the tests, samples were conditioned 23.0 ±0.1 °C for 48 h at 50.0% ± 0.1 RH in a climatic chamber. The flammability of the prepared samples was evaluated in horizontal configuration; the sample (4x50x1 mm^3) was ignited from its short side by a 20 mm methane flame (2x6 s application). The test was repeated at least 3 times for each formulation and parameters like after-flame time (s), char length (mm) and residue (%) were collected. Cone calorimetry (GA01, Noselab ats, Italy) was employed to investigate the combustion behavior of square samples (50x50x1 mm^3) under exposure to a heat of 35 kW/m^2 in horizontal configuration, following an already described procedure. Smaller samples than conventional 10x10 cm^2 were used to reduce the amount of fibers needed for each formulation. Each samples was confined in an aluminum foil holder.(176) The following parameters were collected: time to ignition (TTI, s), peak of heat release rate (PHRR, kW/m2), time to peak (s), total heat release (THR, MJ/m2), average heat of combustion (EHC, MJ/Kg), smoke production rate (SPR, m2/s), total smoke release (TSR, m2/m2) and final residue (%). The test was repeated 3 times to ensure reproducibility and the average of triplicate data is reported.

2.2 Results and discussion

2.2.1 Layer-by-layer assembly

The assembly proposed for this system comprise ammonium polyphosphate or phytic acid as phosphorous-based flame-retardant agent, coupled with halloysite nanotubes stabilized in chitosan. Prior to cellulose fibers coating, the two systems deposition conditions were evaluated via infrared spectroscopy. Following a procedure commonly adopted in the literature, the selected LbL conditions are firstly evaluated in a model surface (i.e. Si wafer). Briefly, LbL assembly is deposited on a Si wafer, and the infrared spectra after each layer, or bi-layer, is recorded. (177) To improve the assembly adhesion, BPEI was used as anchoring layer.(178) This procedure allow allows to gather information on the coating growth regime. Spectra of pure substances are reported in **Figure 16** while **Figure 17** shows the ir spectra for the growth on model substrate.

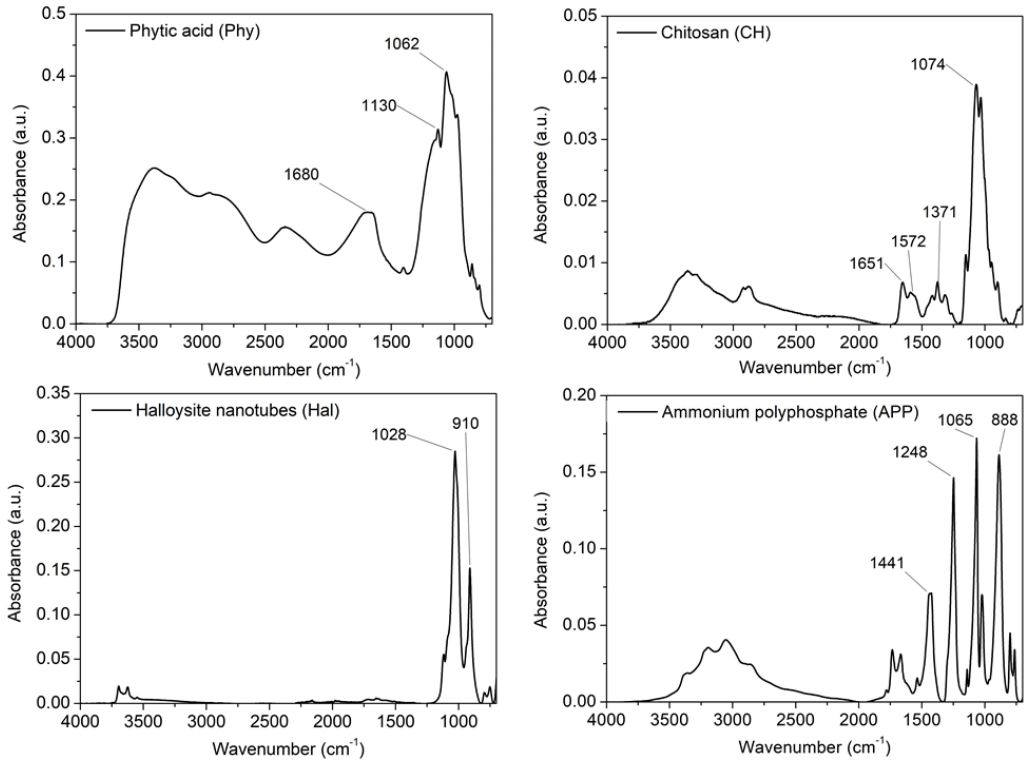


Figure 16: IR-spectra of pure chemicals

Phytic acid show a broad band composed by more than one peak between 900 and 1300 cm^{-1}, in which is possible to find the C-C stretching peak of the inositol ring at 1062 cm^{-1} and the C-O stretching signal at 1130 cm^{-1}.(179) At higher wavenumbers it's possible to find a broad peak centered at 1680 cm^{-1} correlated to O-H bending, while the O-H stretching broad band is visible between 3700 and 3000 cm-1, partially overlapping to the aliphatic C-H stretching band at 2900 cm^{-1}.(180) Chitosan presents too the -OH related stretching signal as broad band between 3700 and 3000 cm^{-1}, overlapped to the amine groups stretching vibrations typically found in the 3550-3330 cm^{-1} region.(180) C-H stretching signals, correlated to CH_2 and CH_3 groups, are visible at 2900 and 2880 cm^{-1}, respectively. Chitosan most intense signal can be seen at 1074 cm^{-1} and can be correlated to the C-O-C group stretching vibration.(181) Characteristic peaks associated to N-H absorption of amine and protonated amine are usually found in the 1650-1500 cm^{-1} range, with the latter producing two band at 1651 and 1572 cm^{-1} related to the asymmetric and symmetric bending vibrations.(180, 181) Halloysite nanotubes most characteristic peaks are found in the fingerprints region, with a sharp peak at 1028 associated to Si-O anti-symmetric stretching vibration and a sharp one at 910 cm^{-1} related to the bending vibration of inner surface hydroxyls.(182) Ammonium polyphosphate yield a well-known spectrum, with well visible signals related to NH_4^+ stretching at 3100, 3050 and 1440 cm^{-1}. A series of sharp peaks between 1500 and 800 cm^{-1} is linked to the phosphorous groups present, with peaks at 1248 and 888 cm^{-1} related to P=O and P-O-P vibrational modes, respectively. A third signal at 1070 cm^{-1} is correlated to the P-O bond.(144, 183) The coating growth was

evaluated for both systems by monitoring the intensity growth of the strong signal at 1073 cm^{-1} correlated to the C-O-C stretching of chitosan.

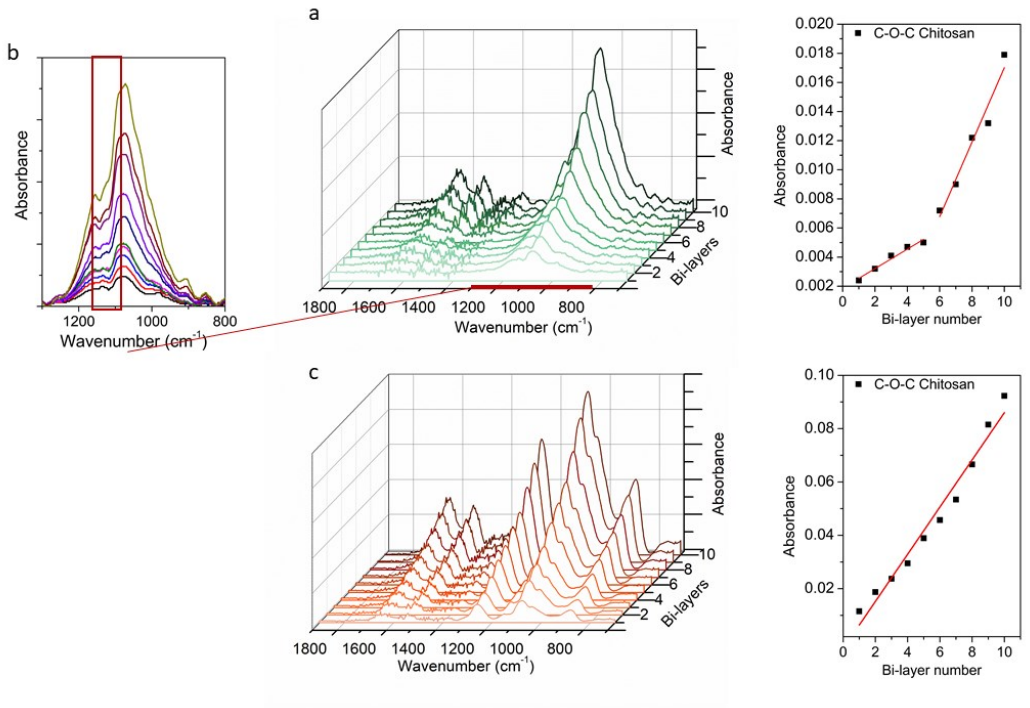


Figure 17: FT-IR spectra plot showing the LbL growth for a) Phy-Hal/CH on a silicon wafer substrate and the correlated BL number vs intensity plot, b) magnification of the portion between 1300 and 800 cm^{-1} ir spectra of Phy-CH/Hal growth and c) APP-Hal/CH on a silicon wafer substrate and the correlated BL number vs intensity plot

For what regard Phy-CH/Hal assembly, the main signals visible are ones related to chitosan, such as the C-O-C stretching vibrations at 1074 cm^{-1}. For this system, the main signals related to phytic acid overlap to the chitosan ones and are therefore difficult evaluation. However, the zoomed in region in **Figure 17 b** clearly points out the formation of a small shoulder at 1150cm^{-1} which increases in intensity by increasing BL numbers. This latter signal can be associated to the C-O stretching of phytic acid.(179) by plotting the peak intensity vs the number of BL it is possible to detect the presence of two different growing regimes, a first one up to 5 BL and a second after 6BL. The change in slope after 5 BLs can suggest an initial growth that proceed with the formation of islands of coating which eventually join together after 6BLs and leading to a more pronounced increase in the C-O-C signal per deposited BL, as visible from figure **Figure 17**. (184-186) The APP-CH/Hal assembly present same chitosan signals, which increase in intensity by increasing BL numbers, while it can be seen two sharp peaks at 1250 and 881 cm^{-1} correlated to the phosphate groups of APP. When put in a plot with BLs number, the signal correlated to C-O-C stretching vibration of chitosan yielded a steady increase in intensity, thus resulting in a linear growth regime. The two coatings have been transferred to the cellulose fibers, 3 and 6 BL have been deposited. Coating growth on fibers was monitored via FT-IR/ATR and scanning electron microscopy and compared to pure compounds IR to investigate signals increase correlated to coating

growth. In **Figure 18** are represented the IR spectra of neat and CH/Hal-Phy coated fibers at increasing number of BLs.

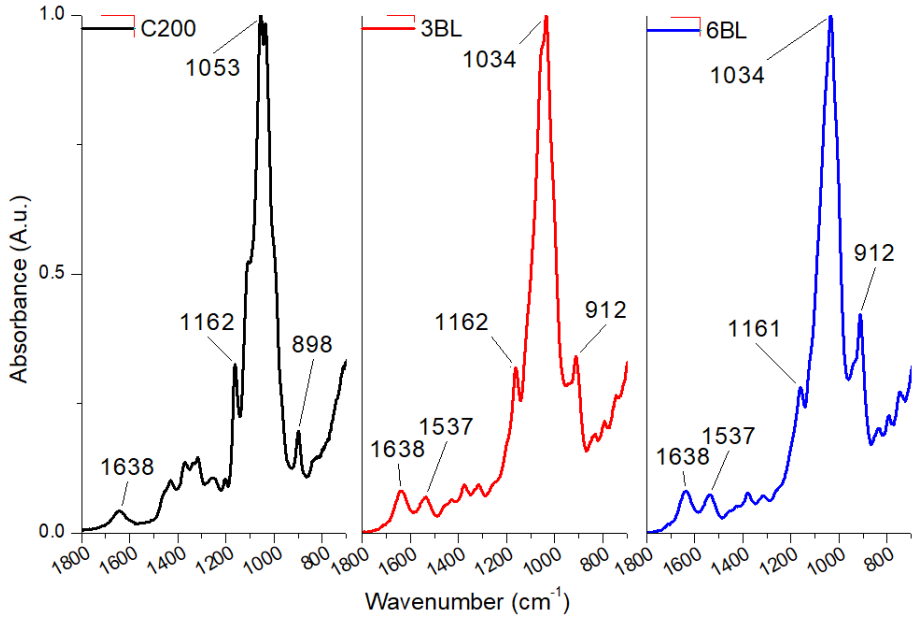


Figure 18: IR spectra of Phy – CH/Hal coated fibers (magnified)

Cellulose fibers IR spectrum has the typical spectrum of a cellulose. Analyzing the region between 1800 and 700 cm^{-1} it's possible to spot the typical bands associated to cellulose. At 1643 cm^{-1} it's possible to spot a band associated to the O-H deformations due to water adsorbed while between 1430 and 1317 cm^{-1} signals related to C-H of cellulose backbone are found. Specifically, at 1428 and 1371 cm^{-1} the C-H deformation of cellulose can be found, together with a signal at 1317 cm^{-1} correlated to the CH_2 wagging. Signal at 1162 cm^{-1} correspond to C-O-C asymmetric stretching of cellulose while the duplet at 1057 and 1034 cm^{-1} is associated to the C-O stretching vibration. The single peak at 900 cm^{-1} can be ascribed to the glucose ring stretching of cellulose.(180, 187, 188) These signals are also visible in the spectra of coated fibers, even if the presence of coating yield new peaks and modifies the relative intensities of the cellulose original signals. Indeed, halloysite nanotube's most visible signal, Si-O anti-symmetric stretching vibration signal at 1035 cm^{-1}, overlap to cellulose C-O stretching vibration, causing an intensity increase of the signal.(182) Moreover the peak at 900 cm^{-1} associated to the glucose ring stretching of cellulose is shifted at 912 cm^{-1} due to an overlapping with the peak of the bending vibration of inner surface hydroxyls of halloysite nanotubes.(182) In **Figure 19** are represented the IR spectra of neat and CH/Hal-APP coated fibers at increasing number of BLs.

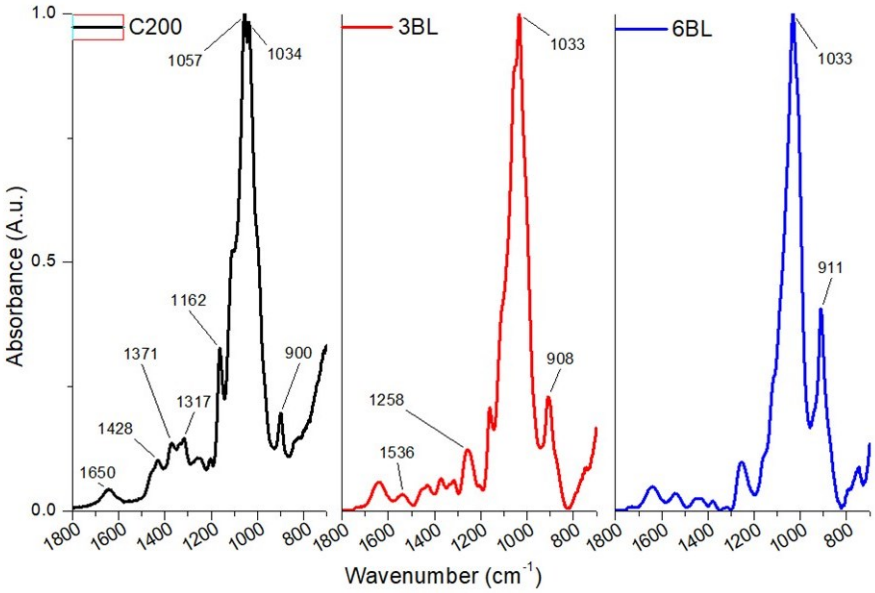


Figure 19: IR spectra of APP – CH/Hal coated fibers (magnified)

IR of CH/Hal-APP system have similar characteristic respect at spectra of CH/Hal-Phy. The main exception is the formation of a visible band at 1258 cm^{-1} associated to the P=O deformation of APP.(189) Fibers morphology was investigated through SEM, visible in **Figure 20**. Neat cellulose presents the typical structure of cellulose, with a corrugated and well visible surface texture.(190-192) LbL coating is visible on the surface for all sample analyzed. More specifically, for Phy system it can be observed the formation of hills-like structures on the surface, which can be attributed to the self-assembled coating which comprise agglomerates of complexes. Indeed, the shape and dimensions of these structures increase with the number of BLs, becoming more evident at 9BL. APP system covers completely the fiber's surface, but leaves small aggregates which seems to increase with the number of BLs forming a coating not completely homogeneous, which can influence its behavior in the final composite. These small aggregates can be attributed to APP crystals that deposit on the surface and act as a sort of nucleating agent for the deposition of further coating on them, resulting in bigger aggregates at higher numbers of BLs.

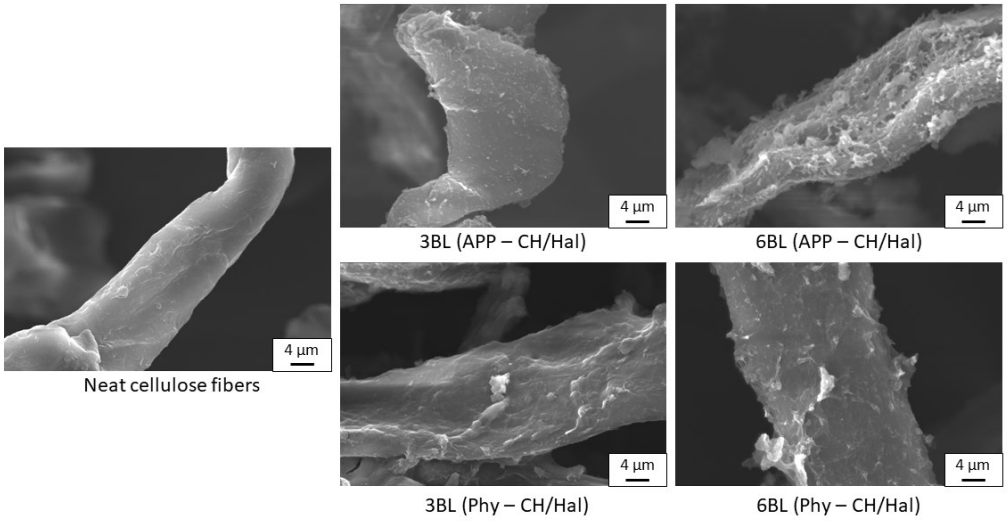


Figure 20: SEM images of treated fibers

2.2.2 Thermal stability

Thermal behavior of Phy-CH/Hal and APP-CH/Hal coated fibers was studied to investigate the influence of coating in thermal stability of coated cellulose fibers. Results from TGA analysis are visible in Figure 21.

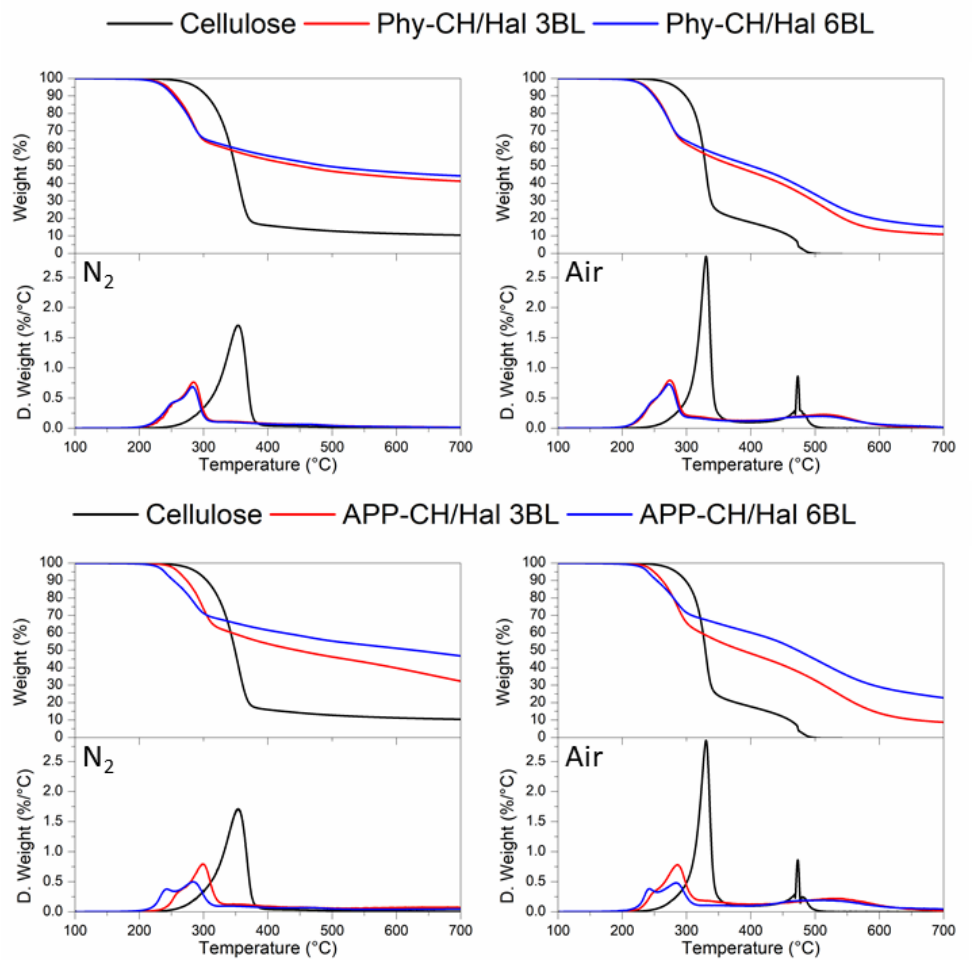


Figure 21: TGA thermograms of treated fibers in nitrogen on the left and in air on the right

Cellulose thermal and thermo-oxidative decomposition path is well known in literature. At temperature lower than 300°C, in inert atmosphere, the depolymerization of the glycosyl units to volatile gases is in competition with their dehydration. After 300°C there's enough energy available to have a rapid cleavage of the glycosidic bond, as visible in **Figure 21** where a rapid weight loss is visible after 300°C.(193) The result of this decomposition step is the formation of a thermally stable char accounting of 10% of initial mass.(48, 49) In an oxidative environment, such as in air, the thermo-oxidative decomposition path is characterized by a two-step process. The step between 250 and 350°C is the result of the production of both volatiles and aliphatic char. The char formed is then further oxidized during the second step, between 350 and 480°C, with the production of CO and CO_2 leaving negligible residue. LbL coating influence the thermal decomposition path by anticipating the T_{on}, as generally reported for phosphate containing system, favoring thus the cellulose decomposition towards char formation which lead to a lower amount of volatile combustible products released.(144, 194) This effect is enhanced by the presence of halloysite, which form an inorganic layer that act as a barrier towards heat and mass transfer, increasing the thermal stability and resulting in a higher final residue,(195, 196) which increase up to 47% of initial mass for the 6BL APP-CH/Hal coated fibers, respect to the 10% residue of neat cellulose. Similar effect is visible also in oxidative atmosphere, with the LbL coating that produces an anticipation of the first decomposition step, but associated to a great increase in char production, with a residue at 400°C that is 2/3 times respect to neat cellulose. As far as the final residue is concerned it should be noted that, being an inorganic component, Hal nanotubes decomposition is mainly due to water release and therefore contribute with nearly their original mass to the final value measured at 700°C.(197, 198) **Table 2** reports TGA values for both systems, as well as neat cellulose ones.

Table 2: TGA values for pure cellulose and lbl coated fibers and

		$T_{on,\,5\%}$ (°C)	Residue at 500°C (%)	Residue at 700°C (%)
N_2	**Cellulose**	289	13	10
	Phy-CH/Hal 3BL	245	47	41
	Phy-CH/Hal 6BL	243	50	44
	APP-CH/Hal 3BL	252	46	33
	APP-CH/Hal 6BL	240	55	47
Air	**Cellulose**	284	0	0
	Phy-CH/Hal 3BL	234	30	11
	Phy-CH/Hal 6BL	233	34	15
	APP-CH/Hal 3BL	249	33	9
	APP-CH/Hal 6BL	240	45	23

This improved char persists along the decomposition, leading to a residue that accounts for 10% and 15% of starting 3 and 6 BL coated fibers, respectively. It has to be noticed that a major increase in residue occur after 3BL, while the difference between 3 and 6BL, in term of residue, are low. This may indicate an already optimal presence of phosphorus at 3BL. It's interesting to nice the residue at 500°C in air. Indeed, untreated cellulose leave little to none residue at that temperature, while all coated fibers present a high residue, accounting to 30-34% of the initial weight for fibers coated with Phy-CH/Hal and reaching 45% for 6Bl of APP-CH/Hal. This observation can be related to the formation of a char residue, more stable than the one naturally formed on cellulose, which can slow down the thermal decomposition path, protecting the inner core of cellulose fibers.

2.2.3 PBS morphology and mechanical properties

Cellulose fibers were melt-blended with PBS in order to produce composites at 15 and 30% wt. of fibers. Their mechanical, thermal and flammability properties were evaluated. SEM images of neat PBS and with untreated cellulose are shown in **Figure 22.**

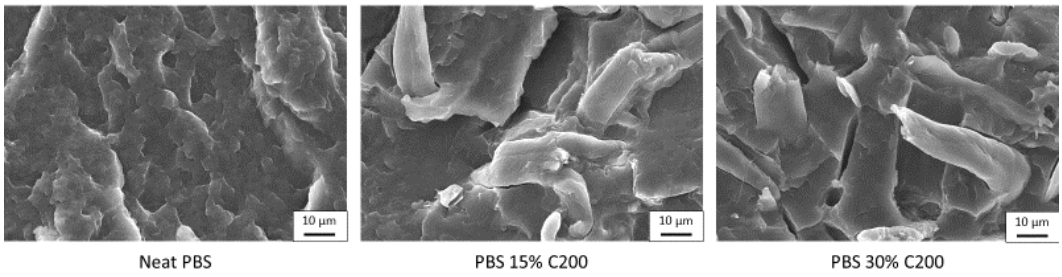


Figure 22: SEM images of PBS composites after brittle fracture

SEM micrographs show good dispersion of fibers in both 15% and 30% of loading. However, it is possible to notice small gaps in the fiber-matrix interface as results of a limited compatibility between natural fibers and PBS.(54, 62, 199) **Figure 23** and **Figure 24** show SEM micrographs of phy-CH/Hal and APP-CH/Hal treated cellulose composites, respectively, after brittle fracture. 3BL samples show an improvement respect to untreated cellulose, even though few vacancies and gaps are still visible for both compounds at 15 and 30%. The beneficial effect of the coating became more visible at higher BLs numbers, with the 6BL samples showing visible reduced gap between fibers and PBS, with a big portion of fibers being completely adhered to the matrix. The presence of phytic acid and chitosan in the coating assert a joint effect with the mechanical gripping given by halloysite nanotubes with PBS (200), with phytic acid and chitosan -OH groups forming weak bonds with the matrix.(201) This effect is helped by the nanotexture imparted by the LbL assembly to the coated fibers, which increase the surface area exposed to the polymer.(202)

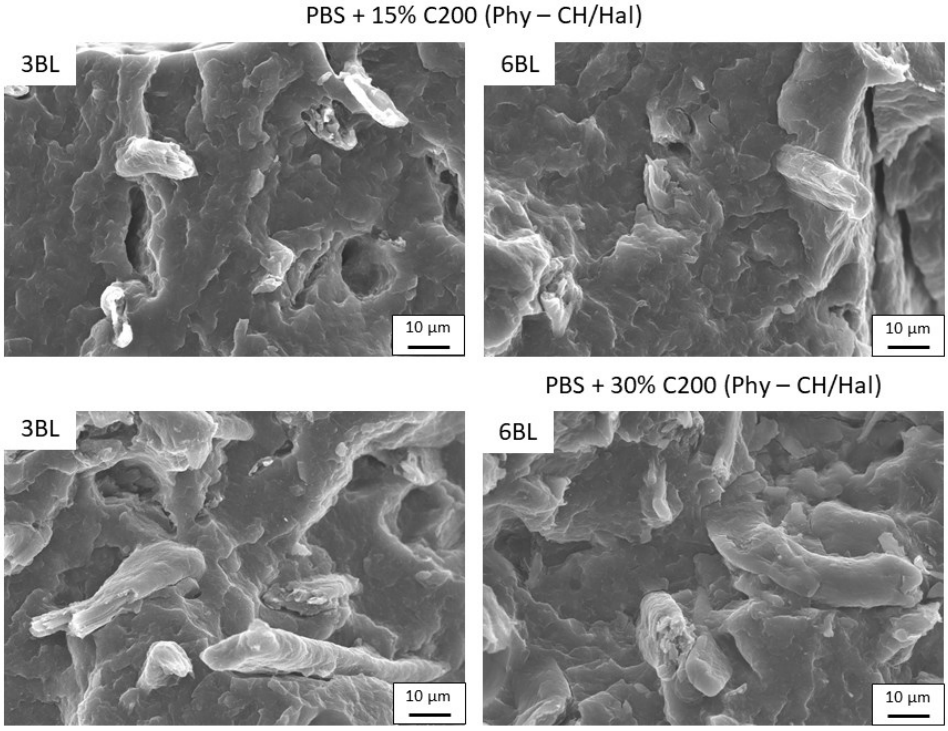


Figure 23: SEM micrographs of PBS composites with Phy-CH/Hal coated fibers after brittle fracture

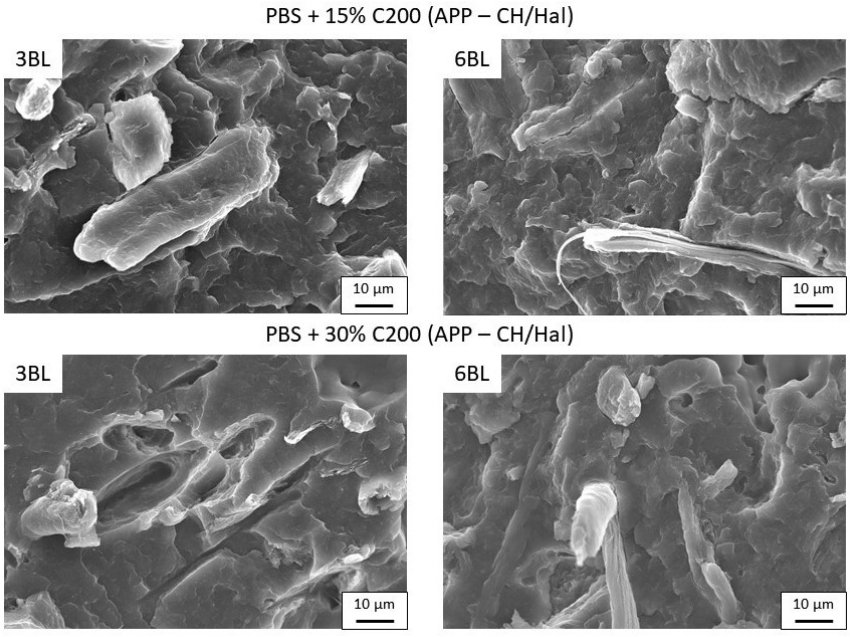


Figure 24: SEM micrographs of PBS composites with APP-CH/Hal coated fibers after brittle fracture

Similar effect is visible also in composites with APP-CH/Hal treated fibers, even though the interphase appears to be slightly worse than the previous system due to the presence of an increased number of gaps between matrix and fibers Indeed, by substituting phytic acid with APP the LbL coating change both in morphology and chemistry, as visible in **Figure 24**, resulting in a more heterogenous fiber dispersion, with fibers completely adhered and other fibers which presents gaps

with the matrix. The mechanical properties of the prepared composites have been tested by tensile test, **Figure 25***: SEM micrographs of PBS composites with APP-CH/Hal coated fibers after brittle fracture*

Table 3 collects the obtained data, while most representing curves of each sample are represented in **Figure 25.**

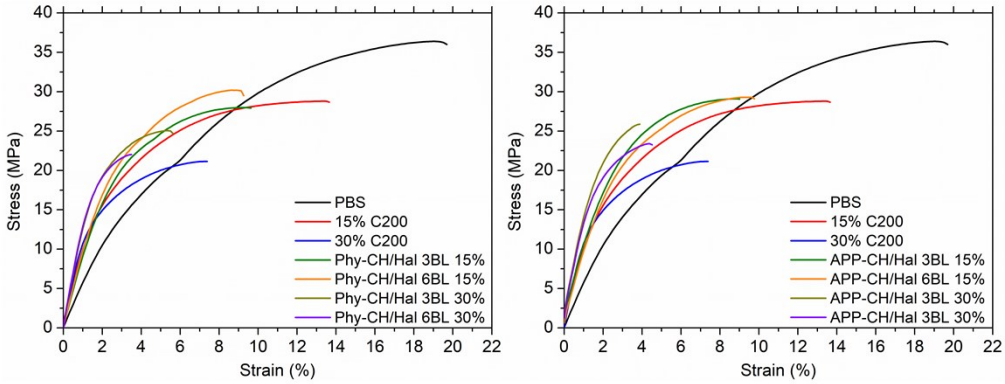


Figure 25: SEM micrographs of PBS composites with APP-CH/Hal coated fibers after brittle fracture

Table 3: Mechanical properties of PBS composites

Sample	Modulus (MPa)	Tensile strength (MPa)	Deformation at break (%)
PBS	608 ± 7	36.8 ± 0.4	20.7 ± 1.7
15% C200	1070 ± 37	27.3 ± 1.4	10.4 ± 3.6
Phy – CH/Hal 3BL 15%	932 ± 115	27.1 ± 1.1	7.8 ± 1.6
Phy – CH/Hal 6Bl 15%	1069 ± 40	29.7 ± 0.6	8.7 ± 1.0
APP – CH/Hal 3BL 15%	985 ± 38	27.9 ± 1.7	7.0 ± 1.8
APP – CH/Hal 6BL 15%	1081 ± 122	29.8 ± 1.4	9.2 ± 2.0
30% C200	1332 ± 165	22 ± 1.7	7.6 ± 0.9
Phy – CH/Hal 3BL 30%	1483 ± 45	24.1 ± 1.1	4.6 ± 0.6
Phy – CH/Hal 6Bl 30%	1449 ± 49	21.2 ± 1.5	4.0 ± 0.6
APP – CH/Hal 3BL 30%	1764 ± 389	24.8 ± 2.1	3.5 ± 0.8
APP – CH/Hal 6BL 30%	1495 ± 403	22.8 ± 0.9	4.3 ± 1.0

The addition of cellulose fibers to PBS increase the modulus and decrease the tensile strength, producing a 75% and 110% increase of modulus for PBS containing 15% and 30%, respectively. However, even though an improvement in adhesion is visible from the morphology study, this effect is not completely reflected in an increase of mechanical properties. Indeed, composites with 15% of coated cellulose fibers do not show relevant improvements in modulus or tensile

strength, on the contrary in certain cases they are lower than untreated fibers. This may be due to the presence of fibers with a different degree of adhesion within the same composite, as visible in **Figure 23** and **Figure 24**. This effect also gives a high standard deviation, reflecting a lack of homogeneity in the samples. This effect is less visible for samples at 30% of coated fibers, in particular for Phy – CH/Hal system. Indeed, sample with neat fibers give a high standard deviation, mainly due the poor interfacial properties between fiber and matrix as well as the formation of aggregates, which leads to non-homogeneous specimens. However, the use of LbL coated fibers lead to more homogeneous samples and an increase in tensile modulus. **Figure 26** collects SEM micrographs of fracture surface after tensile testing.

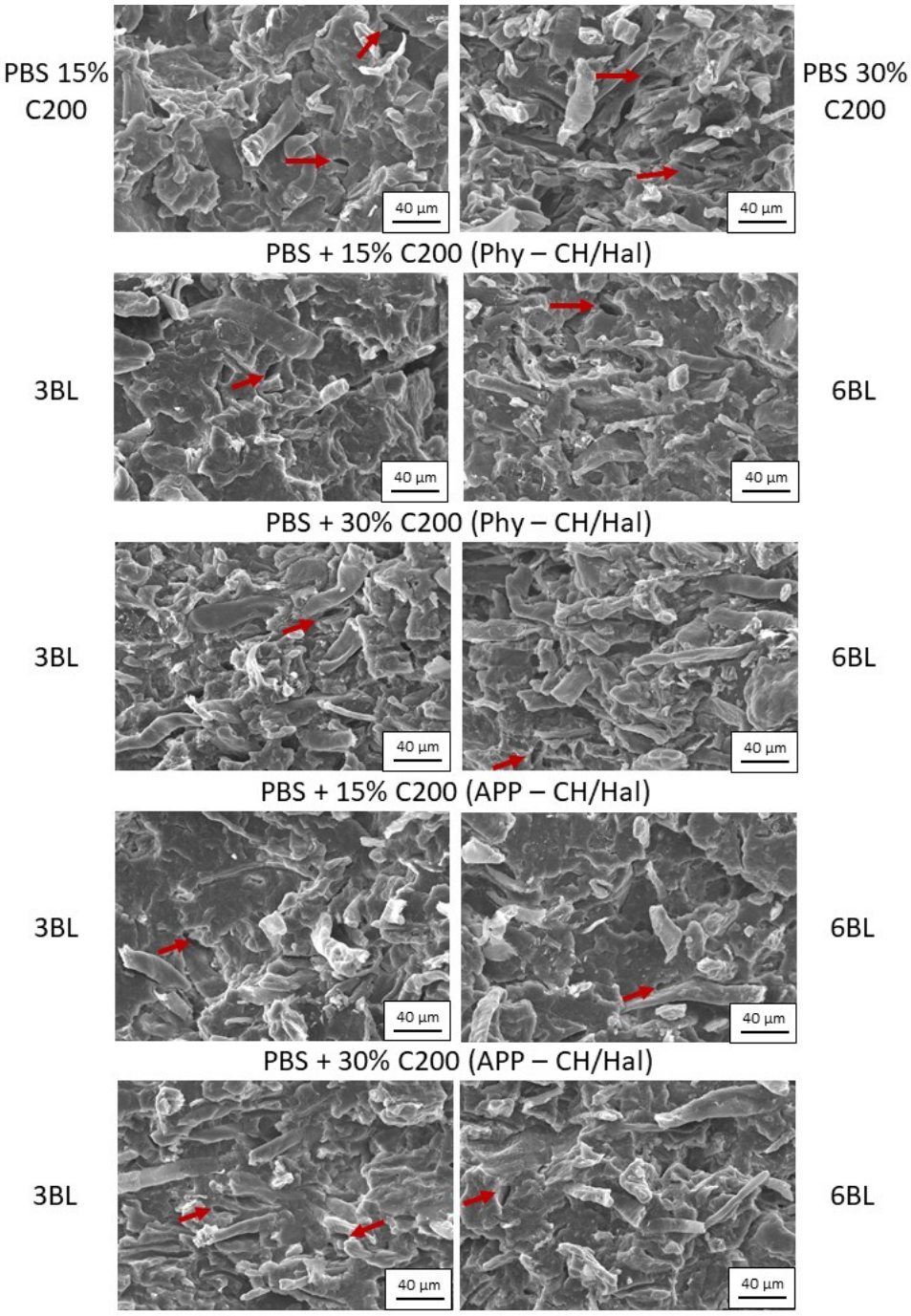


Figure 26: SEM micrographs of tensile-fractured surface

As visible in **Figure 26**, in composites with untreated cellulose, fibers are pulled-out when fracture occurred, resulting in vacancies and holes. This effect is less visible in samples with coated fibers, in which, even though still present, is in competition with fiber fracture as result of a better adhesion with the matrix.

2.2.4 Flame-retardant properties

Fire retardant properties of composites were investigated by flammability tests and cone calorimetry. This set of characterizations provides fundamental information on the simulated behavior of a sample during a fire. Indeed, flammability tests asses

the propensity of the material to start a fire, by evaluating the reaction of the sample to the exposure to a direct flame.(203) Conversely, forced combustion tests are used to evaluate the fire spreading potential of the material, by exposing the sample to a heat flux typically found in developing fire, while also allowing for a preliminary evaluation of the amount of smoke produced during combustion.(204) **Figure 27** shows snapshot at different times of samples during flammability test.

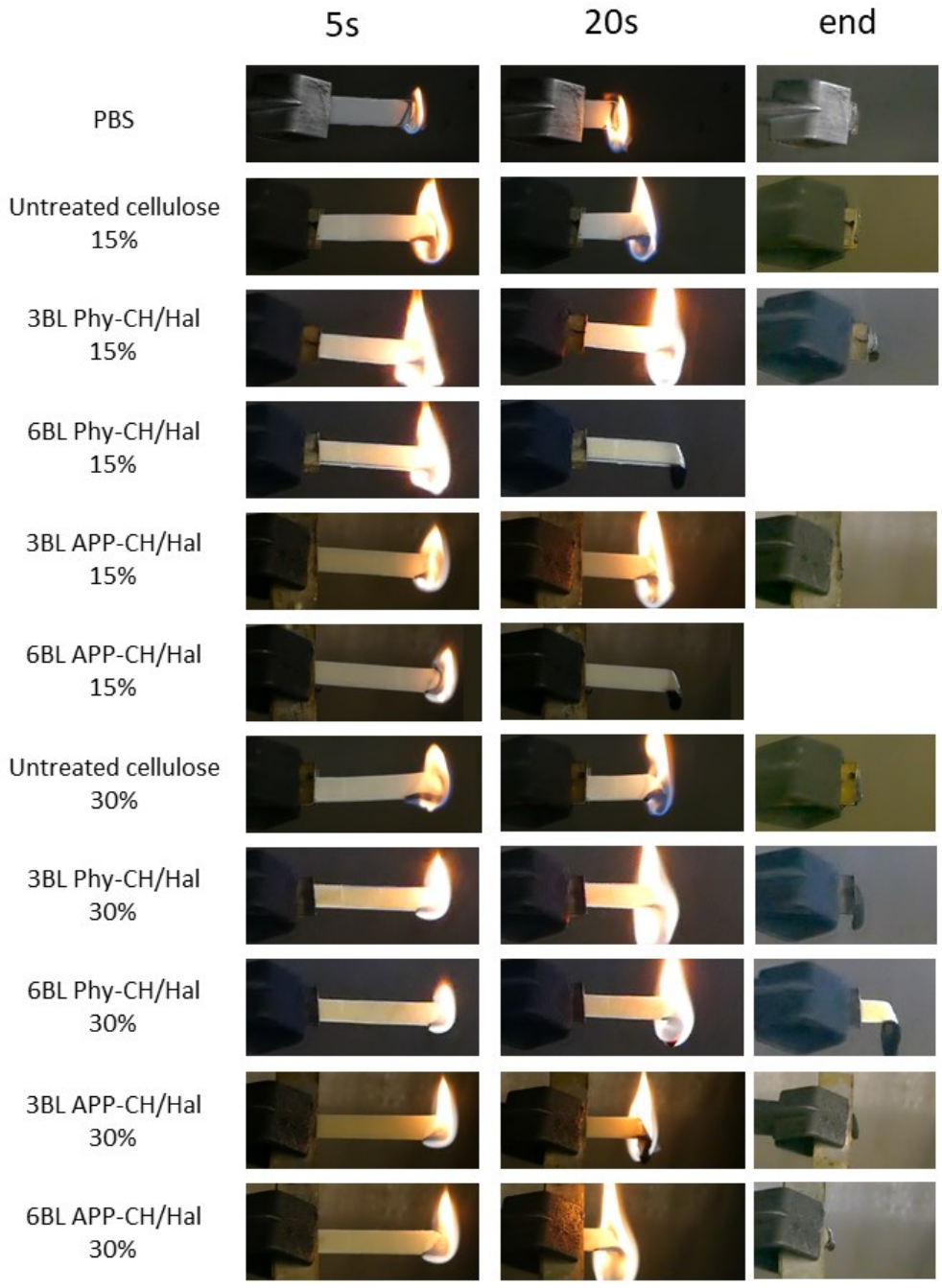


Figure 27: snapshot at various time of flammability test

Polybutylene succinate ignite immediately after flame exposure giving a self-sustaining fire and frequent melt-dripping that lead to the complete consumption of the sample. The addition of cellulose fibers alters little to none this behavior with

samples prone to ignite at flame exposure and giving melt dripping. 3BL coated fibers do not assert a visible effect onto the flammability of composites. However, samples with 6BLs coated cellulose were able to extinguish the flame after 20s, leaving portion of the specimen intact. It has to be noticed that this effect was visible majorly for composites with 15% of cellulose loading and could mainly be attributed to an extinguishing by melt-dripping. Char produced by this mechanism assert a joined barrier effect with halloysite nanotubes, which form a partial barrier on cellulose fibers which form a carbonized network that can partially slow down heat and volatiles transfer, reducing the amount of volatiles released .(195, 205) The char formed by these joined effects is able to slow down the combustion of the sample, which eventually extinguish the flame in samples at 15% of 6BL treated cellulose content, while samples with 30% of cellulose tend to burn almost completely probably due to the presence of more combustible due the higher loading of cellulose. To better explore the effect of coated fibers on final composites, cone calorimetry was used to simulate an evolving fire scenario. Commonly, upon exposure to the heat flux the sample starts decomposing and releases flammable volatiles that ignite when the proper concentration is reached and lead to flaming combustion of the sample. **Figure 28** collects cone calorimetry plots associated to heat release rate (HRR) and total heat released (THR), while numeric data comprising HRR, THR and total smoke released (TSR) are collected in **Table 4**.

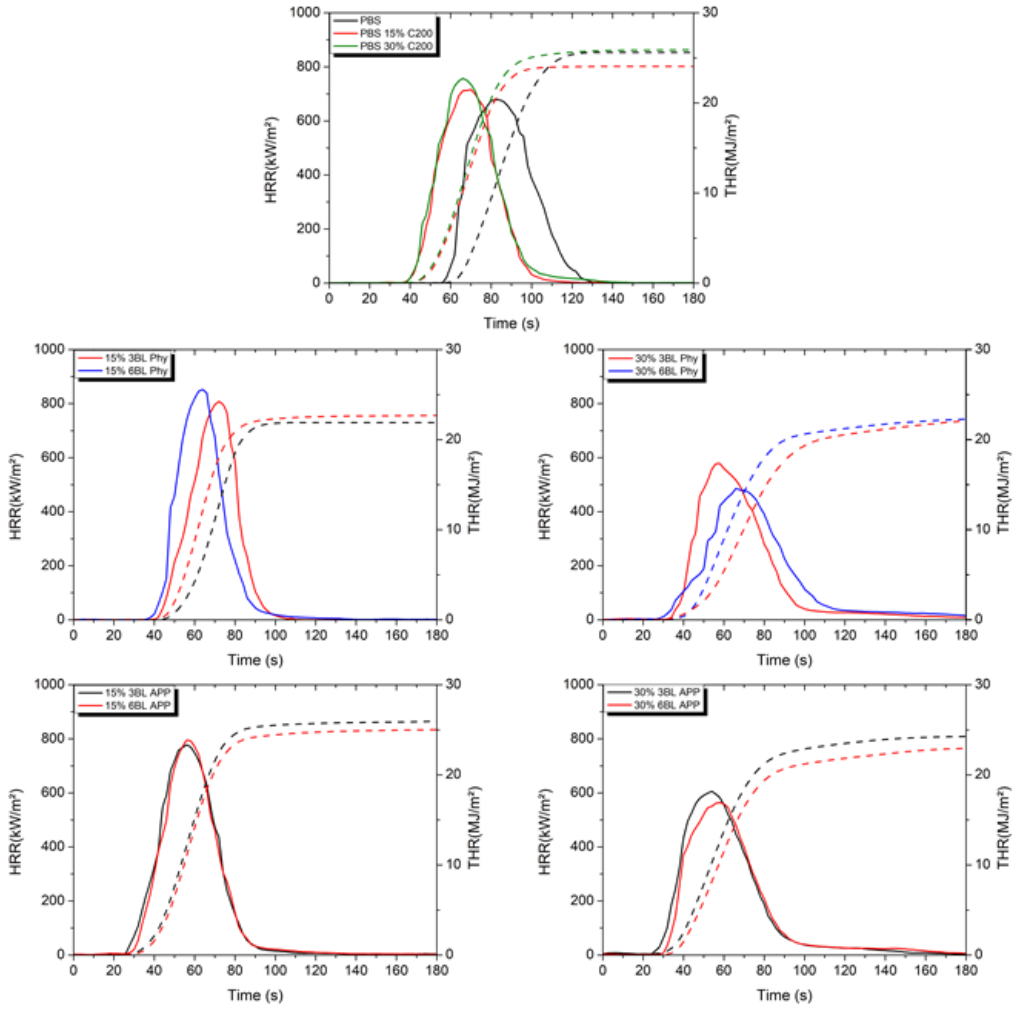


Figure 28: Cone calorimetry results of PBS composites with heat release rate (HRR)and total heat release rate (THR)

Table 4: HRR, THR and TSR of PBS composites

Sample	TTI (s)	HRR_{peak} (KW/m^2)	T. Peak (s)	THR (MJ/m^2)	EHC (MJ/Kg)	TSR (m^2/m^2)
PBS	57 ± 2	679 ± 51	83 ± 1	25.6 ± 0.3	17.3 ± 1.5	133 ± 23
15% C200	39 ± 3	727 ± 26	68 ± 2	24.0 ± 0.4	18.9 ± 0.4	119 ± 19
30% C200	38 ± 2	789 ± 42	66 ± 2	25.9 ± 0.5	19.4 ± 0.2	104 ± 14
Phy – CH/Hal 3BL 15%	39 ± 2	815 ± 15	85 ± 3	21.9 ± 0.7	16.0 ± 0.5	247 ± 33
Phy – CH/Hal 6Bl 15%	40 ± 2	854 ± 32	63 ± 1	22.7 ± 1.4	18.2 ± 0.8	205 ± 43
Phy – CH/Hal 3BL 30%	36 ± 4	595 ± 20	57 ± 4	22.3 ± 0.8	18.8 ± 0.1	241 ± 28
Phy – CH/Hal 6Bl 30%	41 ± 10	551 ± 39	64 ± 8	22.3 ± 0.6	17.9 ± 1.0	251 ± 20
APP – CH/Hal 3BL 15%	24 ± 2	778 ± 40	57 ± 1	25.9 ± 0.7	19.1 ± 1.6	245 ± 18
APP – CH/Hal 6BL 15%	27 ± 2	799 ± 43	57 ± 1	24.9 ± 1.4	20.2 ± 0.2	284 ± 30
APP – CH/Hal 3BL 30%	25 ± 2	606 ± 14	54 ± 1	24.2 ± 0.3	19.6 ± 0.4	265 ± 12
APP – CH/Hal 6BL 30%	29 ± 2	566 ± 7	57 ± 3	22.9 ± 1.2	18.7 ± 0.6	309 ± 3

From cone calorimetry it's apparent that the cellulose addition to PBS asserts a detrimental effect for what regard flammability and fire related properties. Indeed, pkHRR increase by 7 and 16%, for 15%C200 and 30%C200 respectively, respect to neat PBS as the results of adding a highly flammable material in the composite. Moreover, the time to ignition (TTI) visibly decrease as result of the presence of cellulose, which is known to start to decompose earlier than PBS. LbL coated fibers are not able to completely transfer their flame-retardant effect to the material when used in low quantity, such as 15%. This effect is in contradiction with flammability tests, where samples with 15% of cellulose performed better than ones with 30%. A possible explanation is that during combustion the first phenomena that PBS undergo is melting and having molten PBS a low viscosity tends to drip easily. 15% of coated fibers are enough to slow down the burning of the specimen and extinguish the flame by melt dripping. However, when samples are confined in a space, like happens in a fire scenario and simulated by cone calorimetry, PBS can't extinguish by melt dripping, which means that the burning is sustained by the molten PBS composites. Due to the fact that the active components of the system are in the coating, having a low amount of fibers inside the composites means also have an overall low amount of active component. The outcome is that pkHRR increase for all samples, meaning that even if the coating can form a protective layer on cellulose, it is not enough to slow down the combustion of the composite. However, a little protective effect can be observed if THR is considered. On the contrary, high amount of treated cellulose do result in a lower pkHRR and THR, with values for Phy-CH/Hal 6BL of 19% and 30% lower than neat PBS and 30%C200 samples, respectively. The coating on fibers comprise phosphorous

based flame-retardant agent, like phytic acid and APP, halloysite nanotubes as fire barrier agent and chitosan as charring agent. during combustion, APP decomposes releasing ammonia and polyphosphoric acid, while Phy limits its action to release of polyphosphoric acid, which promotes the decomposition of chitosan and cellulose towards a thermally stable char.(206, 207) Char produced by this mechanism assert a joined barrier effect with halloysite nanotubes, which act as a barrier, even if not completely continuous, that concenter flammable gas, which results in the slow down heat and volatiles transfer, improving the thermal stability during combustion.(195, 205) Comparing the two systems under study, system comprising Phy-CH/Hal perform slightly better than APP-CH/Hal, as result of a more homogenous coating on fibers, as seen in previous chapter. Together with the heat released during combustion, smoke production is a fundamental parameter that has to be assessed for evaluate the safety of a material. PBS alone present naturally a lower smoke production respect to other common polymers, such as polyethylene and polyurethane, but still dangerous.(208) Adding cellulose to a polymeric matrix means the partial substitution of a bad burning material with a component which burns efficiently, resulting in a lower smoke production. Indeed, TSR decrease from 133 m^2/m^2 of PBS to 119 and 104 m^2/m^2 when 15 and 30% of cellulose is added, respectively. However, LbL coated fibers are coated with phosphorous based compounds aiming at improved char formation. This produces an inefficient combustion that subsequently leads to a higher smoke production, as visible in **Table 4**, with values that are almost three times the starting one. (209) From the smoke release point of view, phytic acid seems to be more efficient in limiting the smoke production when compared to APP. Putting all this information together, Phy – CH/Hal 6Bl 30% appears to be the most promising material, with 19% and 30% pkHRR reduction respect of neat PBS and 30% C200, respectively, associated to a limited increase in smoke production.

2.3 Conclusion

Short cellulose fibers were successfully coated exploiting LbL approach with flame retardant coatings aiming at improving their FR behavior when employed as natural filler for PBS composites. Halloysite nanotubes were suspended in chitosan and used as positive layer, while APP or phytic acid were used as flame-retardant, negative layer. The flame retardants fibers were then melt-blended with PBS in order to obtain composites with better mechanical properties and flame-retardant properties, aiming to the transfer of coating effect on fibers to the final material. A 75% and 110% modulus increase were visible for composites with 15% and 30% of cellulose, respectively. However, no particular differences are visible between the use of untreated and treated cellulose fibers, with values that remains in a 5% difference range, meaning that coating does not compromise the final mechanical properties. It was observed that composites obtained with APP-CH/Hal assembly present a higher error associated to mechanical testing, in addition to visible irregularities in the composite, indicating the formation of aggregates and poorer dispersion respect to Phy-CH/Hal ones. Flame-retardant properties were assessed

via flammability test and cone calorimetry. Composites containing 15% of 6BL coated fiber of both systems extinguish the flame by melt dripping, while a similar effect was visible only for the Phy-CH/Hal system. Composites behavior in a developing fire scenario was evaluated with cone calorimetry. Phy-CH/Hal was found to be the better performing assembly, with a 19% and 30% pkHRR reduction respect of neat PBS and 30% C200, respectively. these results demonstrate the possibility to use LbL to obtain fibers with better properties that can be transferred to the final composites.

3. Rigid polyurethane foam composites

Thanks to their low thermal conductivity, lightness and ease of processability, PUF are one of the most important insulating material used nowadays.(64) Being so widespread, environmental concern rises from their production and disposal, which can become a problem in the near future. Indeed, often polyurethane use petroleum-based polyols as monomers, as long as isocyanates, which can increase the final environmental impact.(71) A possible way to reduce the impact of the final foam is the substitution of a portion of polyols with natural fiber, in order to provide a more sustainable source of components and give strength to the final foam. Indeed, lignocellulosic fibers can take part to PU reactions thanks to the many hydroxyl groups present on the chains, resulting in the incorporation of fibers into the final polymers.(78, 79) However, if this approach substitute part of the common polyols with natural fibers, at the same time add a highly flammable component to the already flammable foam. Being fire retardancy a prerequisite for many applications, it's therefore necessary to reduce the risk associated to fire implementing flame-retardants in the PUF formulation. In this chapter, the preparation of PUF containing flame-retardant cellulose fibers is discussed. Cellulose fibers were coated, exploiting the Layer-by-Layer technique, with chitosan and sodium hexametaphosphate or chitosan and ammonium polyphosphate, as shown in **Figure 29**

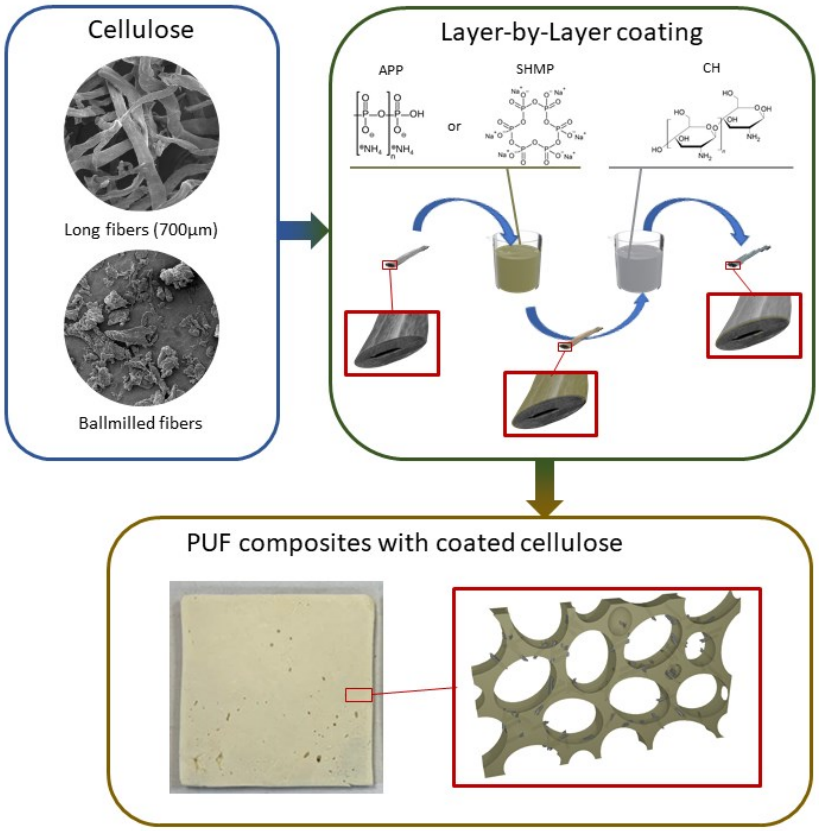


Figure 29: PUF from lbl coated cellulose

Sodium hexametaphosphate and ammonium polyphosphate have proven to be effective flame-retardant agents, in particular when coupled with a charring agent such as chitosan and the cellulose fiber itself. In addition, the former chitosan can improve the adhesion between fibers and polymeric matrix.(126, 210) For this study two types of cellulose fibers were chosen, a long fiber (700µm) and ballmilled fibers, prepared following a previously reported procedure. Ballmilled cellulose were necessary to obtain a higher loading in PUF thanks to their small dimensions, compared to long fiber cellulose.(78) This project has been carried out in collaboration with the Institute for Polymers, Composites and Biomaterials (IPCB - CNR) of Pozzuoli.

3.1 Material and methods

3.1.1 Materials

Commercial bicomponent polyurethane for foaming application, based on methylene diphenyl diisocyanate (MDI, component A) and a mixture of polyols and additives (catalysts, stabilizers and expanding agents), (component B), cream time at 20 ºC 34 s, was purchased by Castro Composites (Pontevedra, Spain). Commercial cellulose fibers (ARBOCEL BC1000 and BWW40) with an average length of 700 and 200 µm, respectively, were kindly provided by J. Rettenmaier & Sohne GmbH (Rosenberg, Germany). Ball-milled cellulose was provided by IPCB-CNR of Naples. Briefly, cellulose fibers Arbocel BWW40 were dried at 90 ◦C under

vacuum for 24 h. Therefore, cellulose samples of (batches of 10.0 ± 0.1 g) were ballmilled in a Retsch PM100 planetary ball milling system (Haan, Germany), using a 125 mL steel milling cup and 25 spheres, 10 mm diameter. The weight ratio spheres/cellulose was 10:1. The ball milling process was carried out for 60 min. The obtained cellulose was characterized by a crystallinity index of 0.15, an aspect ratio (L/D) of 1.5, a circularity of 0.75. Their average lateral size was 12 ±8 µm (major axis) and 7.8 ±4.7 µm (minor axis).(211) Branched poly (ethylene imine) (BPEI, Mw ~25000 Da by light scattering, Mn ~10000 by gel permeation chromatography, according to the material datasheet), chitosan (low molecular weight, < 20000 Da and 75-85% deacetylated chitin, according to the material datasheet), acetic acid and sodium hexametaphosphate (crystalline, +200 mesh, 96%) were purchased from Sigma Aldrich (St- Louis, USA). Suspensions and solutions were prepared using ultrapure water (18.2 MΩ deionized water supplied by a Q20 Millipore system, Italy). Chitosan was solubilized in a 0.5%wt acetic acid aqueous solution to a concentration of 0.5%wt and kept under magnetic stirring overnight. BPEI and SHMP were dissolved in water to 0.1%wt and 1%wt concentration, respectively.

3.1.2 Layer-by-layer assembly

A layer by layer assembly comprising branched poly(ethylenimine), sodium hexametaphosphate and chitosan was studied. Chitosan served as positive layer, while sodium hexametaphosphate was used as negative layer. Branched poly(ethylenimine) was used as anchoring layer. The assembly of 10BL was first studied on a model surface made by a silicon wafer. Briefly, the substrate was immersed in BPEI solution for 10min, washed by static dipping in water and dried by compressed air. IR spectrum was recorded after that. The same procedure was applied for sodium hexametaphosphate, with exception of dipping time that was set to 5min, and spectra were recorded after each layer until 5BL were reached, after that spectra were recorded after each bi-layer until 10BL were obtained. Washing steps were done using water for sodium hexametaphosphate and diluted acetic acid for chitosan. Cellulose fibers were coated following a similar procedure. Briefly, cellulose fibers were rehydrated and the excess of water was discarded by centrifugation (Eppendorf centrifuge 5702). Then, fibers were dispersed in BPEI and sonicated for 10 minutes in order to deposit the anchoring layer and the excess of solution was removed by centrifugation (4400 rpm, 2 min). Fibers were washed with water following the same procedure. The SHMP/CH coating was achieved by alternatively dispersing and sonicating the fibers in the negatively (SHMP) and the positively (CH) charged solutions (5 min each). Each deposition step was followed by excess solution removal by centrifuge and a washing step using water (for BPEI and SHMP) or acetic acid 1% wt. (for CH). Up to 5BL were deposited with this procedure for both 700µm fibers and ball-milled fibers. A scheme of steps followed is visible in **Figure 30.** At the end of the LbL assembly, fibers were washed with water to remove the excess of acetic acid and dried by freeze-drying for 48h.

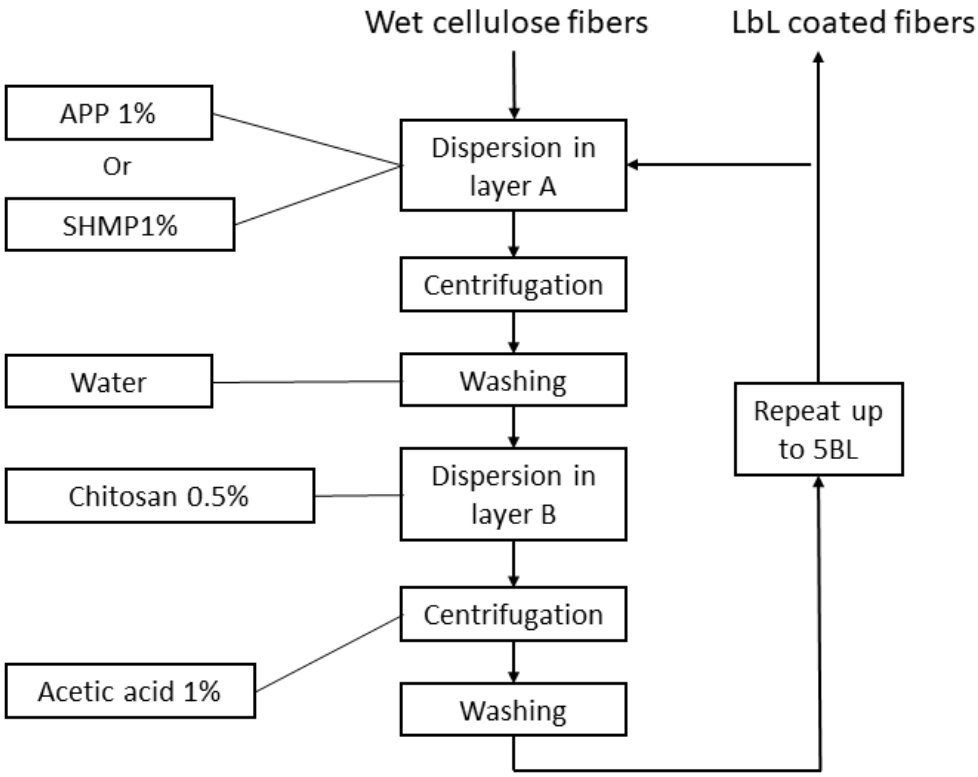


Figure 30: deposition scheme for coated cellulose

3.1.3 Polyurethane foam forming

PUF samples were prepared as follows. The isocyanate component (component A) and the polyol component (component B) were mixed in a 110:100 weight ratio. Then the mixture was immediately poured in an open mold (40 x 40 x 23 cm3) pre-heated in oven at 60 °C and let to foam and polymerize at 25 °C and 50% RH. After 1 day, the external parts of the foams were removed with a knife to obtain samples 2 cm thick. For PUF biocomposite samples, the right amount of cellulose, plain or modified by the above detailed LbL approach (dried in oven at 60 °C overnight, 7.5 or 15 phr), was added to the polyol component (component B). Then the right amount of isocyanate component (isocyanate: polyol 110:100 volume weight ratio) was added to the mixture and the foaming process was performed as previously detailed for neat PUF.

3.1.4 Characterization

Growth on model surface (Si wafer, 100, single side polished) was monitored using a FT-IR spectrophotometer (16 scans and 4 cm^{-1} resolution, Frontier, Perkin Elmer) in transmission mode. Attenuated total reflectance (ATR) Fourier Transform infrared spectroscopy spectra for fibers and composites were collected using the same FT-IR spectroscope equipped with a germanium crystal (16 scans, 4 cm^{-1} resolution). ATR spectra were processed by subtracting the baseline and normalizing by the peak at 1040cm^{-1}. Surface morphology of fibers and composites was studied, after gold sputtering, using a LEO-1450VP Scanning Electron Microscope. Thermal stability of fibers was evaluated by TGA (Discovery, TA

Analysis). Briefly, samples (approx. 10 ± 1mg) were placed into alumina pans and subjected to an isothermal treatment for 15 min at 100°C and then heated at 10°C min^{-1} up to 700°C. Samples were tested both in nitrogen and in air. T_{on} (temperature corresponding to 5 % weight loss), T_{max} (temperature at maximum rate of weight loss), and residue (%) were obtained by these measurements. The morphological analysis of foams was performed by scanning electron microscopy using a SEM FEI Quanta 200 FEG (The Netherlands). Small specimens were cut from the middle of the foams. The inner microstructure of the specimens was analyzed on cryogenically fractured surfaces. Before the analysis, specimens were mounted on aluminum stubs by means of carbon adhesive disks and coated with a thin layer (about 10 nm thick) of gold-palladium alloy using the sputter coating system Emitech K575 (Quorum Technologies LTD, UK).

The sample density was calculated as the ratio between the weight and volume of cubic specimens of about 20 x 20 x 20 mm^3. The weight was measured using an analytical balance (Mettler Toledo L.L.C., USA), and sample dimensions were evaluated using a high-resolution caliper. Before weight measurements, the samples were dried overnight in an oven at 50 °C under vacuum. The calculated density values were averaged among four samples.

The compression behavior of foams was measured in the direction parallel to the foam rise by means of a universal testing machine (Instron model 4505, Norwood, MA, USA) with a calibrated 1 kN load cell. Parallelepiped samples were cut from foamed slabs 20 x 20 x 20 mm3 in size. Compression tests were carried out at 25 °C and 50 % RH and by using a cross-head speed of 3.5 mm/min, according to ASTM D1621. Averaged values of the Young's modulus and stress at yield were obtained by testing five specimens for each sample.

Thermal conductivity (λ) of the foams were measured at 25 °C and 50 % RH by using the multipurpose apparatus (ISOMET, Applied Precision, Bratislava, Slovakia). The measurements were performed on samples pre-conditioned at 50 % RH for 24 h. For each sample, λ values were measured in triplicate on both sides of each panel and the averaged values were calculated.

Cellulose fibers flammability was assessed in horizontal configuration. Briefly, specimens were prepared by drying wet fibers in a mold at 60°C overnight and exposed to a 20mm methane flame (2x3s). Test was repeated 3 times for each formulation and parameters like after-flame time length, char length and final residue were recorded. Cone calorimetry (GA01, ISO 5660, Noselab ats, Italy) was employed to investigate the PU foams combustion behavior of square samples (50x50x15 mm3) under exposure to a heat of 35 kW/m2 in horizontal configuration, following an earlier described procedure. Each sample was confined in an aluminum foil holder.(176) The following parameters were registered: time to ignition (TTI, s), peak of heat release rate (PHRR, kW/m2), time to peak (s), total heat release (THR, MJ/m2), average heat of combustion (EHC, MJ/Kg), smoke production rate (SPR, m2/s), total smoke release (TSR, m2/m2) and final residue

(%). The test was repeated 3 times to ensure reproducibility and the average of triplicate data is reported

3.2 Results and discussion

3.2.1 Layer-by-layer assembly on cellulose fibers

In this work two LbL assemblies were evaluated. Both of them use chitosan as positive polyelectrolyte thanks to its ability to form homogeneous coating on cellulose substrates and its charring properties (212, 213). Sodium hexametaphosphate (SHMP) or ammonium polyphosphate (APP) are selected as negatively charged counterparts. Before coating the fibers, the assembly of the two systems was investigated through deposition on a model silicon wafer surface and monitored using IR spectroscopy.(177) To improve the assembly adhesion, BPEI was used as anchoring layer.(178) IR spectra of pure compounds are analysed in chapter 2.2.1, except SHMP, which is shown in **Figure 31.** SHMP characteristic peaks attributed to phosphate groups can be found in the finger-print region of the spectrum. The peak at 1260 cm-1 is related to the stretching of P=O while at 876 cm-1 it is possible to find the peak related to P-O-P symmetrical stretching.(144, 180)

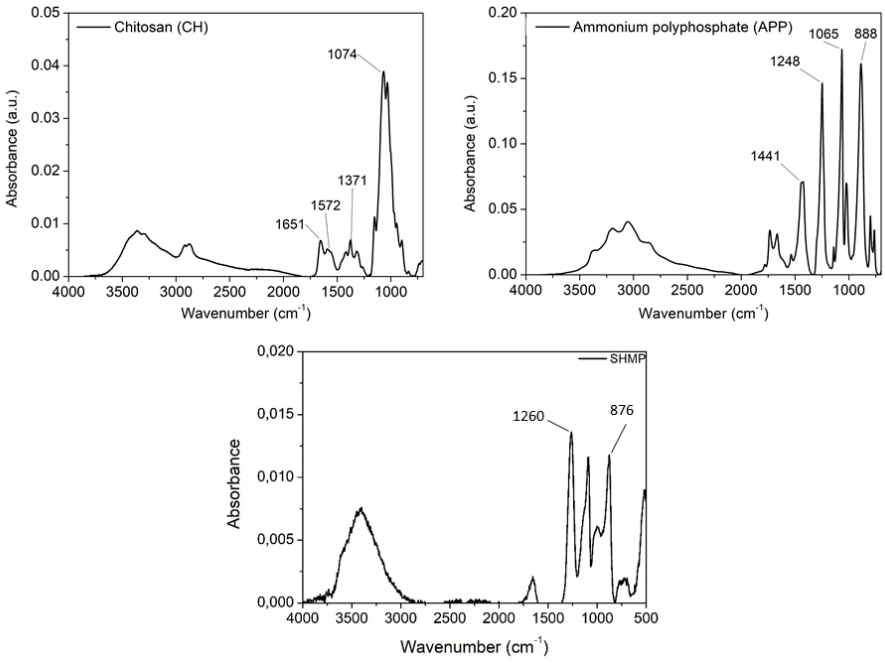


Figure 31: IR spectra of Sodium hexametaphosphate, ammonium phosphate and chitosan

Figure 32 display the spectra collected during the LbL build-up on Si and the BL number vs intensity plots for characteristic peaks of the two components.

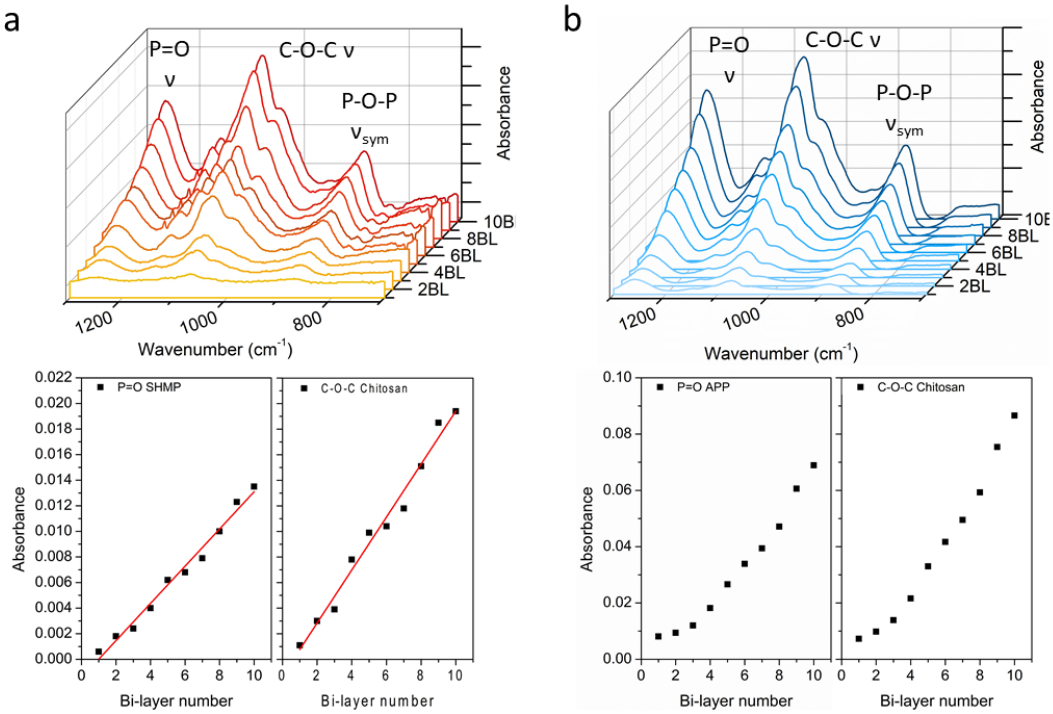


Figure 32: (a) FT-IR spectra plot showing the LbL growth for SHMP-CH on a silicon wafer substrate and the correlated BL number vs intensity, (b) FT-IR spectra plot showing the LbL growth for APP-CH on a silicon wafer substrate and the correlated BL number vs intensity

IR signals for the two systems are similar, especially in the fingerprint region below 1400 cm^{-1}. The typical C-O-C stretching vibration band of CH is well visible for both systems at 1074 cm^{-1} giving the strongest peak in the spectrum.(181) The other two most visible bands in this region of the spectra are the ones correlated to phosphorous compound, more precisely the P=O stretching at 1260 cm^{-1} and the P-O-P symmetrical stretching at 876 cm^{-1}. (144, 180, 214) For each system, the intensity/BL number plot is displayed for both P=O and C-O-C signals. SHMP-CH exhibit a linear growth up to 10BL, while APP-CH show some differences at low BL number. Indeed, the system exhibits two linear regimes. A first initial linear regime up to 3BLs and a second which continue up to 10BLs. This behaviour can commonly occur in layer-by-layer systems and can be ascribed to an uneven coating during the first layers, which eventually reach a complete covering of the substrate after 3 BLs. Indeed, a substantial growth can be seen from 4BLs.(184-186)

3.2.2 Coated fibers characterization

In this work, two kind of cellulose fibers were used, neat cellulose fibers and ballmilled fibers. SEM micrographs of both of them are visible in **Figure 33**. Long cellulose fibers come from a commercial source and were used without any further pre-treatment.

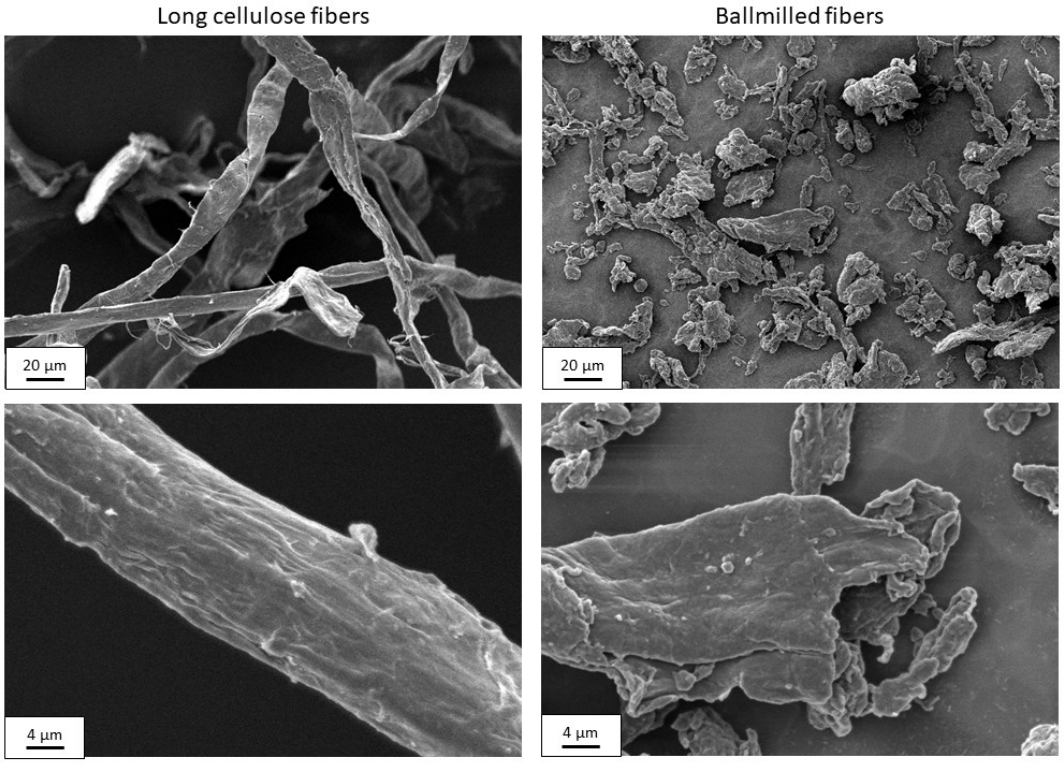


Figure 33: SEM micrographs of long cellulose fibers and ballmilled fibers

As visible from **Figure 33**, shape, dimensions and morphology are different for both fibers. Indeed, long fibers have an average length of 700 µm, a width of 10-20 µm and the typical cellulose corrugated surface.(215) Ballmilled cellulose were obtained by an already studied process in which cellulose fibers are milled in a planetary ball milling system for 60 min. As result of this process, crystalline domains are reduced and fibrous morphology is converted to a quasi-circular shape with dimensions in the order of 10-20 µm.(211)

Both kind of fibers were coated with both LbL systems, resulting in four set of samples. For each of them 1 to 5 BL of coating were deposited. **Figure 34** shows data from ATR-IR spectroscopy of long fiber cellulose (named C700) after coating with both LbL systems.

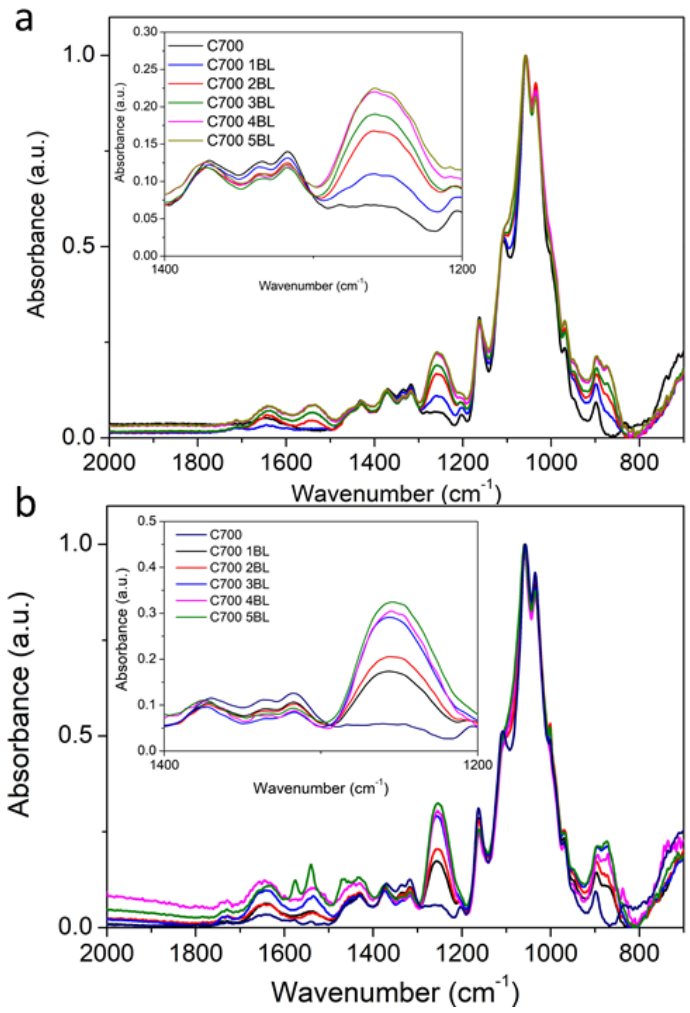


Figure 34: ATR-IR spectra of LbL coating on long cellulose fibers of a) SHMP-CH and b) APP-CH system

Coating presence on fibers surface was investigated through ATR-IR spectroscopy. Unfortunately, one of the strongest peaks in the coating, the C-O-C stretching of chitosan, is not suitable for evaluation due to the overlapping with the strong cellulose signal in the same region. Conversely, phosphorous related signals do not overlap with cellulose fibers signals and they were analyzed confirm the presence of the coating on fibers. To obtain a semi-quantitative information, all spectra were normalized to the 1060 cm^{-1} peak, being a strong cellulose peak, and the trend of peak at 875 cm^{-1} and 1255 cm^{-1}, correlated to P-O-P and P=O stretching of APP or SHMP, was observed. It can be noticed from **Figure 34** that the intensity for peak at 1255 cm^{-1} increase steadily for both systems, indicating an increase in the coating amount on fibers.(170, 210) **Figure 35** display SEM micrographs of coated fibers, both C700 and ballmilled.

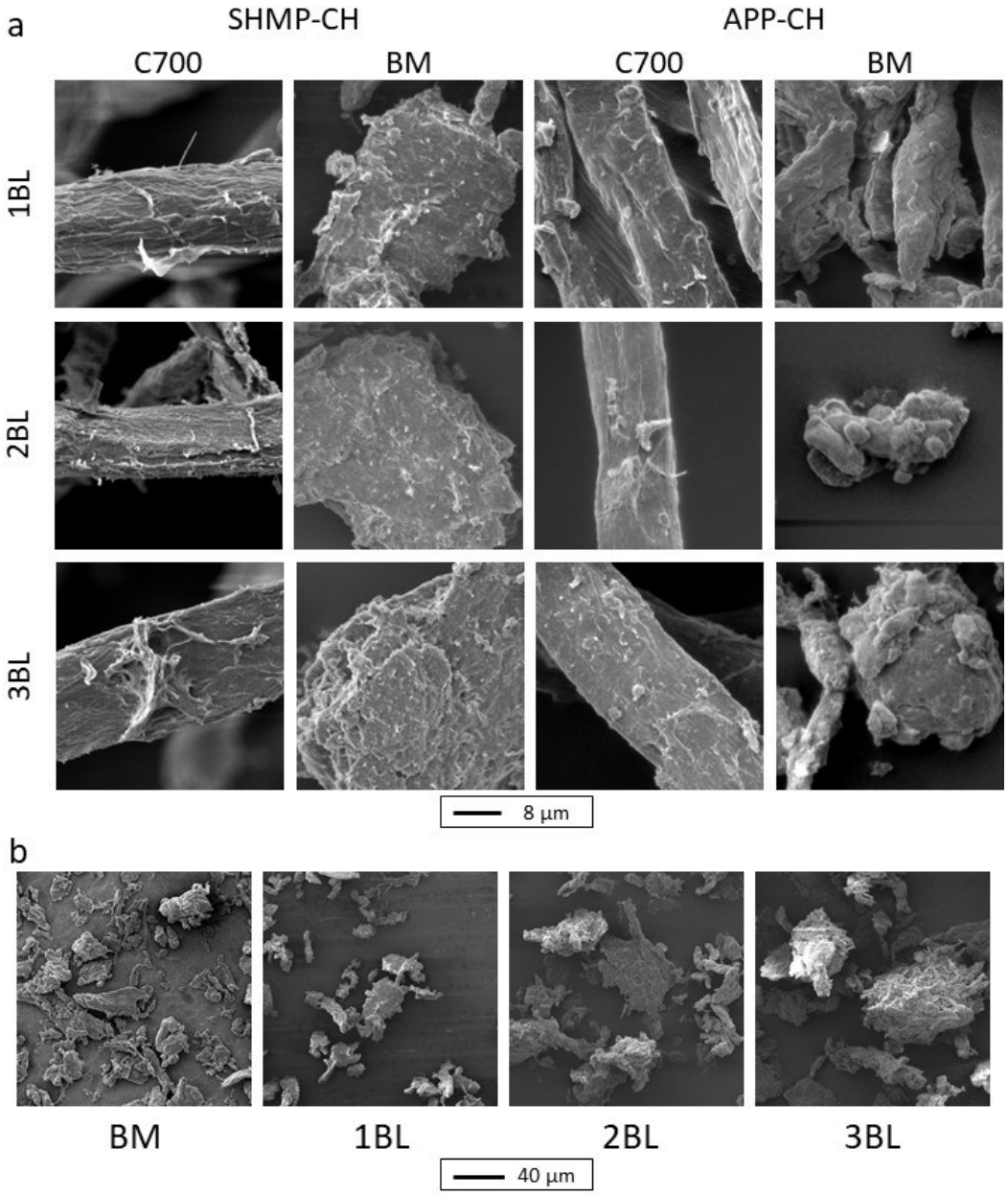


Figure 35: SEM micrographs of a) coated fibers with the two systems, b) BM fibers coated with 1 to 3 BLs of SHMP-CH LbL assembly

Coating deposited on the surface alters the fibers morphology, which becomes rougher. Filaments and film-like plates expand from the surface as indication of the presence of coating. Moreover, as visible in **Figure 35**b, coated ballmilled appears to be bigger than uncoated. This could be due the aggregation of small particles upon during, with the LbL coating helping the adhesion between them. Even though, coating assembly seems to grow by increasing BLs numbers.

3.2.3 Thermal stability

To understand the coating effect on the decomposition path of the coated fibers, the thermal and thermo-oxidative stability was investigated by thermogravimetric analysis, displayed in **Figure 36** and reported in **Table 5.**

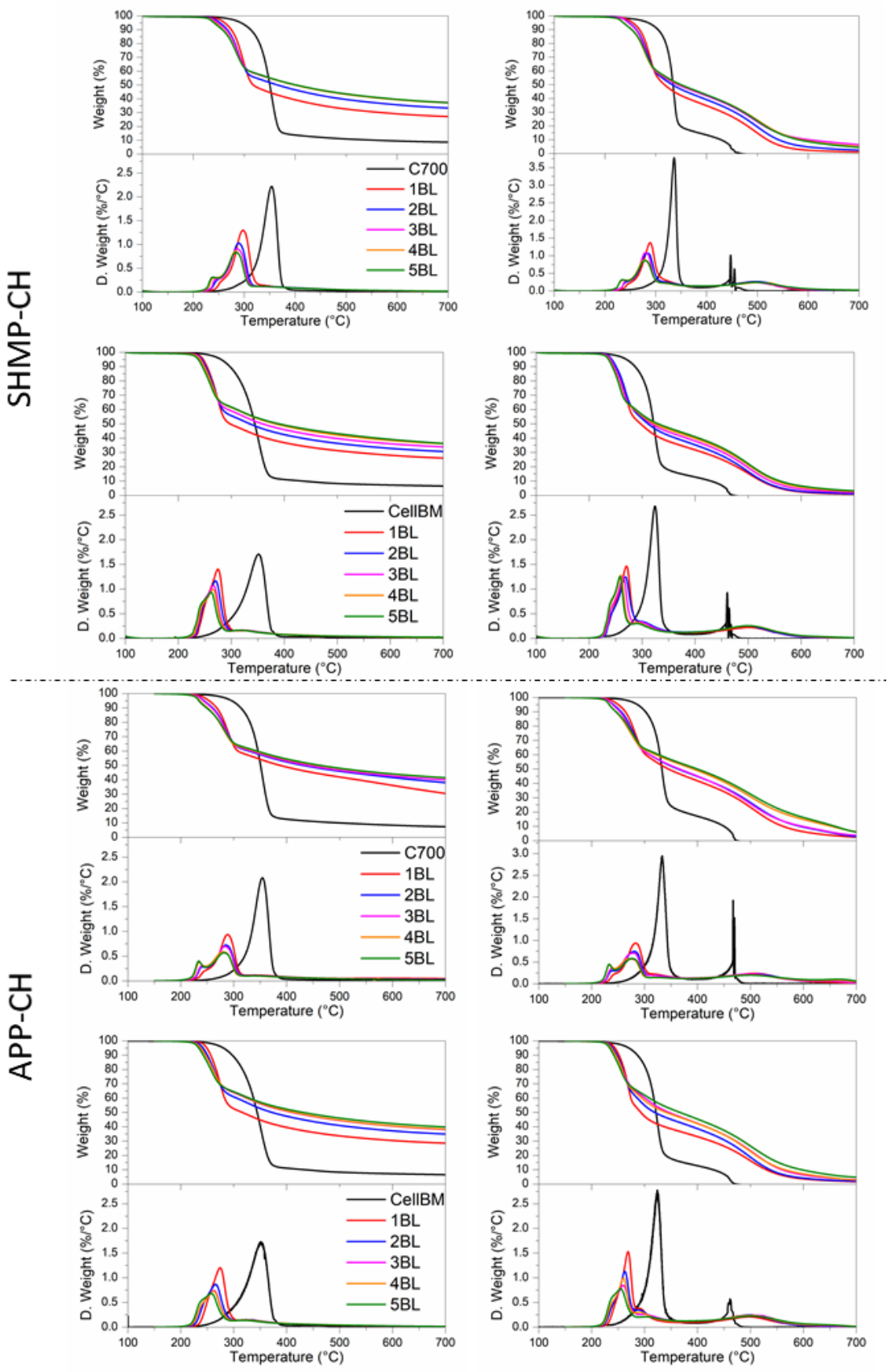


Figure 36: TG plots of C700 and BM fibers (in Nitrogen and Air) for both LbL systems

Table 5: TGA data for PUF composites

	N_2			Air		
	$T_{on,5\%}$ (°C)	**Residue at 500°C (%)**	**Residue at 700°C (%)**	**$T_{on,5\%}$ (°C)**	**Residue at 500°C (%)**	**Residue at 700°C (%)**
C700	294	11	9	285	0	0
CellBM	281	8	6	271	0	0
C700 SHMP-CH 1BL	262	33	27	255	15	1
C700 SHMP-CH 2BL	253	40	33	248	19	2
C700 SHMP-CH 3BL	249	44	37	246	24	5
C700 SHMP-CH 4BL	243	44	37	237	24	5
C700 SHMP-CH 5BL	241	44	37	237	25	7
CellBM SHMP-CH 1BL	247	31	26	243	15	1
CellBM SHMP-CH 2BL	245	36	31	240	16	1
CellBM SHMP-CH 3BL	243	40	34	237	19	3
CellBM SHMP-CH 4BL	241	42	36	237	21	3
CellBM SHMP-CH 5BL	238	43	36	237	22	3
C700 APP-CH 1BL	254	42	31	250	23	3
C700 APP-CH 2BL	244	47	38	241	26	4
C700 APP-CH 3BL	243	47	40	240	27	4
C700 APP-CH 4BL	236	48	42	233	31	6
C700 APP-CH 5BL	234	48	42	233	33	6
CellBM APP-CH 1BL	249	34	29	244	16	2
CellBM APP-CH 2BL	242	41	35	240	19	2
CellBM APP-CH 3BL	238	45	38	237	23	3
CellBM APP-CH 4BL	238	45	38	237	24	3
CellBM APP-CH 5BL	234	46	40	234	27	5

Neat C700 and BM cellulose show the typical thermal decomposition pathway of cellulose both in oxidative and non-oxidative atmosphere, as described in chapter 2.2.1. However, the thermal stability of BM cellulose slightly decrease as result of the ballmilling process, which by reducing the crystallinity of cellulose also impacts the $T_{on,\ 5\%}$ that is decreased from 297°C of neat cellulose to 283°C, in inert atmosphere(211, 216) The anticipation of onset decomposition temperature is observed also for LbL treated fibers, with the $T_{on,\ 5\%}$ diminishing for all samples with values from 297°C of C700 to 234°C for 5BL APP-CH coated C700 fibers in nitrogen. This is commonly reported for systems containing phosphates that are

well-known to favor dehydration processes pushing the cellulose decomposition towards char formation(194).The more pronounced difference is observed for 1BL treated fibers, which yield a final residue of 25% and 26% for BM and C700 fibers, respectively, in SHMP-CH assembly and similar values for APP-CH systems. The deposition of additional BL, gradually improves the amount of char produced at 800°C with diminishing results above 3 deposited BL. This behavior can point out that 3 bi-layers are enough to provide the optimal phosphorous content to the system, which can take part into the char formation. An increase of coating materials does not improve the final residue. Such behavior has been already observed on other cellulose-based materials.(217) In the presence of air, cellulose goes through a two-step thermal oxidation process. As already observed in inert atmosphere, the presence of LbL coating increase the char formed after the first decomposition step. The so produced charred residues show improved oxidative stability as their oxidation during the second weight loss step is slower allowing to reach higher temperature. Indeed, residue at 500°C of coated fibers (both BM and C700) account to 15% for both of them, while neat cellulose at the same temperature leave negligible residue (<1%). The above observed improved char forming ability can be ascribed to the dual action of SHMP or APP, which can directly enhance the cellulose char formation while also constructing a protective insulating layer with CH, which further contributes to char formation by reducing heat gradients.(36) Following TGA results, flammability of LbL coated fibers has been evaluated to investigate their flame-retardant properties and select the best assembly to be used in PUF composites. To this aim, horizontal flame tests were performed on specimens obtained from drying wet fibers (C700) at 70°C in a mold, in this way a self-sustaining, yet very fragile, bar was obtained for both systems under investigation. Due that there was no visible effect of higher BL numbers from TGA and wanting to find a balance between properties and process steps required for coating, only 1, 2 and 3BL samples were tested and snapshots of flammability test are visible in **Figure 37**.

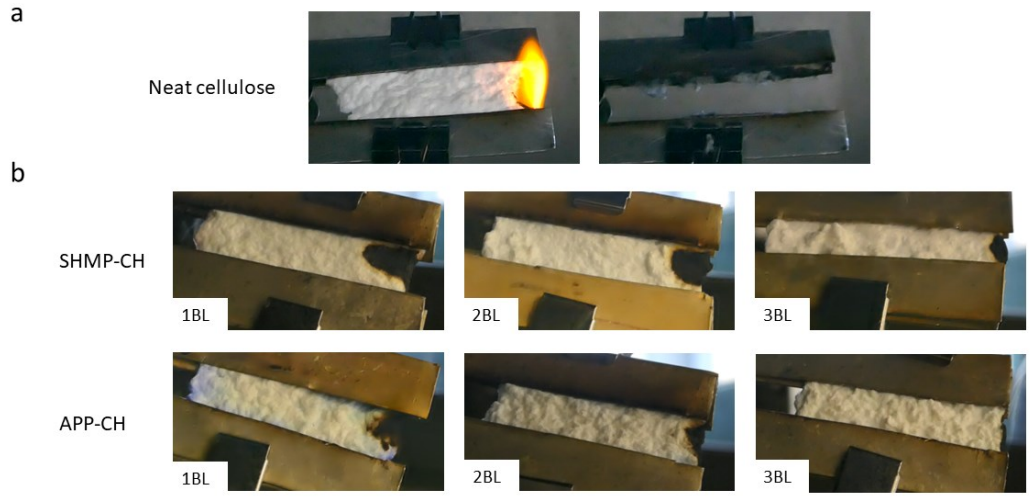


Figure 37: a) untreated cellulose fibers flammability test and b) C700 samples after flammability test

The same procedure was not applicable to BM fibers due to their powder form which gave specimen too fragile to be tested in this way, therefore they were tested in form of powder with similar results respect to C700 fibers and test for SHMP-CH formulation is visible in **Figure 38**.

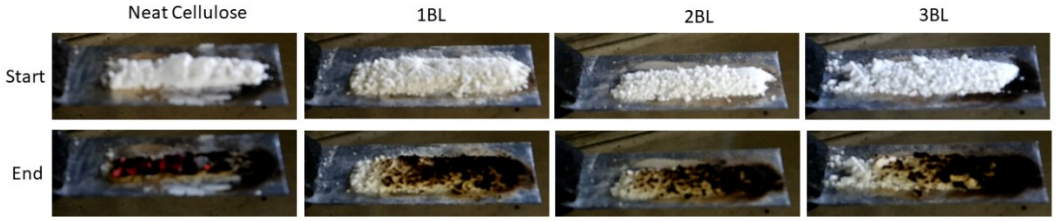


Figure 38: Flammability test for BM fibers coated with SHMP-CH assembly

Neat cellulose fibers are extremely flammable and after ignition the flame spread along all the surface, consuming it completely leaving no residue. Conversely for 1BL and 2BL coated samples a self-extinguishing behavior was observed after a couple of seconds from the removal of the ignition source without afterglow. It has to be noticed that in half of 1BL samples flames spread all along the surface, burning all the sample and leaving a fragile, black charred residue. Surprisingly, sample at 3BL gave a non-ignitability behavior forming a black char as soon as the flame is applied which prevent the ignition of the specimen. Ballmilled cellulose presented similar behavior. Indeed, untreated ballmilled fibers burn completely when exposed to a flame, but when LbL fibers are tested, a black char is formed as soon as the flame is applied, slowing down the fire growth and thus leaving almost intact the sample. For this reasons, 3BL coated fibers were then chosen as candidate for PUF composites due to their good balance between flame-retardancy properties and production steps required.

3.2.4 Polyurethane foaming and physical properties

Coated cellulose fibers were used as filler for PUF composites and a first screening was done using C700 as substrate for both LbL systems. Composites with 2.5, 5 and 7.5 phr of cellulose were prepared by the Institute of Polymers, Composites and Biomaterials of Pozzuoli (IPCB-CNR) and are visible in **Figure 39**.

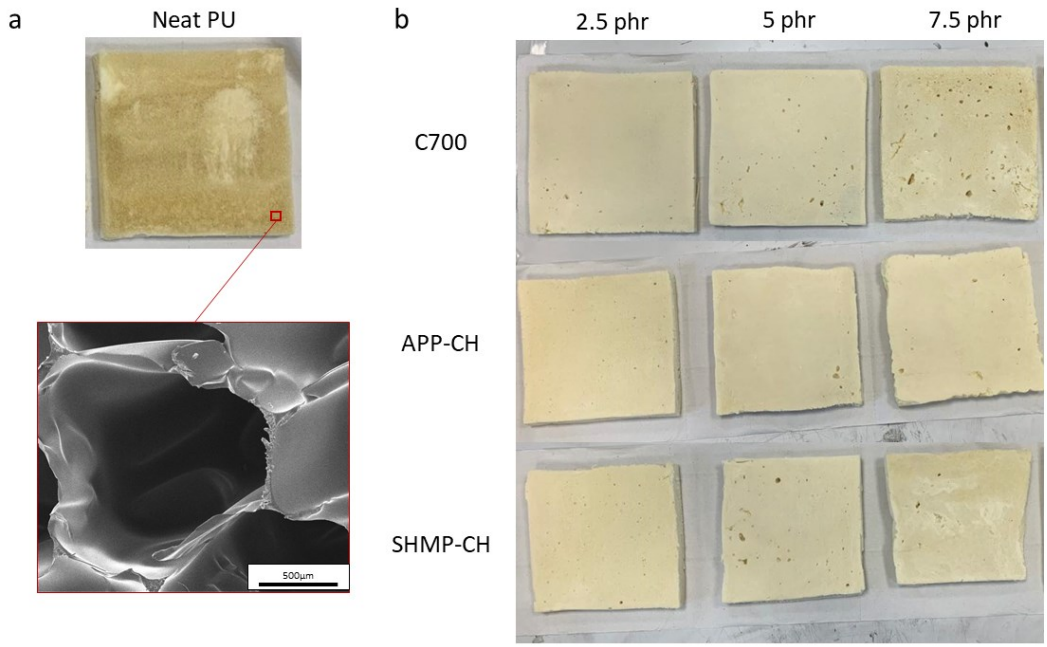


Figure 39: a) neat PU reference with digital photo and SEM micrograph and b) digital images of PUF samples prepared with untreated cellulose and coated cellulose

The PU foamability is affected by the presence of cellulose fibers, resulting in visually less homogenous PUF respect to neat PU. As expected this effect increase with the concentration of cellulose and can be noticed that all samples at 7.5phr presents irregularities in shape and surface aspect, with holes clearly visible. This effect is due to the length of cellulose fibers used, which tend to touch and form aggregates, which eventually interfere with cells formation and thus leaving holes in the final PUF. This effect limits the possible maximum loading of fibers, which can result in a lower flame-retardant effect given by the coated fibers. However, it can be noticed that the presence of coating on fibers seems to help in diminishing holes in PUF, as visible in **Figure 39b**, where less holes can be seen in samples, in particular for 7.5phr containing PUF. In an effort to increase the concentration of cellulose into the final foam, ballmilled fibers were incorporated into the PU foaming at 7.5 and 15 phr and resulting PUF are visible in **Figure 40**.

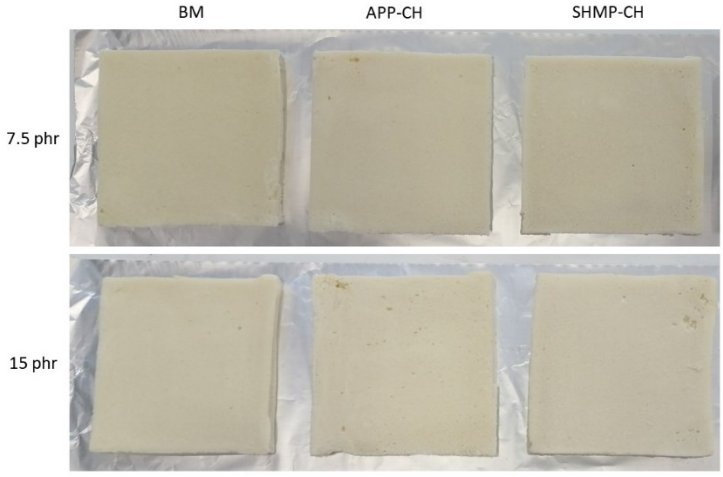


Figure 40: digital images of PUF samples prepared with untreated BM cellulose and lbl coated BM cellulose

Surface of 7.5 phr PUF with BM cellulose is visibly better respect to samples prepared with long fibers. Being BM fibers smaller and round shaped can form less aggregate and entanglements, having the chance to alter less the foaming mixture respect to C700 fibers, resulting in possible higher loading concentration. Samples at 15phr still present some holes on the surface, but with an overall homogeneous aspect. SHMP-CH was chosen to investigate more in-deep the effect of cellulosic filler into the microscopic aspects that lead to these results. **Figure 41** shows SEM micrographs of PUF at 7.5 and 15 phr content of C700 or BM fibers.

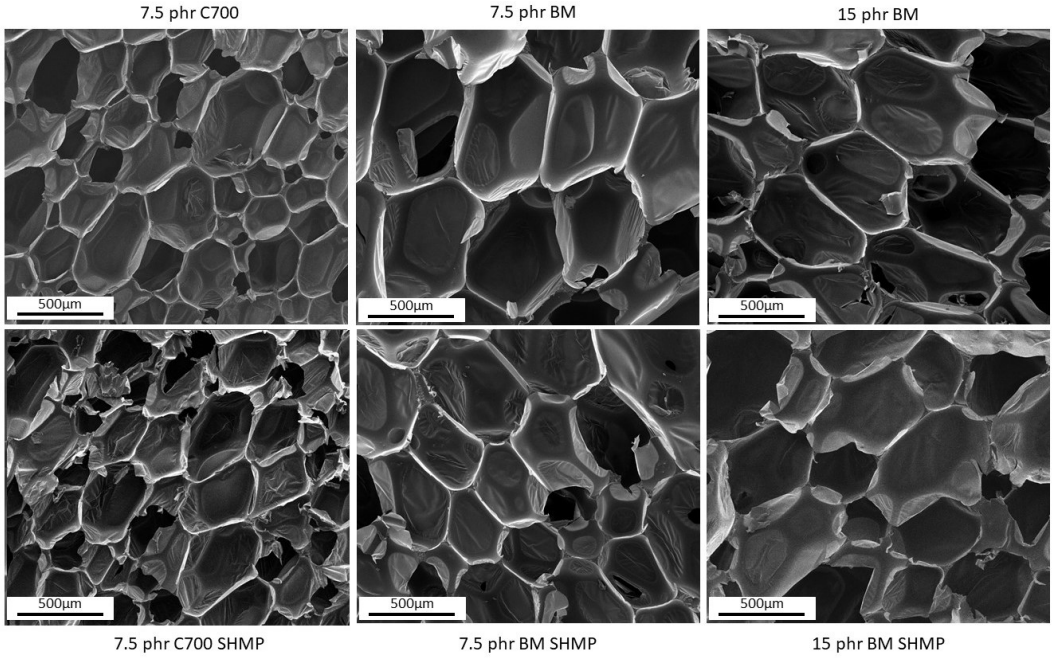


Figure 41: SEM images of PUF with 7.5 and 15 phr of C700 or BM cellulose, uncoated or coated

PUF without fibers added present the regular structure associated to closed cells polymeric foams, with cells with dimensions of 750 ± 50 µm of diameter. The addition of cellulose fibers alters the cells structure and dimensions respect to neat PU, visible in **Figure 39a**. Indeed, the presence of cellulose acts as nucleating agent for gas and reduce the coalescence of bubbles, leading to smaller cells, as already reported in previous works.(78, 218) Samples containing LbL coated fibers have a wider range of cell dimensions, with sample made with 3BL SHMP-CH coated C700 presenting irregular cells ranging from tenths to hundreds of microns of diameter. Moreover, many cells assume an irregular shape as result of the disruption caused by long fibers, which lead many cells to join together, contributing to increase the range of cells dimensions. and joined together. This effect is accentuated by the presence of coating and can be the cause of the difficulty of preparing samples with higher percentage of long fibers. The PUF morphology is correlated to mechanical and thermal properties, in **Table 6** are visible data regarding compression tests and the thermal conductivity of the discussed samples which can be correlated to cells dimension and foamability of samples.

Table 6: data from compression tests and thermal conductivity for PUF previously studied by SEM

Sample	Density (kg/m^3)	Thermal conductivity (W/(m K))	Specific modulus ($MPa/(g/cm^3)$)	Specific stress at yield ($MPa/(g/cm^3)$)
Neat PU	41.9 ± 0.8	0.0441 ± 0.0008	189.3 ± 28.2	12.6 ± 1.3
7.5 phr C700	41.7 ± 1.5	0.0387 ± 0.0003	148.5 ± 4.6	8.0 ± 0.1
7.5 phr C700 3BL SHMP-CH	47.1 ± 2.1	0.0394 ± 0.0006	106.8 ± 20.9	6.1 ± 0.1
7.5 phr BM	40.7 ± 1.6	0.0394 ± 0.0007	143.4 ± 11.9	8.4 ± 1.9
7.5 phr BM 3BL SHMP-CH	40.2 ± 0.7	0.0389 ± 0.0006	190.7 ± 26.7	9.6 ± 0.6
15 phr BM	39.8 ± 1.1	0.0401 ± 0.0003	111.1 ± 22.9	8.0 ± 0.3
15 phr BM 3BL SHMP-CH	40.0 ± 1.0	0.0411 ± 0.0004	135.4 ± 6.3	7.6 ± 0.1

As expected from SEM analysis, sample with LbL coated C700 present higher density respect to all other samples, mainly due the structure collapsing and smaller cells. The inclusion of cellulose has a detrimental effect on mechanical properties, such as modulus and stress at yield, while at the same time reduce thermal conductivities for all composites which can be possibly attributed associated to the cellulosic fillers together with the cells size reduction.(77, 219) Interestingly, analyzing each couple of PUF (7.5phr BM with 7.5 phr coated BM) it's possible to notice that the coating seems to mitigate the loss in mechanical properties.

3.2.5 PU foam flame retardancy

Forced combustion tests have been selected to evaluate the flame-retardant characteristics of the prepared bio-PUF. During the test the sample is exposed to an impinging heat flux of 35 kW/m2 that simulate a fire in its early stage.(204) This triggers the sample thermal decomposition towards the production of combustible volatiles that ignite upon reaching the flammability limits and lead to the flaming combustion of the specimen. Heat and smoke release parameters as a function of time are then evaluated. **Figure 42** displays HRR and SPR plots as well as their integral value for all tested PUF, while all data are condensed in **Table 7**.

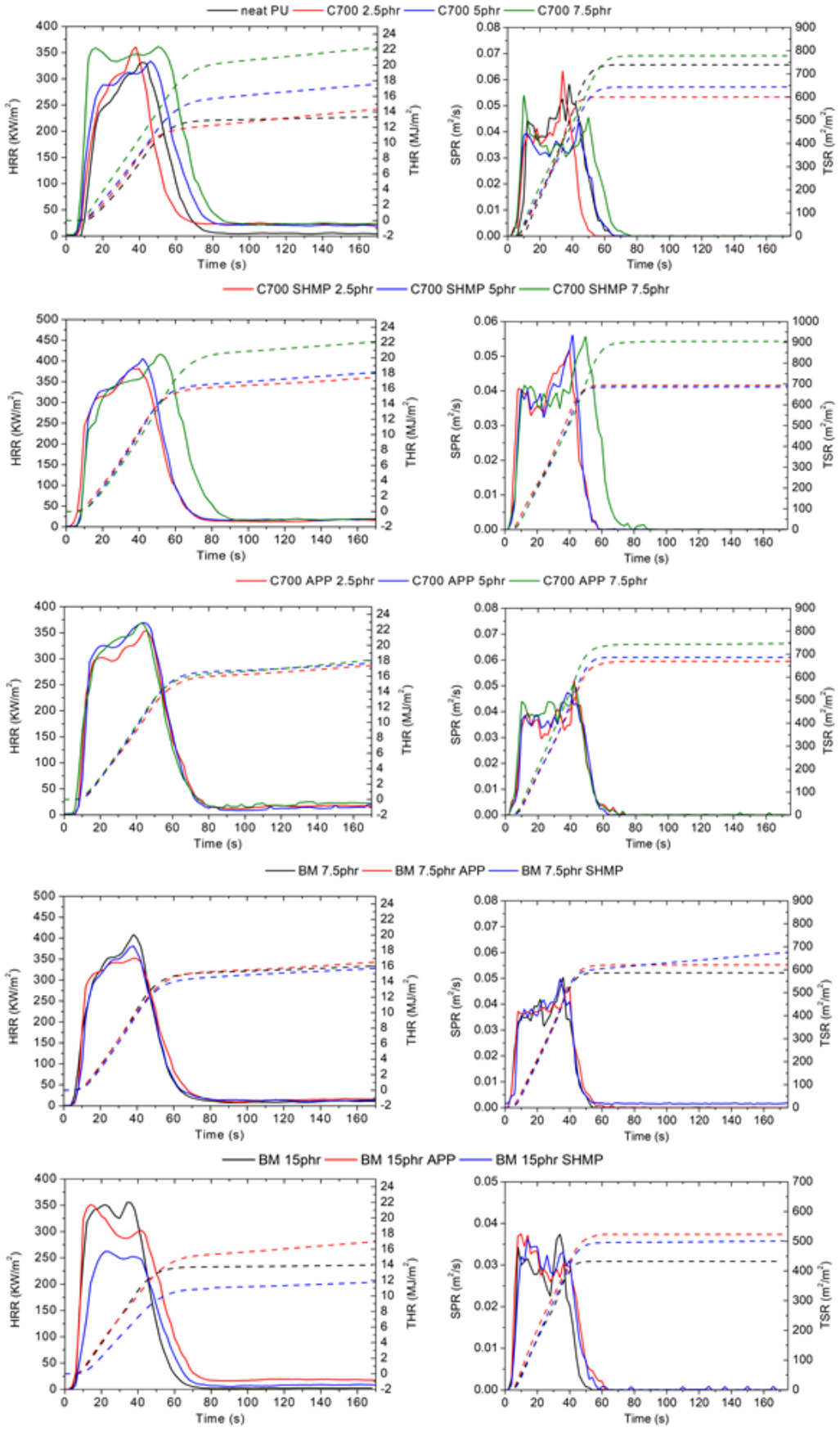


Figure 42: Heat release rate (HRR), total heat release rate (THR), smoke production rate (SPR) and total smoke release (TSR) for PUF made with untreated and coated BM cellulose

Table 7: data from cone calorimetry for all PUF samples

Sample	TTI (s)	HRR_{peak} (KW/m^2)	T Peak (s)	THR (MJ/m^2)	EHC (MJ/Kg)	TSR (m^2/m^2)
PU	8 ± 1	340 ± 5	43 ± 2	13.3 ± 1.3	18.0 ± 1.0	736 ± 48
2.5 phr C700	6 ± 2	362 ± 19	37 ± 1	14.4 ± 1.2	21.4 ± 1.1	597 ± 84
5 phr C700	5 ± 1	336 ± 10	47 ± 1	17.8 ± 0.9	23.8 ± 0.6	640 ± 23
7.5 phr C700	6 ± 2	396 ± 56	34 ± 14	22.7 ± 2.6	24.6 ± 0.8	773 ± 118
2.5 phr C700 3BL SHMP-CH	4 ± 2	396 ± 25	41 ± 4	17.7 ± 2.1	22.5 ± 2.1	692 ± 26
5 phr C700 3BL SHMP-CH	5 ± 1	408 ± 54	41 ± 1	18.2 ± 2	23.8 ± 0.5	683 ± 89
7.5 phr C700 3BL SHMP-CH	9 ± 4	430 ± 30	53 ± 3	22.4 ± 1.7	23.1 ± 1.1	873 ± 34
2.5 phr C700 3BL APP-CH	7 ± 1	355 ± 11	45 ± 1	17.5 ± 0.6	23.9 ± 0.9	658 ± 37
5 phr C700 3BL APP-CH	8 ± 2	382 ± 17	46 ± 2	17.9 ± 0.6	23.4 ± 0.7	673 ± 10
7.5 phr C700 3BL APP-CH	5 ± 1	368 ± 9	42 ± 1	18.4 ± 0.8	22.6 ± 1.4	744 ± 80
7.5 phr BM	3 ± 1	411 ± 9	38 ± 2	16.1 ± 1.1	20.1 ± 1.1	585 ± 24
15 phr BM	5 ± 1	375 ± 52	27 ± 9	13.9 ± 1.5	17.4 ± 2.5	430 ± 39
7.5 phr BM 3BL SHMP-CH	5 ± 1	388 ± 18	39 ± 3	15.7 ± 0.6	21.2 ± 0.9	592 ± 6
15 phr BM 3BL SHMP-CH	5 ± 2	265 ± 8	25 ± 3	11.9 ± 0.2	16.9 ± 0.3	498 ± 34
7.5 phr BM 3BL APP-CH	5 ± 1	357 ± 12	35 ± 7	16.6 ± 0.9	21.7 ± 0.8	617 ± 42
15 phr BM 3BL APP-CH	4 ± 1	352 ± 1	13 ± 1	17.0 ± 0.5	21.8 ± 0.2	523 ± 12

From an overall point of view, the addition of cellulose to the PU foam produces an increase in combustion rates and a decrease in the smoke produced, with the exception of 7.5phr of C700, where both HRR and TSR increase. Indeed, differently from the PU matrix, cellulose is easily burned producing an increase in HRR values proportional to its content. On the other hand, by being completely consumed during combustion the cellulose smoke production is extremely low.(192) Thus, as the PU content is decreased the TSR values are positively affected decreased proportionally to the cellulose content. The main exception to this is the sample containing 7.5phr of C700, both untreated and LbL coated, where an increase in all parameters is observed. This effect can be caused by the uneven dispersion of cellulose in the sample, resulting in a material that burns well, producing more smokes than neat PU. When cellulose concentration is increased to 15phr, a visible decrease in smoke production is visible, associated to a slight

increase in HRR and THR, even though the high error associated to this measure can indicate the presence of uneven distribution of fibers in the sample. In order to notice an influence of coated cellulose on flame-retardancy of PUF obtained, high contents are needed. Indeed, samples with less than 7.5 phr of treated cellulose present same values, if not worse, than their respective samples with untreated cellulose. This effect was visible for both systems investigated, even though APP-CH assembly performed slightly better than SHMP-CH. However, when 15phr coated cellulose is used, SHMP-CH assembly prove to be effective in transferring the flame-retardant properties of fibers to the PUF. Indeed, Instead, a pkHRR reduction of 30% compared to 15phr of untreated fibers and 22% respect to neat PU was observed. Moreover, smoke production is just slightly affected if compared to untreated cellulose, with a final 32% reduction respect to neat PUF. Among the two systems, only SHMP-CH presented a good efficacy in transferring its flame-retardant properties to final PUF. This can be the result of a more homogeneous coating on fibers, with an optimal phosphorous content. APP-CH assembly fails to transfer its properties to final PUF, this could be due to a thinner coating on fibers, which can be enough to protect them from flame when used alone, but not enough to impact the burning behaviour of a polymeric matrix.

3.3 Conclusions

In this study, two LbL systems comprising a flame-retardant agent (SHMP or APP) and chitosan were used to coat neat or ballmilled cellulose fibers, which were then used as bio-sourced fillers in PUF forming. The LbL growth of both systems was evaluated on a model substrate and on fiber surface, showing good correlation between the two different substrates. Fibers flammability was tested pointing out how 3BL coated fibers can yield a non-ignitability behavior. This result suggested 3 as the optimal number of BL to be deposited on fibers for the preparation of the PUF composites. Cellulose fibers were successfully incorporated in the PUF forming with a maximum concentration of 7.5 phr and 15 phr for long fibers and ballmilled fibers, respectively, without significant alterations in mechanical properties and slight better thermal conductivity. Cone calorimetry was used to assess the flame-retardant behavior of PUF containing cellulose fibers. On overall, PUF containing cellulose presented higher pkHRR, and lower smoke production. Among all formulations tested, PUF containing 15phr of ballmilled cellulose coated with 3BL SHMP-CH showed the best results. Indeed, a 30% reduction in pkHRR respect to the use of untreated cellulose and 22% respect to neat PU was observed, with a significant reduction in smoke production. This effect was possible thanks to the combination of cellulose size from ballmilling and flame-retardant LbL coating.

4. Cellulose fibers lightweight materials

In chapter 2 and 3, the LbL technique was used with the aim of increase the compatibility between cellulose fibers and a polymeric matrix and at the same time provide flame retardant properties. In this chapter cellulose fibers were coated with an assembly similar to the one used in chapter 3, but with different deposition conditions, able to favor the formation, upon drying, of a stable 3D lightweight structure with high flame retardancy. The production of stable lightweight structure made of cellulose or lignocellulosic fibers is a matter of interest in many fields, as seen in chapter 1.2.3 which highlighted the wide number of studies comprising nanocellulose exploitation for making stable porous 3D structures.(86, 220-222) Even if nanocellulose present outstanding properties, pulp fibers appears to be more appealing in an industrial context, mainly due to their ease of handling, reduced cost and less environmental impact.(90) However, the development of porous fiber network made by pulp fibers can face some limitations and challenges, mainly due to the poor fiber-fiber interactions that leads to weak materials. Although classic foaming approaches, like foaming using surfactants like sodium dodecyl sulfate, and more innovative ones, like solvent exchange,(93) have been attempted with acceptable results, the stability and the mechanical properties of the obtained porous structure are limited by the nature of the fiber-fiber interaction.(92) Moreover, as seen previously, cellulose-rich materials exploitation is limited by their high flammability, that limits the range of possible applications. Among all methods investigated in literature for imparting flame retardants properties to cellulose, the LbL appears to be one of the most promising method, which in addition can help to improve the desired fiber-fiber interactions. In this chapter, the LbL was used with the double aim of impart flame-retardant properties to cellulose fibers and improve the fiber-fiber interactions.(160, 223, 224) Having this in mind, in this work two different assemblies were tested for the production of rigid cellulose lightweight materials and thus the discussion part of this chapter will be divided in two sections, as presented in **Figure 43.**

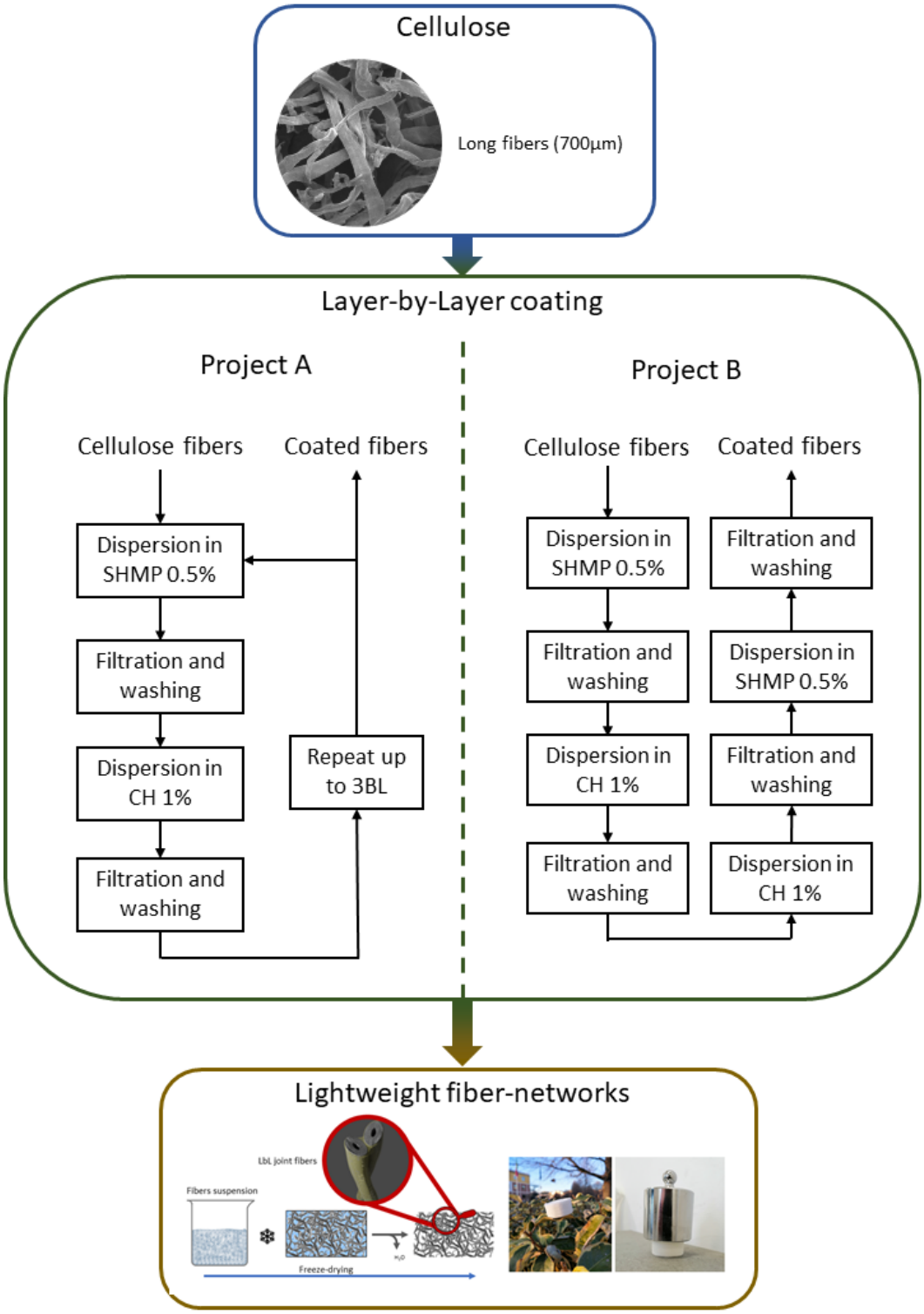


Figure 43: lightweight fiber-networks from lbl coated cellulose fibers

The first section reports an assembly comprising the same components of chapter 3, Chitosan and sodium hexametaphosphate, but with conditions of deposition tailored to be more effective in enhance fiber-fiber interactions and thus make stable 3D structures upon freeze-drying.

The second assembly, disclosed in the second section, introduce cellulose nanofibers with the aim of increase mechanical properties and changes phosphorous

source in phytic acid, commonly obtained from agricultural wastes and products,(225) to exploit a completely bio-sourced system.

Both projects were done in collaboration with the Royal Institute of Technology (KTH) of Stockholm. Polyelectrolyte adsorption measurements and study were done during the visiting period as part of the PhD program.

4.1 Materials and methods

4.1.1 Materials

Commercial cellulose fibers (ARBOCEL BC1000) with an average length of 700 μm were kindly provided by J.Rettenmaier & Sohne GmbH (Rosenberg, Germany). Branched poly(ethylene imine) (BPEI, Mw ~25000 Da by light scattering, Mn ~10000 by gel permeation chromatography, according to the material datasheet), chitosan (low molecular weight, < 20000 Da and 75-85% deacetylated chitin, according to the material datasheet), acetic acid, sodium hexametaphosphate (crystalline, +200 mesh, 96%), phytic acid (50% wt. solution) and sodium acetate were purchased from Sigma Aldrich (St- Louis, USA). Cellulose nanofibrils were purchased from Rise (Sweden). Suspensions and solutions were prepared using ultrapure water (18.2 MΩ deionized water supplied by a Q20 Millipore system, Italy). More specifically, chitosan was solubilized in a 1%wt acetic acid aqueous solution at a concentration of 1%wt and kept under magnetic stirring overnight. BPEI and SHMP were dissolved in water to 0.1%wt and 0.5%wt concentration, respectively. Analytical grade potassium polyvinyl sulfonate (KPVS) was purchased from Wako Pure Chemicals (Japan) and polydiallyldimethylammonium chloride purchased from Sigma-Aldrich (Stockholm, Sweden) was ultrafiltrated using a tangential flow equipment before use.

4.1.2 Layer by layer assembly

In this chapter, two assemblies are discussed:

a) Branched poly(ethylenimine), sodium hexametaphosphate and chitosan were used in form of solution at 0.1%, 0.5% and 1% wt. respectively to obtain a lbl assembly. The assembly of 10BL was first studied on a model surface made by a silicon wafer and FT-IR spectroscope. The SHMP/CH coating was achieved by a first dipping in BPEI solution (5 min) followed by alternatively dipping the Si wafer in the negatively (SHMP) and positively (CH) charged solutions (5 min each). Each deposition was followed by excess solution removal by dip in water (for BPEI and SHMP) or acetic acid 1% wt. (for CH). To transfer the same assembly, cellulose fibers were rehydrated and the excess of water was discarded. Then, fibers were dispersed in BPEI and sonicated for 10 minutes in order to deposit the anchoring layer. The SHMP/CH coating was achieved by alternatively dispersing and sonicating the fibers in the negatively (SHMP) and the positively (CH) charged solutions (5 min each). Each deposition step was

followed by excess solution removal by centrifuge and a washing step using water (for BPEI and SHMP) or acetic acid 1% wt. (for CH). Up to 3BL were deposited with this procedure. At the end of the LbL assembly, fibers were washed with water to remove the excess of acetic acid.

b) A quad-layer layer by layer assembly comprising phytic acid, cellulose nanofibers and chitosan was also studied. BPEI was used as 0.5%wt solution and pH was set to 8 using NaOH. Chitosan was used as 1% solution in an acetate buffer at pH5. CNF was used as 0.2 or 0.4% suspension and pH6. Phytic acid was used as 1 or 2.5% solution. Briefly, cellulose fibers were rehydrated and the excess of water was discarded. Then, fibers were dispersed in BPEI and mechanically stirred for 10 minutes in order to deposit the anchoring layer. Fibers were then separated by filtration on a nylon filter (200 mesh) and washed with water for 5 minutes following the same procedure. Phy, CNF and Ch were deposited following the same procedure, with the exception of contact time that was set to 5 minutes. Each deposition step was followed by a washing step using water (for Phy and CNF) or pH5 acetate buffer (for CH). Three different systems were then obtained, as shown in **Table 8.**

Table 8: deposition solution concentration for the 3 assemblies proposed

	Deposition solution concentration				
	BPEI (%wt.)	Phy (%wt.)	CH (%wt.)	CNF (%wt.)	CH (%wt.)
Phy1CNF0.2	0.5	1	1	0.2	1
Phy2.5CNF0.2	0.5	2.5	1	0.2	1
Phy1CNF0.4	0.5	1	1	0.4	1

4.1.3 Porous fiber network preparation

The wet fibers were suspended in water in order to achieve a weight ratio of 1:11.5 between the fibers and water aiming at a final density of the fiber network of 75kg/m^3. The resulting dispersion was subsequently cast into molds and subjected to freezing at a temperature of -40°C for a duration of 12 hours. Samples were subsequently freeze-dried for 48 hours using a vacuum freeze-dryer (Toption TOPT-10A, vacuum freeze dryer).

4.1.4 Characterization

Growth on model surface (Si wafer, 100, single side polished) was monitored using a FT-IR spectrophotometer (16 scans and 4 cm^{-1} resolution, Frontier, Perkin Elmer) in transmission mode. Attenuated total reflectance (ATR) Fourier Transform infrared spectroscopy spectra for fibers and composites were collected using the same FT-IR spectroscope equipped with a germanium crystal. (16 scans, 4 cm^{-1} resolution). Surface morphology of fibers and composites was studied, after gold sputtering, using a LEO-1450VP Scanning Electron Microscope. Thermal stability

of fibers was evaluated by TGA (Discovery, TA Analysis). Briefly, samples (approx. 10 ± 1mg) were placed into alumina pans and subjected to an isothermal treatment for 15 min at 100°C and then heated at 10°C min^{-1} up to 700°C. Samples were tested both in nitrogen and in air. T_{on} (temperature corresponding to 5 % weight loss), T_{max} (temperature at maximum rate of weight loss), and residue (%) were obtained by these measurements

Polyelectrolyte titration was used to measure the charge density of BPEI, CH and SHMP using a rapid particle charge titration instrument (Stabino, Meerbusch, Germany) according to a previously described method.(226) The calculation of the charge density is based on 1:1 stoichiometric charge ratio between the studied chemicals and the oppositely charged polyelectrolytes. Potassium polyvinyl sulfate (KPVS) was used to titrate BPEI and CH, while a specially cleaned polydiallyldimethylammonium chloride (PolyDADMAC), was used for the titration of CNF, Phy and SHMP. BPEI, SHMP and CH were adsorbed onto the cellulose fibers by LbL as described under 5.1.2. Filtrates after deposition of each adsorbed layer were collected after centrifugation. The concentration of BPEI, SHMP and CH in the filtrates was determined by titration with KPVS or PolyDADMAC and the adsorbed mass of the BPEI, SHMP and CH was back-calculated from the remaining chemicals in the filtrate. The same procedure was applied to Phy-CH-CNF assemblies. The flammability of the prepared samples was evaluated in horizontal and vertical configuration; the sample (80x25x10 mm3) was ignited from its short side by a 20 mm methane flame (flame application time: 2x6 s). The test was repeated at least 2 times for each formulation; during the test, parameters such as after-flame time (the time for which flame persists after the ignition source has been removed on the basis of ISO 13943, expressed in s) and final residue (%). Cone calorimetry (GA01, Noselab ats, Italy) was employed to investigate the combustion behavior of square samples (50x50x15 mm3) under exposure to a heat of 35 kW/m^2 in horizontal configuration, following an earlier described procedure. Each sample was confined in an aluminum foil holder.(176) The following parameters were registered time to ignition (TTI, s), peak of heat release rate (PHRR, kW/m2), time to peak (s), total heat release (THR, MJ/m2), average heat of combustion (EHC, MJ/Kg), smoke production rate (SPR, m2/s), total smoke release (TSR, m2/m2) and final residue (%). The test was repeated 3 times to ensure reproducibility and the average of triplicate data is reported; the experimental error was assessed as standard deviation (σ). Raman spectra of sample after cone calorimetry were obtained on an InVia Raman Microscope (Renishaw, New Mills, UK argon laser source 514nm) coupled with a Leica DM 2500 optical microscope. D and G band were fitted with Lorentz functions in order to determine their ratio.

4.2 SHMP-CH assembly results and discussion

4.2.1 Coating growth and assembly on fibers

Up to 10BLs of LbL assembly were deposited on a model silicon substrate in order to study the layers build-up with transmission IR spectroscopy. (177) To improve adhesion between substrate and assembly, both on silicon and on fibers, BPEI was employed as anchoring layer as already described in previous chapters. Spectra of pure substances, such as BPEI, CH and SHMP were collected by drop casting on Si wafer and their IR spectra were measured. Pure substances IR spectra analysis are reported in chapter 2.2.1 and 3.2.1 and they will not be further discussed. **Figure 44** shows the spectra during the build-up the LbL systems on silicon wafer up to 10 BL and the intensity vs BL number plot for the characteristic peaks of CH and SHMP. Signal intensity increase steadily as the number of deposited BL increases, showing the successful LbL assembly of the selected components. The absorbance at 1260 cm^{-1} and 1074 cm^{-1}, corresponding to P=O group of SHMP and C-O-C stretching of chitosan respectively, plotted as function of the deposited BL number suggest a linear regime growth.(217) The LbL assembly was then transferred to cellulose fibers with the target of studying the effect of 1, 2 and 3 BL in the formation of stable 3D lightweight structure. Surface morphology of coated fibers was studied through SEM and a collection of micrographs is visible in **Figure 44b**.

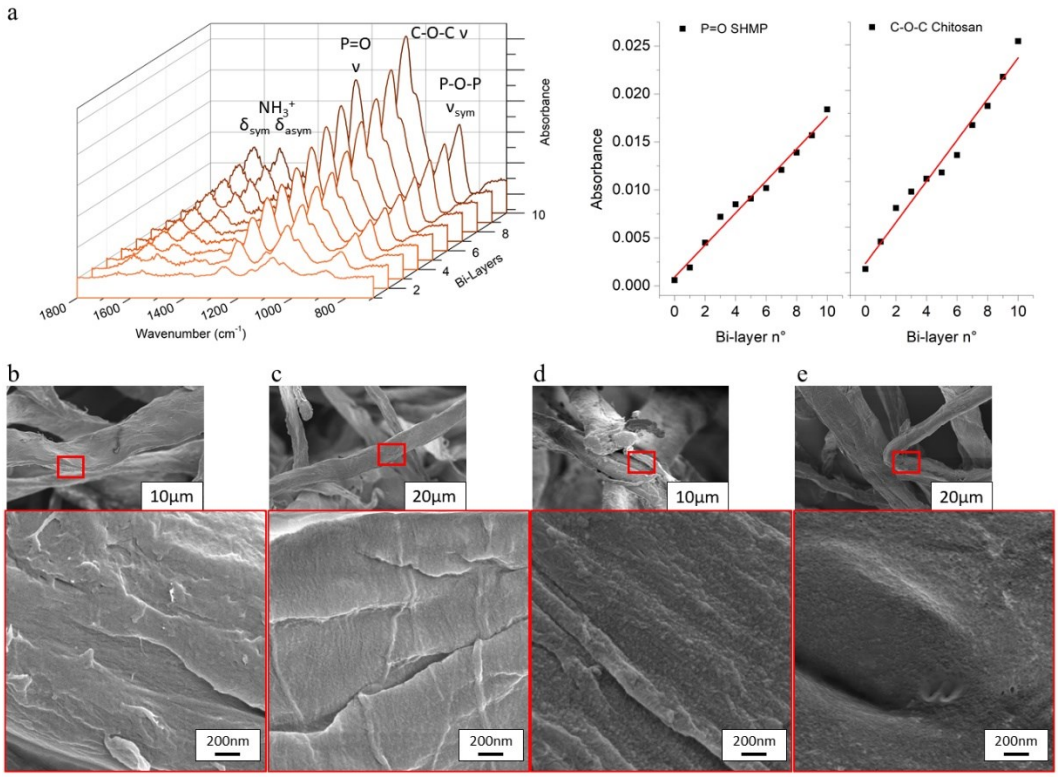


Figure 44: a) FT-IR spectra showing the LbL growth on a silicon wafer substrate, SEM images of b) neat cellulose fibers, c) 1BL, d) 2BL, e) 3BL coated fibers

Cellulose fibers used are the same employed for PUF of chapter 3 and have an average length of 700µm and a width in the range of 10-20µm. By SEM is visible

the typical surface texture and morphology, which does not seem to change much after 1 and 2 BL, indicating the build-up of a very thin coating on the surface. However, after 3BLs, coating became more visible with a change in texture and morphology of the fiber, indeed the formation of a homogeneous coating can be easily observed. **Figure 45** show ATR-IR of fibers, which was used to confirm the LbL coating presence and gather semi-quantitative information about it.

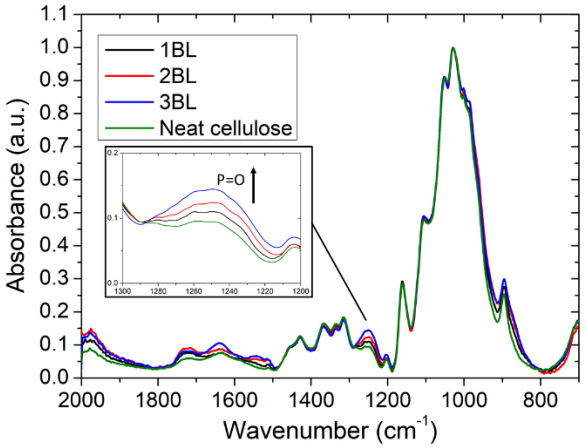


Figure 45: ATR-IR of 1,2 and 3BL coated cellulose fibers vs neat un-coated cellulose

As already seen in the previous chapters, cellulose signals overlap to the most intense peak of CH, making it extremely difficult to spot. Nevertheless, signals related to SHMP such as P=O band are not significantly overlapping to cellulose ones and therefore become a valid target for coating growth evaluation. Even though is not possible to use ATR-IR, in these conditions, for quantitative analysis, it is still possible to notice that its intensity increase by increasing the number of BLs, thus supporting the coating growth. In an attempt to shift from a qualitative point of view to a quantitative one, polyelectrolytes titration was exploited to determine the amount of polyelectrolyte added to fiber surface at each layer. This was possible by titrating the non-adsorbed components after each layer deposition and fiber separation and back-calculating the adsorbed amount knowing the amount of cellulose fibers employed in the deposition. To do so, charge densities of SHMP and CH were calculated and found to be 11.31 meq/g and 6.31 meq/g, respectively, resulting thus in an estimated charge neutralization complexation ratio of 1:2 (w/w). The results of this study are shown in **Figure 46**

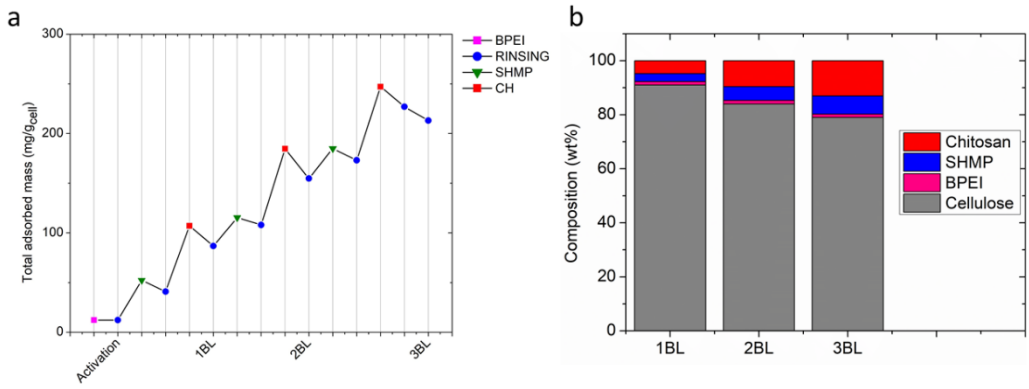


Figure 46: a) Total adsorbed mass for cellulose-rich fibers as evaluated with charge titration for each individual adsorption step including rinsing during the build-up of 3BL, b) composition of dry fibers in %wt., calculated from the charge titration measurement

The adsorbed mass increases steadily after each deposition, confirming that the linear growth observed on silicon wafer was maintained also on cellulose fibers. It can be noticed also that a slight decrease in adsorbed mass happens after each rinsing step, which is likely due to the desorption of excess polyelectrolytes which are loosely bound to the layer. From this analysis it is possible to calculate a coating composition, both respect each component and respect to cellulose fibers. Indeed, coating accounts for 9, 16 and 21% for 1, 2 and 3BL of the total mass of the composite, respectively. CH is the main component of the coating for all compositions, comprising of 53 to 62% of the coating weight. The content of SHMP in the coating account for half the amount of CH, as predicted from the estimated charge neutralization complexation ratio of 1:2 (w/w) calculated from charge density determination.

4.2.2 Low density fiber network forming and characterization

Self-standing porous fiber networks were prepared by freeze-drying suspensions of coated fibers as depicted in **Figure 47**.

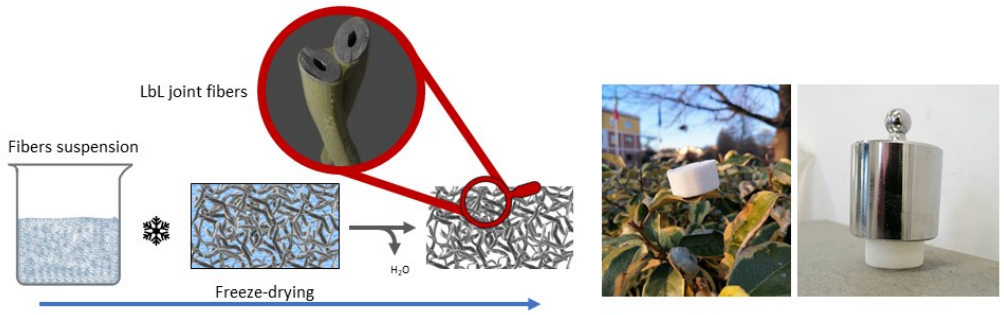


Figure 47: scheme of fiber network preparation

Figure 48 shows digital images of the material prepared from 3BL coated fibers, SEM images at different magnifications and stress/strain plots from compression tests.

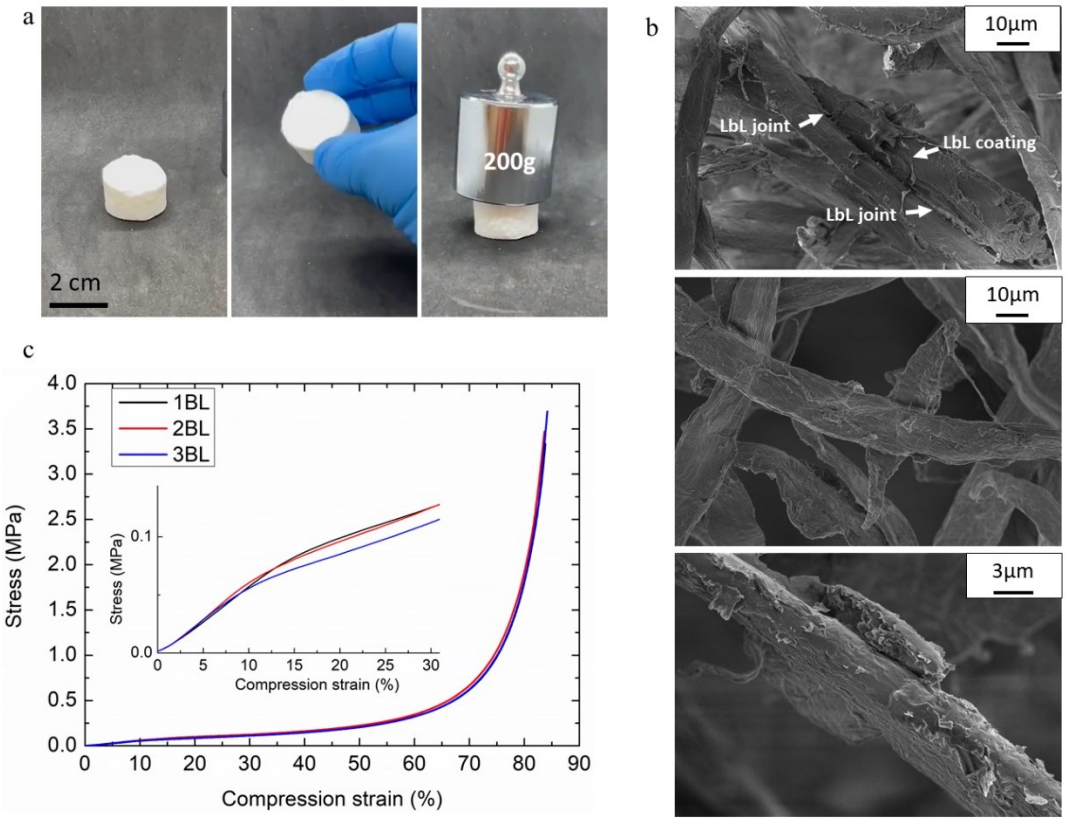


Figure 48: Fiber network morphological and mechanical characterization, a) digital images of the as prepared fiber networks, b) SEM images at different magnification of a 3BL sample in which is visible the coating interconnection between fibers, c) compression stress/strain plots for 1, 2 and3BL samples with an insert showing higher magnification of the compression range 0 to 30%.

Freeze-drying is an already known method for producing lightweight materials based on nanoscale cellulose fibers.(222, 227) As visible in **Figure 48a**, freeze-drying coated cellulose fibers produces porous fiber-network that can be easily handled and does not break when compressed by a static weight (100 times its weight). This result was impossible to obtain by freeze-drying untreated fibers, which results in the formation of an extremely soft structure that collapse when removed from the silicone mold, as visible in **Figure 49**.



Figure 49: untreated fibers after freeze-drying

By looking closely at the fiber network SEM micrographs, it's possible to see that the fibers are frozen in a self-sustaining 3D structure. One of the main contribute to

the structure integrity is the physical interlocking between fibers strong because the fibers are physically connected to each other. However, high magnification micrographs reveal the presence of bridges between fibers due to the interlocking of the LbL coatings as fibers are pushed together by ice crystal formation. Indeed, during the freezing process, fibers tend to be pushed away from each other by the crystals formed, decreasing the distance among them and coming to close contact. This effect, together with the difficulties in preparing a stable structure with untreated cellulose, suggests that coating assert a fundamental role in maintaining the 3D structure of the final network producing an exoskeleton at air/cellulose interface. This film forming joints effect is more visible as the number of BLs increase and for 3BLs the bridges are easier to detect due to the amount of adsorbed coating, as visible in **Figure 48b**. When compressed, samples show the typical behavior of rigid foams. Samples collapse progressively eventually reaching a densification stage at high deformations.(228) As visible from **Figure 48c**, the measured stress/strain plots for 1, 2 and 3BL samples are almost superimposable, suggesting that the modulus and the compression strength are not correlated to the coating amount on fibers a such low BLs number. The materials prepared have an average compression modulus of 0.60 ± 0.03 MPa. Even though it was not possible to produce a reference material made by only un-coated cellulose fibers, it is possible to use similar fiber networks prepared from self-assembled and cross-linked fibers present in literature as comparison.(93) These latter show a compressive modulus ranging from 0.6 to 1.1 MPa, depending on density, while other cellulose-based foams produced with cellulose nanofibrils achieved higher compressive moduli.(229) This suggests that the materials developed in this work could easily be handled and employed as a lightweight panel where no particular mechanical strength is required. A consideration has to be made regarding the components of the LbL coating. Indeed, chitosan and sodium hexametaphosphate were already used in chapter 3 on both long fibers and ballmilled fibers, but their freeze-drying didn't give any sort of porous structure, with fibers that tend to behave like untreated fibers. This shows how the parameters of LbL assembly, such as solution concentration, can influence the final properties if the materials. In this particular case, the concentration used allow a higher content of chitosan in the coating, which, having a good filming capacity thanks to the high number of hydrogen bonds formed, allow the formation of bridges between fibers, helping the formation of stronger structures that can behave in a foam-like style.

4.2.3 Thermal stability

Thermogravimetric analyses in nitrogen and air were used to investigate the thermal and thermo-oxidative stability of the prepared fiber networks. Collected plots are reported in **Figure 50** and their numerical data are reported in **Table 9.**

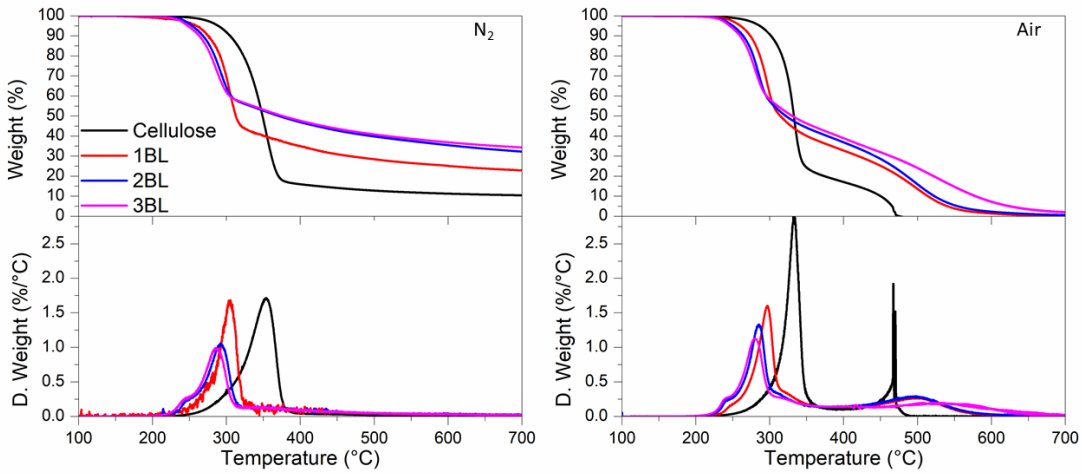


Figure 50: TG plots of neat cellulose and 1, 2 and 3 BL fiber networks in a) nitrogen and b) air

Table 9: data from thermogravimetric analysis of neat and coated fibers

		$T_{on,\ 5\%}$ (°C)	Residue at 500°C (%)	Residue at 800°C (%)
N_2	**Cellulose**	289	13	10
	1BL	260	28	22
	2BL	254	40	30
	3BL	248	41	33
Air	**Cellulose**	284	0	<1%
	1BL	261	14	<1%
	2BL	250	16	<1%
	3BL	246	24	<1

In inert atmosphere, cellulose shows its well-known single decomposition step, as already described in chapter 2.2.2. Meanwhile, LbL-treated cellulose fiber exhibit an early decomposition ($T_{on5\%}$ of 289 and 260°C for neat cellulose and coated fibers, respectively), which is generally reported for phosphate containing systems, as visible also for assemblies in chapter 2 and 3. This effect is considered positive since it favors the cellulose decomposition towards char formation(194) and results in the release of a reduced amount of volatile combustible products.(144) An

increase of up to 33% (for 3BL sample) can be observed in the final residues at 800°C indicating a substantial improvement in cellulose char formation. Interestingly, the amount of residue collected at the end of the test does not increase with the number of deposited BL in a proportional way, suggesting that increasing the number of deposited BL produces diminishing results in char formation during TG tests. Such behavior, suggest that good char forming efficiency can be achieved even at low BL numbers, as already observed on other cellulose-based substrates and as seen in previous chapters.(217) In air, cellulose undergo a two steps thermal oxidation path as previously described in chapter 2. Also, in oxidative environment the presence of the LbL coating anticipate the thermal decomposition and increase the char formation during the first step, with a residual weight at 400°C that is nearly double for LbL coated fibers respect to untreated fibers. The oxidation of such residues occurs gradually and persist up to higher temperatures than neat cellulose, suggesting thus a more stable residue. Indeed, at 600°C, 3Bl coated fibers still show a residual 10% weight, evidencing thus how the presence of the coating can simultaneously improve the quality and amount of char produced. This occurs as a consequence of the double effect exerted by SHMP that can directly improve the cellulose char formation while also building up a protective insulating layer with CH, which further improves char production due to a heat shielding effect.(217)

4.2.4 Flammability and combustion properties

To investigate the flame-retardant properties of the prepared fiber networks, flammability tests (in both horizontal and vertical configuration) and forced combustion tests by cone calorimetry have been performed. **Figure 51** collects digital images of the samples during flammability tests and numeric values are reported in Errore. L'origine riferimento non è stata trovata.**.** Results were compared to a commercial rigid PUF with similar density.

Table 10: Flammability test data

	Horizontal		**Vertical**	
Sample	After-flame time (s)	Residue (%)	After-flame time (s)	Residue (%)
C700	215 ± 1	2 ± 1	/	/
1 BL	26 ± 1	94 ± 1	37 ± 1	9 ± 1
2 BL	5 ± 3	98 ± 1	5 ± 1	89 ± 1
3 BL	<1	98 ± 1	<1	88 ± 1
PU	110 ± 10	30 ± 10	75 ± 5	40 ± 2

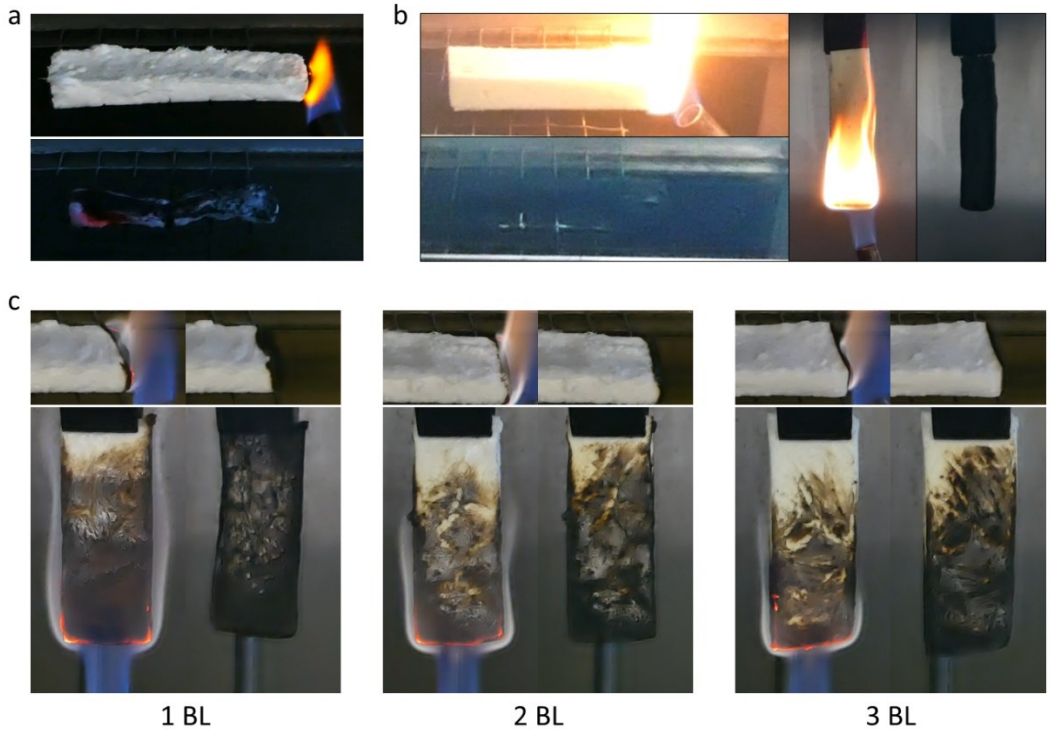


Figure 51: Flammability test snapshots of a) horizontal flame test of freeze-dried neat cellulose, b) horizontal and vertical flame test snapshot of a commercial PU foams, c) horizontal and vertical flame test for 1BL, 2BL, and 3BL foams (from left to right) with the flame and after the flame was removed

Flammability in horizontal configuration was firstly evaluated as this is typically adopted for foamed materials. Sample behavior was compared to untreated cellulose, compacted in the same shape and density as samples of fiber network, and to a commercially available rigid polyurethane foam. this latter has been selected as comparison due to the widespread use of this class of foams in many industrial products and applications.(230)

Upon exposure to the methane flame the neat cellulose fibers quickly ignite and undergo complete combustion with vigorous flames. Sample prepared with coated fibers present a different behavior. Indeed, with only 1 BL deposited, after ignition the flame is not able to spread and it rapidly extinguishes leaving the majority of the sample intact. An improved effect was visible for 2BL and 3BL samples, which self-extinguished the flame immediately after removal of the methane flame. Flammability in vertical configuration was also performed. This setup has harsher conditions respect to the horizontal one. Conventionally is considered a key test for evaluating the fire safety of dense materials such as nanocomposites and polymer composites.(231) The 1BL sample burned completely after the methane flame removal forming a stable carbon structure. However, 2BL samples extinguished the flame after few seconds, leaving the structure of the sample almost intact, in a classic example of self-extinguishing behavior. 3BL samples gave the best results as it self-extinguished immediately after methane flame was removed, leaving a charred residue only where the flame was directly applied. Such results clearly point

out the extreme fire safety achieved by the fiber networks especially if compared with the reference commercial PU foams that burned completely during both horizontal and vertical flame tests. Forced combustion tests were also performed evaluating the reaction of the samples when exposed to an irradiating heat flux of 35 kW/m^2, which is a value typically found in developing fires. **Figure 52** collects cone calorimetry plots associated to HRR and SPR as well as their integral values, numerical data are visible in **Table 11.** As for flammability tests, neat cellulose fibers and commercial PUF were employed as reference sample.

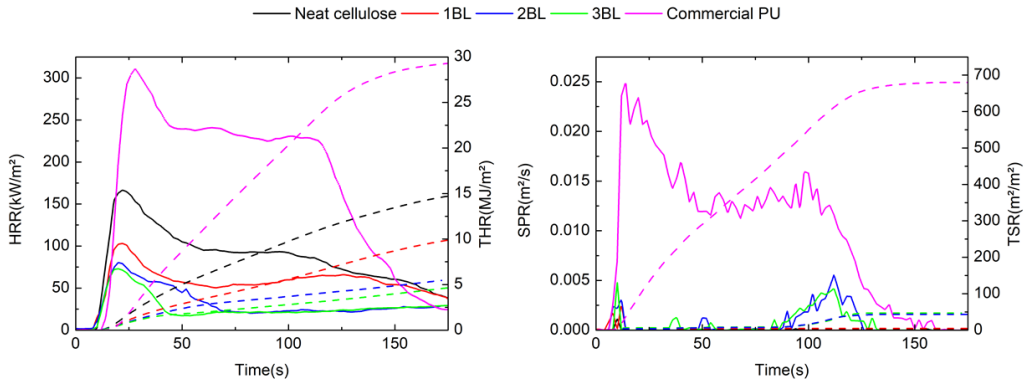


Figure 52: Heat release rate (HRR), total heat release rate (THR), smoke production rate (SPR) and total smoke release (TSR) for porous fibers network and PUF

Table 11: Time to ignition (TTI), heat release rate (HRR), total heat release (THR) and total smoke production (TSR) from cone calorimetry

Sample	TTI (s)	HRR_{peak} (kW/m^2)	T peak (s)	THR (MJ/m^2)	TSR (m^2/m^2)	EHC (MJ/Kg)	Residue (%)
Cellulose	10 ± 1	167 ± 2	23 ± 1	16.5 ± 0.4	1.2 ± 0.2	9.8 ± 0.1	< 1
1 BL	9 ± 1	105 ± 7	21 ± 2	13.9 ± 1.6	4.2 ± 3.0	9.8 ± 0.6	5.5 ± 0.7
2 BL	9 ± 1	83 ± 1	20 ± 2	6.9 ± 0.5	33.7 ± 14.1	5.9 ± 2.2	16.1 ± 3.5
3 BL	9 ± 1	73 ± 1	19 ± 1	4.2 ± 0.9	42.2 ± 18.9	4.0 ± 0.7	22.9 ± 1.4
PU	9 ± 1	311 ± 24	28 ± 1	31.0 ± 1.6	679.4 ± 37.8	19.7 ± 1.1	20.9 ± 1.1

Neat cellulose fibers quickly ignite and burn with vigorous flames reaching a pkHRR of 167 kW/m^2 leaving almost no residue (final residue < 1%). The burning behavior of the fibers assembled in the porous networks is greatly influenced by the presence of LbL coating. Indeed, during combustion an extensive charring of the samples occurs allowing the samples to maintain their original shape and structure. This leads to conspicuous reductions in both pkHRR and THR values. A single BL produces a 38% reduction in pkHRR and 31% in THR thus showing the great FR potential of this system. The best performances were obtained with 3BL with a pkHRR and THR reduction of 56% and 68%, respectively. It is worth highlighting that 2 and 3BLs samples achieve extremely low HRR values (below 100 kW/m^2),

which are well below the reference PU foam and similar to high performing foams such as phenolic resins.(232) The char forming properties of the SHMP/CH pair is at the basis of these excellent results, by producing a thermally stable carbonaceous structure they protect the underneath fiber by limiting heat and mass transfer. Moreover, thanks to the presence of SHMP and the protective structures, the release of combustible volatiles from the sample is limited, favoring thus the cellulose char formation. This results in a single BL is that is enough to stop flame spread in horizontal configuration since after ignition the release of flammable volatiles is not enough to sustain combustion leading to a self-extinguishing behavior even after multiple flame applications. When 2 and 3BL are used, the flame-retardant properties are further improved, with the same results obtained also in vertical configuration. By cone calorimetry, the above-mentioned phenomena considerably hinder the combustion rates of the samples and is visible in a strong reduction in pkHRR and THR values. The downside of this inefficient combustion is the inevitable in TSR values with respect to neat cellulose. However, it is worth mentioning that TSR values commonly measured for synthetic foams are typically one order of magnitude higher than what measured for these LbL-stabilized fiber networks as evidenced by the results achieved by the employed rigid PU reference (679.4 Vs 42.2 m^2/m^2 for the PU and the 3BLs sample, respectively). Smoke is one of the biggest dangers during an evolving fire and is considered one of the main causes associated to fire casualties. This due to its incapacitating effects that prevent people from escape and produce long term damage.(233) The relatively low TSR values measured further highlight the potentialities of the prepared fiber networks in replacing commercial petroleum-based foams. This fact can be further highlighted by performing a comparison of pkHRR and TSR from cone calorimetry tests of other FR rigid foam from the literature background (**Figure 53**).(234-240)

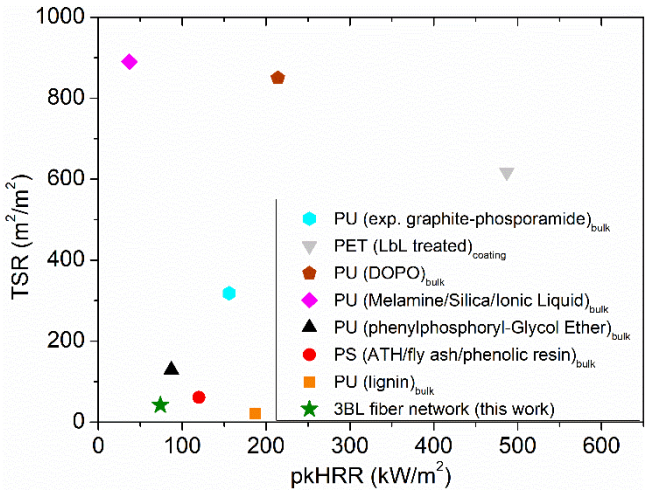


Figure 53: Comparison of cone calorimetry results of different rigid FR foams from the literature background. PET: polyethylene terephthalate, PS: polystyrene, DOPO: 9, 10-dihydro-9-oxa-10-phosphaphenanthrene-10-oxide, ATH: aluminumtrihydroxide

The performed comparison clearly highlights how the limited pkHRR and TSR values of the porous fiber networks prepared in this manuscript actually outperform the values achieved by widely employed rigid foams such as PS, PET and PU.

4.2.5 Post combustion residue analysis

The combustion residues collected after cone calorimetry tests were characterized by means of SEM and Raman. **Figure 54** collects the SEM micrographs of residue obtained from cone calorimetry for porous fibers network coming from treated fibers.

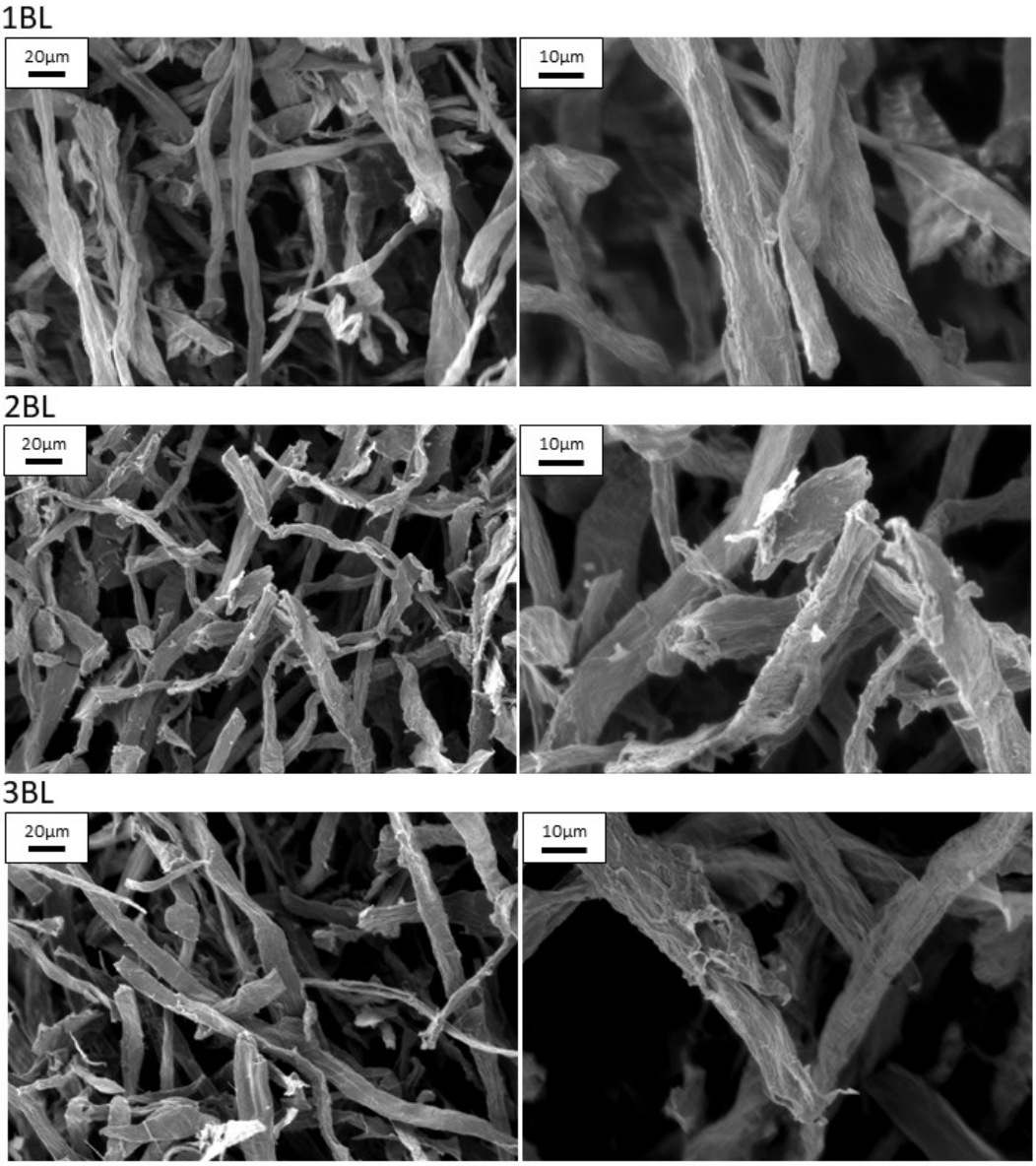


Figure 54: SEM micrographs of porous fibers network from LbL coated fibers

A self-sustaining residue which can be easily handled is produced after combustion of fiber networks prepared from coated cellulose. This is particularly visible for 2 and 3 BL samples, which are also the best performing samples. SEM investigations show a structure that resembles the one of the unburned fiber-network with coating

that becomes more wrinkled due the char formation processes that occurred during combustion. No significantly differences are visible between residues coming from 1, 2 and 3 BLs at this magnification. This indicate the formation of a homogenous char all along fibers, even at low BLs number. Raman spectra of residues are visible in **Figure 55.**

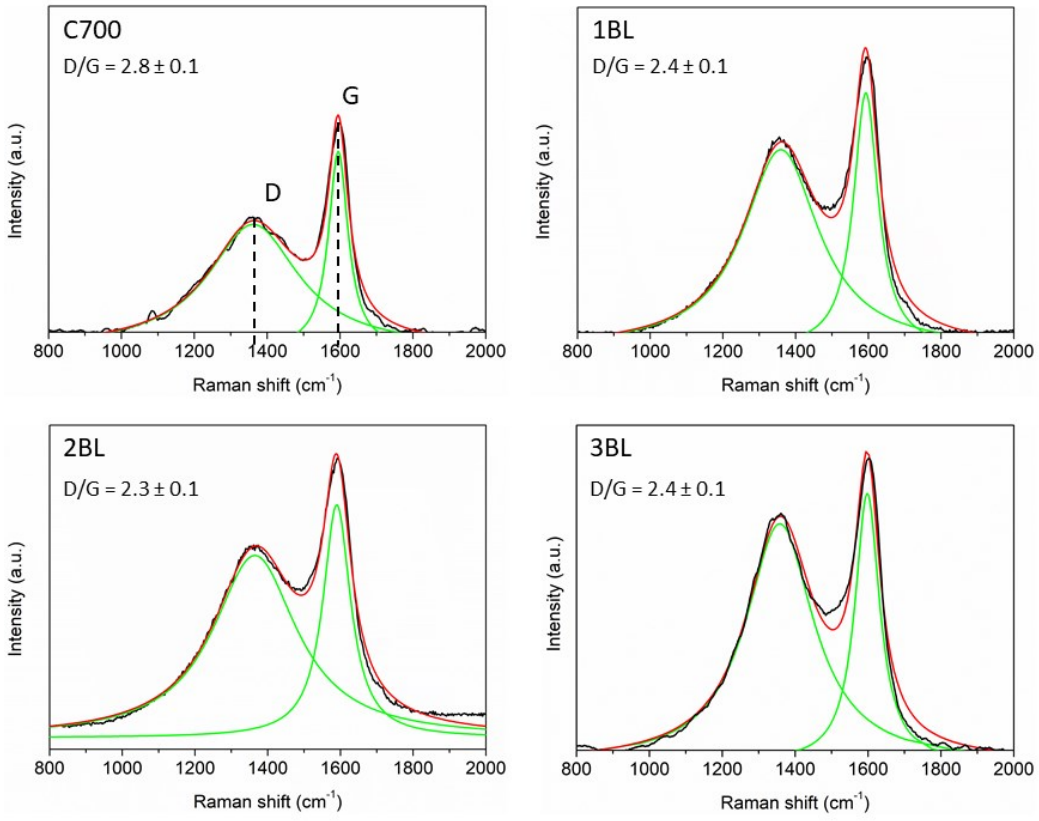


Figure 55: Raman spectra of fiber network residues with deconvoluted fittings of peak D and G

Raman spectroscopy points out the formation of two characteristic signals known as G and D bands normally found in graphene and graphene related materials.(241) The G-band is linked to the stretching of sp^2 carbons and is the primary mode in graphene and graphite. The D-band is known as the disorder- or defect-band and is normally associated to the presence of edges, curvature and inclusions close to sp^2 carbon rings. These latter two bands are often broadened in residues produced from cellulose pyrolysis, as results of the contribution of several additional peaks associated to the complexity of the structures produced upon thermal decomposition.(242) This is also observed, for the D band, on the Raman spectrum of the shrunken and brittle residue collected from neat cellulose after cone calorimetry. Conversely, the presence of a well-defined G and D bands suggests an improved graphitization degree of the cellulose network (**Figure 54** and **Figure 55**). The evaluation of the ratio between the area underneath the G and D bands, which is often employed to evaluate the quality of the produced char structure, support this hypothesis. The collected signals present D/G values similar to what already reported for graphene oxide containing combustion residues, ranging from 2.2 to

2.4.(181) 1 and 2 BLs fiber networks show similar results (Figure 55: Raman spectra of fiber network residues with deconvoluted fittings of peak D and G). This further confirms the crucial role of the LbL coating in promoting cellulose char forming decomposition pathways that considerably reduce the production of combustible volatiles.

A preliminary FR mechanism for these LbL-enabled fiber networks can be therefore hypothesized based on the performed characterization and it is illustrated in **Figure 56** and described in more details below.

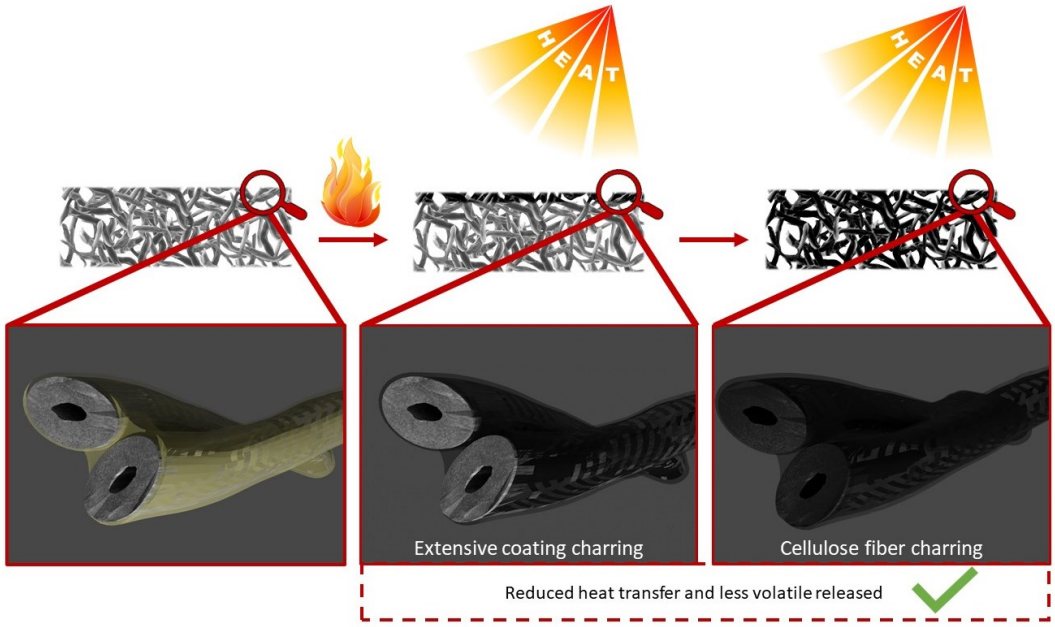


Figure 56: Schematic representation of the fiber network flame-retardant mechanism upon exposure to a flame or heat flux

When exposure to a flame or a heat flux, CH undergoes extensive charring thanks to the presence of SHMP,.(173) SHMP also favors the dehydration of cellulose glycosyl units towards the production of a thermally stable char. The coating charring helps in maintaining the fiber network structural integrity thus resulting in reduced heating rates that also promote cellulose char production from the bulk.(243) The overall process considerably limits the amount of volatiles feeding to the flame thus producing the observed self-extinguishing behavior in flammability tests and low heat release rates during cone calorimetry. Such high FR efficiency can thus be ascribed to the homogeneity of the deposited CH/SHMP assembly that can exert a considerable FR effect even at such low BL numbers by producing a continuous exoskeleton at the air/cellulose interface. These results are comparable to what reported in literature for studies with similar assemblies, comprising SHMP and CH, on cotton fabrics. However, it has to be noticed that higher add-ons were obtained when single fibers are used instead of fabrics, such as this study. This allows to reduce the number of BLs necessary to have a

significant flame-retardant effect, with evident flame retardancy even after 1BL, respect to 10-15 BLS required for textiles, evidencing the great potentiality of this approach. (100, 244)

4.3 Phy-CNF-Ch assemblies results and discussion

4.3.1 Coating growth and assembly on fibers

A first evaluation of the lbl assembly was obtained by depositing Phy1CNF0.2 on a mode substrate and IR spectra collected are presented in **Figure 57**. IR spectra analysis of pure chemicals, such as BPEI, CH and Phy are reported in chapter 2.2.1 and they will not be further discussed. BPEI was used to improve adhesion between the assembly and the substrate, as in chapter 2 and 3.

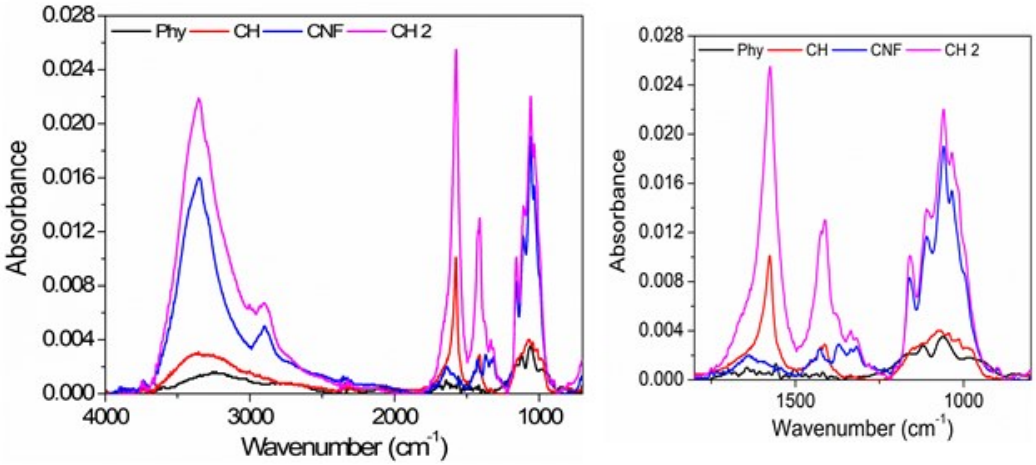


Figure 57: IR spectra of Phy-CH-CNF assembly on Si-wafer, with magnification of portion between 1800 and 850 cm[1]

As visible from **Figure 57**, each layer deposited on Si wafer give the characteristic peaks associated to the component deposited. This can be easily seen in the increase of peak at 1074 cm^{-1} associated to C-O-C stretching vibrations of chitosan.(181) However, due to the fact that this study focus its attention on the deposition of few layers, only 1 QL were measured, confirming the assembly growth. To study the influence of deposition solution concentration, three systems with different concentration of Phy and CNF were evaluated and polyelectrolyte titrations were used to investigate the differences in coating composition as consequence of it. Results obtained are visible in **Figure 58**.

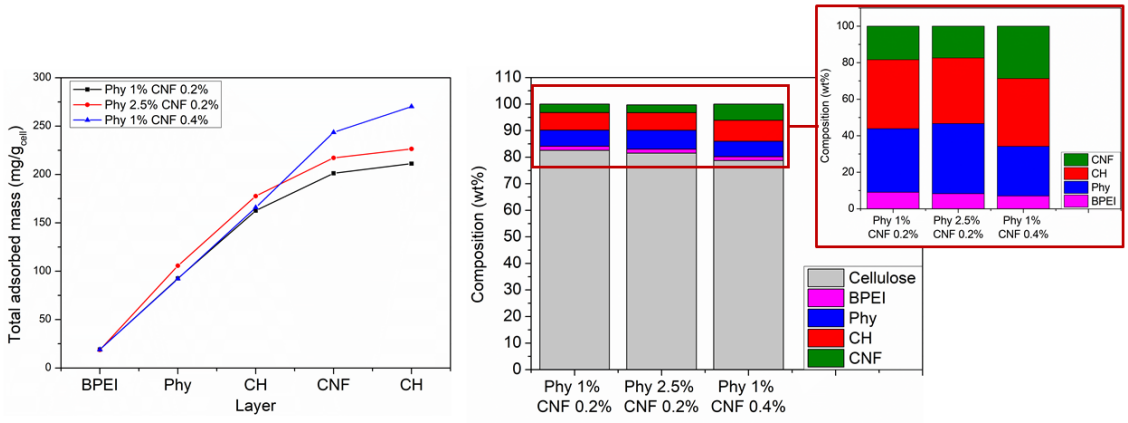


Figure 58: polyelectrolytes titration results with total adsorbed mass after each deposited layer, coated fibers composition and coating composition

Polyelectrolytes titration allow to determine the amount of each polyelectrolyte assembled on fibers, which is back calculated from the non-adsorbed components after each step.(226) The charge densities of Phy and CNF were found to be 6 meq/g and 0.51 meq/g, respectively, while CH charge density was 5.33 meq/g due to the pH change respect to previous study. Results obtained show that the use of solution at higher concentration during the deposition gives an increase in deposited polyelectrolytes. Indeed, increasing Phy solution concentration from 1 to 2.5%, leads to a 20% increase in the deposited amount of Phy on cellulose, while CNF is almost doubled when the solution concentration is increased to 0.4%wt. This points out the possibility to tailor the coating composition by changing the deposition conditions as a possible alternative way respect to increase the layer numbers. The morphology of the so coated fibers was investigated by SEM. Collected micrographs are reported in **Figure 59**.

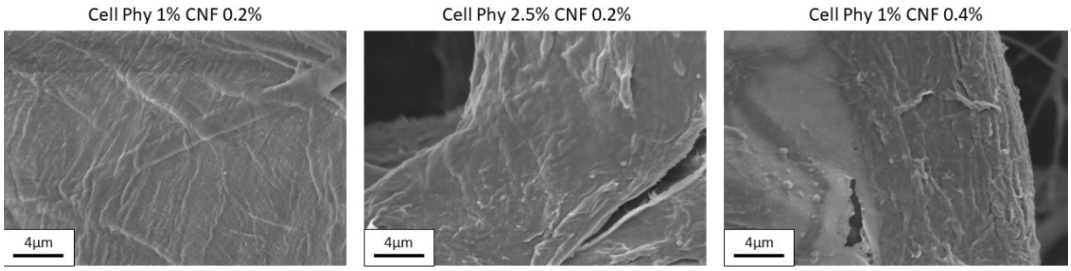


Figure 59: SEM micrographs of coated fibers

Compared to typical morphology of natural fibers, visible in chapter 3.2.2, lbl treated fibers present a homogeneous coating with cellulose nanofibrils that can be seen as part of the coating. The three systems do not show particular differences among each other, nevertheless, comparing the coated fiber with materials obtained in chapter 4.2 it's possible to notice a thicker coating with a higher tendency of film formation, with add-ons comparable, if not higher than 2BL of SHMP-CH coating.

4.3.2 Low density fiber network morphology and mechanical properties

Low density fiber networks were prepared by freeze-drying as reported in chapter 4.2. Freeze-drying of coated fibers produce self-standing porous materials which can be easily handled with a density of 85 ± 3 kg/m^3. The 3D microstructure of the obtained fiber networks was investigated via SEM analysis and their images are visible in **Figure 60.**

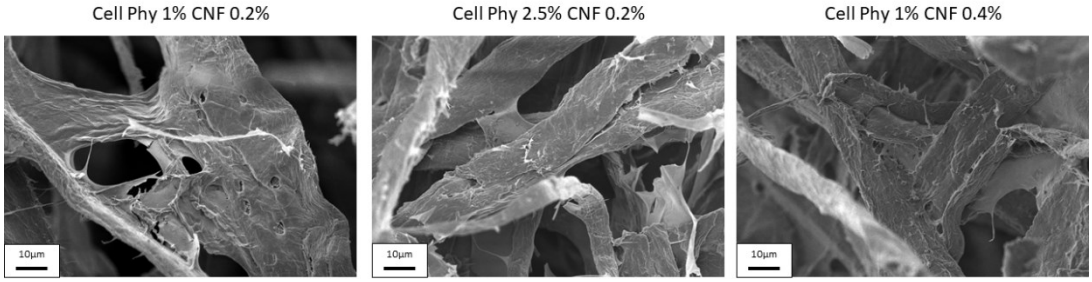


Figure 60: SEM micrographs of lightweight fiber-networks obtained from freeze drying

Obtained materials were compared to ones previously described in chapter 4.2. As for previous materials, the structural integrity is given principally by the physical interlocking of fibers due to the lbl coating. However, the presence of both chitosan and cellulose nanofibers, which are well known for their filming abilities,(245, 246) increase significantly the contribute given by the coating. Indeed, the coating acts as a sort of exoskeleton on fibers producing well visible bridges among them, as visible in **Figure 60.** It has to be noticed that this effect seems to be more prominent in Phy1%CNF0.4% coated fibers, probably due to the higher CNF content. To investigate the effect of the employed different concentrations on mechanical properties compressive strength tests were performed and data collected are presented in **Figure 61**.

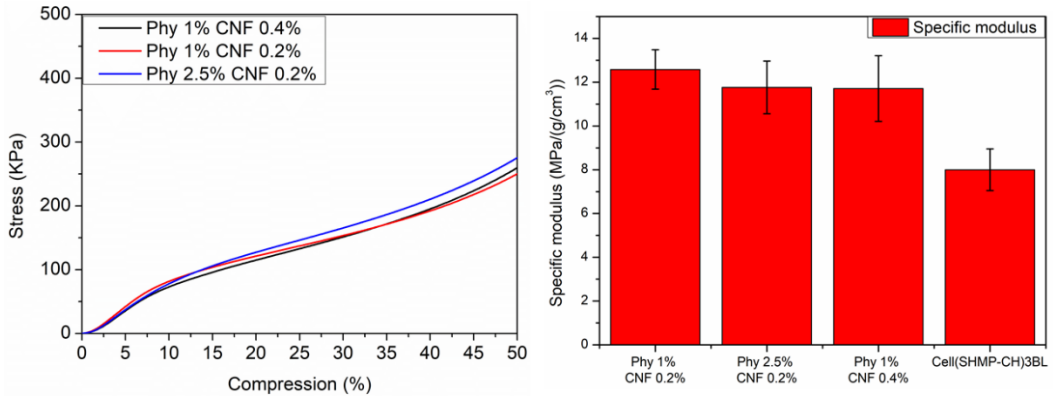


Figure 61: Compression stress test for cellulose lightweight materials and comparison with previously obtained one

The obtained fibers-networks behave like rigid open cells foams. Indeed, when compressed, samples show a progressive collapse of inner structure which lead to a densification stage at high compression, as commonly occurs for rigid foams.(181) Compressive modulus present a slight increase respect to fiber-networks prepared previously, indicating a reinforcing effect given by cellulose nanofibers, which can be mainly attributed to the formation of an higher number of bridge between fibers, as visible in **Figure 60**. However, no significant variations can be seen among the three systems, which present modulus ranging from 0.95 ± 0.04 MPa of Phy2.5%CNF0.2% to 1.05 ± 0.03 MPa of Phy1%CNF0.2%. These results are comparable to what obtained in literature from similar porous fiber network prepared from self-assembled and cross-linked cellulose fibers.(93) Cellulose porous fiber-networks thermal conductivities were also measured and compared to materials reported in literature, as visible in **Figure 62**.

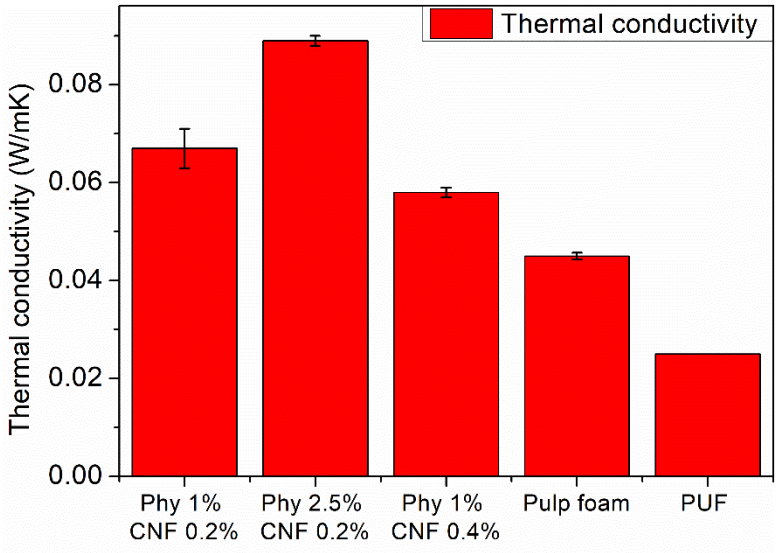


Figure 62: thermal conductivity of lightweight materials from this work compared to a pulp foam made by borate crosslinking and a water-blown PUF of similar density. (134, 243)

Thermal conductivities of obtained cellulose porous lightweight materials fall all below 0.1 W/mK with the best performing one reaching 0.058 W/mK, which is the one containing more CNF. However, compared to common materials like PUF, all samples present higher conductivities.

4.3.3 Fire-retardant properties

Flame-retardancy of obtained materials was tested by horizontal flammability test and cone calorimetry. Pictures from flammability test of Phy1CNF0.2 are visible in **Figure 63**, while cone calorimetry data are available in **Figure 64** and **Table 12.**

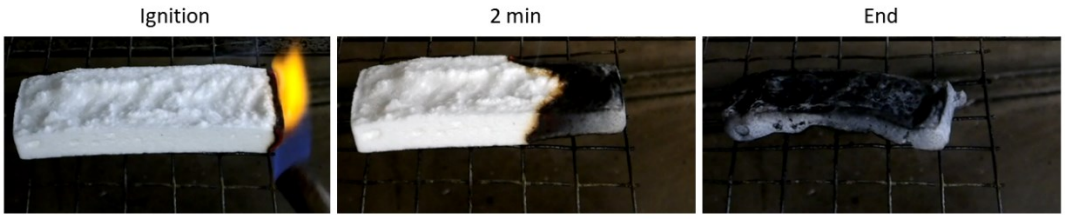


Figure 63: Smoldering during flammability test of Phy1CNF0.2

Phy1CNF0.2 extinguish the flame after few seconds, while phy2.5CNF0.2 and Phy1CNF0.4 extinguish the flame as soon as the methane flame is removed. However, all samples presented smoldering, which slowly consume completely the sample, leaving a fragile residue accounting less than 3% of residue respect of initial weight, as visible **Figure 64**.

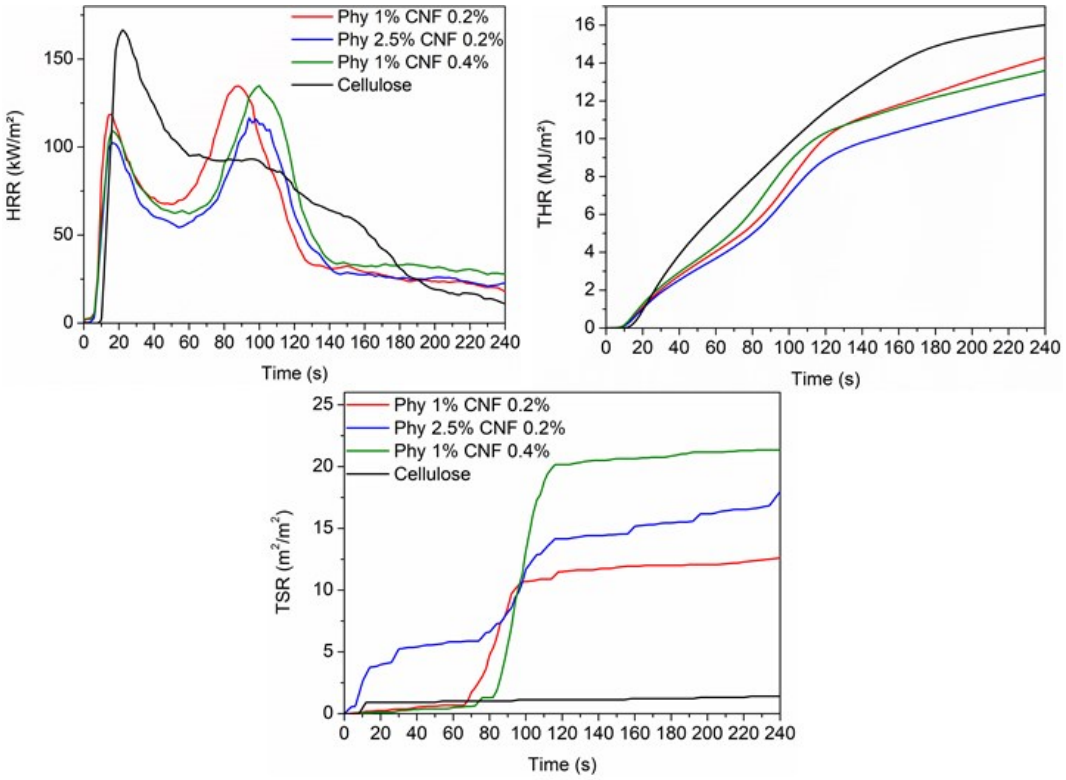


Figure 64: cone calorimetry data for cellulose based porous lightweight materials

Table 12: cone calorimetry data

Sample	TTI (s)	HRR_{peak} (kW/m^2)	T peak (s)	THR (MJ/m^2)	TSR (m^2/m^2)	EHC (MJ/Kg)	Residue (%)
Cellulose	10 ± 1	167 ± 2	23 ± 1	16.5 ± 0.4	1.2 ± 0.2	9.8 ± 0.1	< 1
Phy1% CNF0.2%	6 ± 2	141 ± 4	89 ± 7	13.5 ± 0.5	12.2 ± 6	11.7 ± 0.5	2.4 ± 0.2
Phy2.5% CNF0.2%	6 ± 2	125 ± 7	97 ± 7	12.4 ± 0.2	16.4 ± 1.5	11.5 ± 0.5	3.2 ± 0.2
Phy1% CNF0.4%	6 ± 2	141 ± 5	101 ± 1	14.5 ± 0.8	21.9 ± 2.8	11.7 ± 0.6	2.2 ± 0.2

Compared to untreated cellulose fibers, which was discussed in chapter 4.2.4, treated cellulose present lower pkHRR and THR. Indeed, during combustion a protective char layer is formed on the sample surface, producing a decrease in pkHRR. However, as already seen in other materials like wood,(247) after few seconds the protective char layer breaks and the sample underneath is consumed, producing a second HRR peak. A small difference can be seen in between samples made with less Phy and one with higher concentration. However, this small difference falls in the error range, resulting not enough to provide useful information.

4.4 Conclusions

The preparation of low density, flame-retardant fiber network has been discussed in this chapter. In the first part, the LbL approach was used to coat fibers surface with an assembly comprising chitosan and sodium hexametaphosphate, with the aim of building a flame-retardant coating able to improve the fiber-fiber adhesion. Prior to fibers functionalization, LbL assembly growth was studied on a model substrate, such as silicon wafer, which shows the typical behavior of a linear growing, such as seen in chapter 3.2.1. Moreover, the composition of the coating in the first 3 BLs was studied by polyelectrolyte titration. Thanks to this, it was possible to calculate the percentage composition of coating, with chitosan accounting for the 63% wt. of it at 3BL, while SHMP account to 32%. Cellulose content was estimated to be in the range between 80 to 90%. Freeze-drying was used to prepare porous fiber networks with 1, 2 and 3 BLs treated cellulose fibers. The coating has been proved to contribute to increase the fiber-fiber interactions by forming bridge-like structures, becoming a key factor for the formation of self-sustainable lightweight materials. The so enabled 3D structure show open porosities where cellulose fibers are interconnected by the coating. The flame retardancy of these lightweight materials has been assessed by flammability test and cone calorimetry. Fibers network coming from coated cellulose fibers were able to self-extinguish the flame both in horizontal and vertical configuration, with 3BL fibers leaving the highest residue. Extremely low combustion rate was displayed by 3BL coated fibers lightweight materials, with values lower than 100 kW/m^2 and extremely low smoke production, accounted to be one magnitude lower than

commercially available PU foams. After burning, a carbonaceous structure on cellulose fibers is formed, which maintains intact the shape of original fibers. The result is a self-sustaining residue that does not collapse. Such results are comparable to ones obtained using synthetic polymers and are even more impressive considering the high amount of cellulose involved. The major limitations of these materials were found to be related to the limited mechanical properties and, consequently, to non-optimal fiber-fiber interactions. For these reasons, in the second part of the study, a quad-layer comprising cellulose nanofibers was investigated, aiming at an improvement of fiber-fiber interactions and increase in mechanical properties. Moreover, phytic acid was included as bio-based flame retardant and three different deposition conditions were investigated, each of them resulting in three coatings with different polyelectrolytes contents. Long cellulose fibers were coated with a system made by the sequence Phy-CH-CNF-CH and then freeze-dried following the same procedure used for SHMP-CH ones, resulting in the production of porous lightweight fiber-networks. Three deposition conditions were evaluated, in which Phy and CNF concentration of deposition solutions were changed, resulting in three different coatings on cellulose fibers. The composition of each coating was investigated by polyelectrolyte titrations, resulting in samples with an average 80% cellulose content and different coating composition. Indeed, it has been proved that solutions with higher concentration deposit on fibers a higher quantity of polyelectrolytes, with CNF content in the coating increasing from 17% to 29% when solution concentration was increased from 0.2% to 0.4%. Regarding this, CNF has proven to be beneficial in increase interactions among fibers, favoring the formation of bridges of coating which connects fibers together, resulting in a 66% increase in modulus respect of SHMP-CH assembly. However, among the different systems evaluated, the concentration of CNF in the coating was not relevant, resulting in samples with nearly identical compressive moduli. Phytic acid content, on the contrary, presents a slight influence on flame-retardant properties. Indeed, samples with a higher content of Phy, present a 25% reduction respect to neat cellulose. Even though the obtained materials present lower pkHRR and THR respect of neat cellulose, the fire-retardant properties are not as good as ones for lightweight materials obtained from SHMP-CH coated fibers. This could be ascribed to a better flame-retardant efficiency of SHMP.

5. General conclusions and future perspectives

The versatility of LbL approach as tool for producing fiber-based materials has been investigated through the last three chapters, with application ranging from bulk polymers, like PBS, and low-density materials. Cellulose fibers were selected as universal substrate for surface modification and its application in the different fields. Cellulose fibers have a natural hydrophilicity that, when coupled with functional groups resulting from pulping processes, favor the deposition of polyelectrolytes. With this in mind, BPEI was selected as anchoring layer for all assemblies proposed in this elaborate, which showed to be effective in promoting the subsequent growth of polyelectrolytes layers.

In chapter 2, cellulose fibers were employed in the fabrication of PBS composites with maximum loading of 30%. Two hybrid organic-inorganic systems were proposed for that application, with both of them comprising halloysite nanotubes suspended in chitosan coupled with either ammonium polyphosphate or phytic acid. The principal results obtained can be summarized as follow:

- Both coatings were successfully assembled up to 6BL on cellulose fibers and used to prepared composites.
- Coated fibers can be melt-blended with PBS yielding composites with up to 30% content of fibers
- The composite mechanical properties were not modified by LbL
- The flame-retardant properties were improved resulting in lower pkHRR and formulations with self-extinguishing behavior

In chapter 3, long cellulose fibers and ballmilled fibers were coated with two different LbL assemblies and used to prepare PUF composites. The use of LbL on fibers allowed to obtain:

- Both long fibers and ballmilled cellulose were coated with APP-CH or SHMP-CH assemblies up to 5BL which imparted them flame-retardant properties
- Coated fibers can be used to prepare PUF composites with content up to 15phr for ballmilled cellulose and 7.5phr for long fibers
- Thermal conductivities PUF were not significantly affected by coated cellulose
- The flame-retardant properties of PUF composites were improved in term of pkHRR reduction and smoke production

In chapter 4, long cellulose fibers were coated with two lbl systems and used to produce self-standing lightweight fiber-networks by freeze-drying. Resulting in:

- Both systems produced lightweight materials that can be easily handled, are self-sustaining and can bear moderate loads
- CNF has been proved to improve mechanical properties when used as component in a lbl assembly
- Materials obtained from SHMP-CH assembly resulted in enhanced flame-retardant properties

Results obtained evidenced the great flexibility of LbL approach as viable method to modify cellulose fibers surface, introducing functionalities and improving adhesion with matrix of various nature. However, further studies need to be carried out to overcome the showed limitations. Indeed, even if in chapter 3 was visible an improvement in the fiber-matrix adhesion, more work needs to be done to further improve it. Moreover, it lacks a complete processing study which consider all processing parameters commonly used. To this aim future studies should be focused on:

- Evaluation of ending layers in order to improve the affinity with PBS matrix
- In-deep investigation of processing parameters, such as temperature, residence time and screw speed, with Phy-CH/Hal coated fibers, as shown to be the most effective of the two
- Evaluating the effect of increasing cellulose content in the final composite

The use of cellulose fibers in PUF biocomposites also showed some limitations. Indeed, cellulose content was limited by its shape, with a maximum content of 7.5phr of long fibers obtained, contraposed to 15phr when ballmilled fibers were used. LbL approach presented promising results, even though the decrease in flammability was not outstanding. Possible solutions could be:

- Increase cellulose content
- Study of LbL coating with higher BLs number and alternative formulations

Cellulose lightweight materials presented in this thesis present great potentiality to be exploited as insulation materials. However, more studies need to be done focusing majorly the process sustainability. Indeed, freeze-drying of solutions for obtaining lightweight materials is a widely used procedure at research level, which however does not scale-up well. This leads to the necessity to find alternative processes that can transfer results obtained in the small-scale research to an industrial product. Possible routes can be:

- Evaluation of alternative, ambient pressure, foaming methods, such as surfactant aided foaming.
- Being new materials with interesting properties, a study of the environmental impact compared to commercial common insulation materials should be performed

- Evaluation for a reduction in density for CNF containing materials for improving thermal insulations properties

6. References

1. (2023) O. Global Plastics Outlook: Plastics use by polymer - projections
2. Directive (EU) 2019/904 of the European Parliament and of the Council of 5 June 2019 on the reduction of the impact of certain plastic products on the environment, (2019).
3. Ramamoorthy SK, Skrifvars M, Persson A. A Review of Natural Fibers Used in Biocomposites: Plant, Animal and Regenerated Cellulose Fibers. Polymer Reviews. 2015;55(1):107-62.
4. Neto GCdO, Micheline Maia Teixeira, Gabriel Luis Victorino Souza, Valquiria Demarchi Arns, Tucci HNP, Amorim M. Assessment of the Eco-Efficiency of the Circular Economy in the Recovery of Cellulose from the Shredding of TextileWaste. Polymers. 2022;14:1317.
5. Seki Y, Selli F, Erdoğan ÜH, Atagür M, Seydibeyoğlu MÖ. A review on alternative raw materials for sustainable production: novel plant fibers. Cellulose. 2022;29(9):4877-918.
6. Jagadeesh P, Puttegowda M, Boonyasopon P, Rangappa SM, Khan A, Siengchin S. Recent developments and challenges in natural fiber composites: A review. Polymer Composites. 2022;43(5):2545-61.
7. Popescu C-M, Singurel G, Popescu M-C, Vasile C, Argyropoulos DS, Willför S. Vibrational spectroscopy and X-ray diffraction methods to establish the differences between hardwood and softwood. Carbohydrate Polymers. 2009;77(4):851-7.
8. R. R, R P, M. T. Cell wall chemistry. Handbook of wood chemistry and wood composites: Taylor & Francis; 2012.
9. Klemm D, Heublein B, Fink HP, Bohn A. Cellulose: Fascinating biopolymer and sustainable raw material. Angewandte Chemie - International Edition2005. p. 3358-93.
10. Gibson LJ. The hierarchical structure and mechanics of plant materials. Journal of th Royal Society Interface. 2012;9:2749-66.
11. Shinichiro Iwamoto, Kentaro Abe, Yano H. The Effect of Hemicelluloses on Wood Pulp Nanofibrillation and Nanofiber Network Characteristics. Biomacromolecules. 2008;9:1022 - 6.
12. T. H, P. F, B. H. Sorption of spruce O-acetylated galactoglucomannans onto different pulp fibres. Cellulose. 2003;10:317 - 24.
13. M. Sefik Tunc, Heiningen ARPv. Hemicellulose Extraction of Mixed Southern Hardwood with Water at 150°C: Effect of Time. Industrial & Engineering Chemistry Research. 2008;47:7031 - 7.
14. Sixta DH. Handbook of Pulp: Wiley; 2006.
15. Hult EL, Larsson PT, Iversen T. Cellulose fibril aggregation — an inherent property of kraft pulps. Polymer. 2001;42(8):3309-14.

16. Phillips M. Benjamin Chew Tilghman, and the origin of the sulfite process for delignification of wood. Journal of Chemical Education. 1943;20:444-7.
17. Gonzalo A, Bimbela F, Sánchez JL, Labidi J, Marín F, Arauzo J. Evaluation of different agricultural residues as raw materials for pulp and paper production using a semichemical process. Journal of Cleaner Production. 2017;156:184-93.
18. E.-L. Hult PTL, T. Iversen. Cellulose fibril aggregation - an inherent property of kraft pulps. Polymer. 2001;42:3309 - 14.
19. Young RA. Comparison of the properties of chemical cellulose pulps. Cellulose. 1994;1(2):107-30.
20. Östenson M, Järund H, Toriz G, Gatenholm P. Determination of Surface Functional Groups in Lignocellulosic Materials by Chemical Derivatization and ESCA Analysis. Cellulose. 2006;13(2):157-70.
21. Suess HU. Pulp Bleaching Today Backmatter. De Gruyter; 2010. p. 307-10.
22. Jonoobi M, Harun J, Shakeri A, Mishra M, Oksman K. Chemical composition, crystallinity and thermal degradation of bleached and unbleached kenaf bast (Hibiscus cannabinus) pulp and nanofiber. BioResources. 2009;4(2):626-39.
23. Phanthong P, Reubroycharoen P, Hao X, Xu G, Abudula A, Guan G. Nanocellulose: Extraction and application. Carbon Resources Conversion. 2018;1(1):32-43.
24. Habibi Y, Goffin A-L, Schiltz N, Duquesne E, Dubois P, Dufresne A. Bionanocomposites based on poly (ε-caprolactone)-grafted cellulose nanocrystals by ring-opening polymerization. Journal of Materials Chemistry. 2008;18(41):5002-10.
25. Saito T, Kimura S, Nishiyama Y, Isogai A. Cellulose Nanofibers Prepared by TEMPO-Mediated Oxidation of Native Cellulose. Biomacromolecules. 2007;8(8):2485-91.
26. Camarero Espinosa S, Kuhnt T, Foster EJ, Weder C. Isolation of thermally stable cellulose nanocrystals by phosphoric acid hydrolysis. Biomacromolecules. 2013;14(4):1223-30.
27. Reid MS, Villalobos M, Cranston ED. Benchmarking Cellulose Nanocrystals: From the Laboratory to Industrial Production. Langmuir. 2017;33(7):1583-98.
28. Siqueira G, Abdillahi H, Bras J, Dufresne A. High reinforcing capability cellulose nanocrystals extracted from Syngonanthus nitens (Capim Dourado). Cellulose. 2009;17(2):289-98.
29. Ilari Filpponen DSA. Regular Linking of Cellulose Nanocrystals via Click Chemistry: Synthesis and Formation of Cellulose Nanoplatelet Gels. Biomacromolecules. 2010;11:1060 - 6.
30. Iwamoto S, Nakagaito AN, Yano H. Nano-fibrillation of pulp fibers for the processing of transparent nanocomposites. Applied Physics A. 2007;89(2):461-6.

31. Iwamoto S, Nakagaito AN, Yano H, Nogi M. Optically transparent composites reinforced with plant fiber-based nanofibers. Applied Physics A. 2005;81(6):1109-12.
32. Zhang L, Tsuzuki T, Wang X. Preparation of cellulose nanofiber from softwood pulp by ball milling. Cellulose. 2015;22(3):1729-41.
33. Nechyporchuk O, Belgacem MN, Bras J. Production of cellulose nanofibrils: A review of recent advances. Industrial Crops and Products. 2016;93:2-25.
34. Jozala AF, de Lencastre-Novaes LC, Lopes AM, de Carvalho Santos-Ebinuma V, Mazzola PG, Pessoa A, Jr., et al. Bacterial nanocellulose production and application: a 10-year overview. Appl Microbiol Biotechnol. 2016;100(5):2063-72.
35. Michael Jacob I. Microcellulose Vs Nanocellulose – A Review. World Journal of Advanced Engineering Technology and Sciences. 2022;5(2):001-15.
36. Stoudmann N, Nowack B, Som C. Prospective environmental risk assessment of nanocellulose for Europe. Environmental Science: Nano. 2019;6(8):2520-31.
37. Małachowska E, Dubowik M, Lipkiewicz A, Przybysz K, Przybysz P. Analysis of Cellulose Pulp Characteristics and Processing Parameters for Efficient Paper Production. Sustainability. 2020;12(17):7219.
38. Mateo S, Peinado S, Morillas-Gutiérrez F, La Rubia MD, Moya AJ. Nanocellulose from Agricultural Wastes: Products and Applications—A Review. Processes. 2021;9(9):1594.
39. Maldas D, Kokta BV, Daneault C. Influence of coupling agents and treatments on the mechanical properties of cellulose fiber–polystyrene composites. Journal of Applied Polymer Science. 1989;37(3):751-75.
40. Marais S, Gouanvé F, Bonnesoeur A, Grenet J, Poncin-Epaillard F, Morvan C, et al. Unsaturated polyester composites reinforced with flax fibers: effect of cold plasma and autoclave treatments on mechanical and permeation properties. Composites Part A: Applied Science and Manufacturing. 2005;36(7):975-86.
41. Ho M-p, Wang H, Lee J-H, Ho C-k, Lau K-t, Leng J, et al. Critical factors on manufacturing processes of natural fibre composites. Composites Part B: Engineering. 2012;43(8):3549-62.
42. Christian Gauss, Kim L. Pickering, Joshua Tshuma, McDonald-Wharry J. Production and Assessment of Poly(Lactic Acid) Matrix Composites Reinforced with Regenerated Cellulose Fibres for Fused Deposition Modelling. Polymers. 2022;14:3991.
43. Yussuf AA, Massoumi I, Hassan A. Comparison of Polylactic Acid/Kenaf and Polylactic Acid/Rise Husk Composites: The Influence of the Natural Fibers on the Mechanical, Thermal and Biodegradability Properties. Journal of Polymers and the Environment. 2010;18(3):422-9.
44. Mazzanti V, Salzano de Luna M, Pariante R, Mollica F, Filippone G. Natural fiber-induced degradation in PLA-hemp biocomposites in the molten state. Composites Part A: Applied Science and Manufacturing. 2020;137:105990.

45. Cichosz S, Masek A. Cellulose structure and property changes indicated via wetting-drying cycles. Polymer Degradation and Stability. 2019;167:33-43.
46. Poletto M, Júnior HLO, Zattera AJ. Thermal Decomposition of Natural Fibers: Kinetics and Degradation Mechanisms. 2015:515-45.
47. Thomason JL, Rudeiros-Fernández JL. Thermal degradation behaviour of natural fibres at thermoplastic composite processing temperatures. Polymer Degradation and Stability. 2021;188:109594.
48. Mészáros E, Jakab E, Várhegyi G. TG/MS, Py-GC/MS and THM-GC/MS study of the composition and thermal behavior of extractive components of Robinia pseudoacacia. Journal of Analytical and Applied Pyrolysis. 2007;79(1-2):61-70.
49. Gabor Varhegyi, Morten Gunnar Grønli, Blasi CD. Effects of Sample Origin, Extraction, and Hot-Water Washing on the Devolatilization Kinetics of Chestnut Wood. Industrial & Engineering Chemistry Research. 2004;43(10):2356-67.
50. Xu J, Guo BH. Poly(butylene succinate) and its copolymers: research, development and industrialization. Biotechnol J. 2010;5(11):1149-63.
51. Song H, Lee SY. Production of succinic acid by bacterial fermentation. Enzyme and Microbial Technology. 2006;39(3):352-61.
52. Yim H, Haselbeck R, Niu W, Pujol-Baxley C, Burgard A, Boldt J, et al. Metabolic engineering of Escherichia coli for direct production of 1,4-butanediol. Nat Chem Biol. 2011;7(7):445-52.
53. Chung H, Yang JE, Ha JY, Chae TU, Shin JH, Gustavsson M, et al. Bio-based production of monomers and polymers by metabolically engineered microorganisms. Curr Opin Biotechnol. 2015;36:73-84.
54. Liu L, Yu J, Cheng L, Yang X. Biodegradability of poly(butylene succinate) (PBS) composite reinforced with jute fibre. Polymer Degradation and Stability. 2009;94(1):90-4.
55. Gowman A, Wang T, Rodriguez-Uribe A, Mohanty AK, Misra M. Bio-poly(butylene succinate) and Its Composites with Grape Pomace: Mechanical Performance and Thermal Properties. ACS Omega. 2018;3(11):15205-16.
56. Feng Y, Shen H, Qu J, Liu B, He H, Han L. Preparation and properties of PBS/sisal-fiber composites. Polymer Engineering & Science. 2011;51(3):474-81.
57. Liu HY, Chen FQ, Guo RB, Zhang G, Qu J. Effect of compatibilizer on the properties of PBS/lignin composites prepared via a vane extruder. Journal of Polymer Engineering. 2015;35(9):829-37.
58. Mochane MJ, Magagula SI, Sefadi JS, Mokhena TC. A Review on Green Composites Based on Natural Fiber-Reinforced Polybutylene Succinate (PBS). Polymers (Basel). 2021;13(8).
59. Soatthiyanon N, Aumnate C, Srikulkit K. Rheological, tensile, and thermal properties of poly(butylene succinate) composites filled with two types of cellulose (kenaf cellulose fiber and commercial cellulose). Polymer Composites. 2020;41(7):2777-91.

60. Zhao Y, Qiu J, Feng H, Zhang M. The interfacial modification of rice straw fiber reinforced poly(butylene succinate) composites: Effect of aminosilane with different alkoxy groups. Journal of Applied Polymer Science. 2012;125(4):3211-20.
61. Calabia B, Ninomiya F, Yagi H, Oishi A, Taguchi K, Kunioka M, et al. Biodegradable Poly(butylene succinate) Composites Reinforced by Cotton Fiber with Silane Coupling Agent. Polymers. 2013;5(1):128-41.
62. Liu L, Yu J, Cheng L, Qu W. Mechanical properties of poly(butylene succinate) (PBS) biocomposites reinforced with surface modified jute fibre. Composites Part A: Applied Science and Manufacturing. 2009;40(5):669-74.
63. Key World Energy Statistics 2021. International Energy Agency; 2021.
64. Hasanzadeh R, Azdast T, Lee PC, Park CB. A review of the state-of-the-art on thermal insulation performance of polymeric foams. Thermal Science and Engineering Progress: Elsevier Ltd; 2023.
65. Zabalza Bribián I, Valero Capilla A, Aranda Usón A. Life cycle assessment of building materials: Comparative analysis of energy and environmental impacts and evaluation of the eco-efficiency improvement potential. Building and Environment. 2011;46(5):1133-40.
66. Cabulis U, Kirpluks M, Stirna U, Lopez MJ, Del Carmen Vargas-Garcia M, Suárez-Estrella F, et al., editors. Rigid polyurethane foams obtained from tall oil and filled with natural fibers: Application as a support for immobilization of lignin-degrading microorganisms. Journal of Cellular Plastics; 2012.
67. Marson A, Masiero M, Modesti M, Scipioni A, Manzardo A. Life Cycle Assessment of Polyurethane Foams from Polyols Obtained through Chemical Recycling. ACS Omega. 2021;6(2):1718-24.
68. Suresh KI. Rigid polyurethane foams from cardanol: Synthesis, structural characterization, and evaluation of polyol and foam properties. ACS Sustainable Chemistry and Engineering. 2013;1(2):232-42.
69. Cifarelli A, Boggioni L, Vignali A, Tritto I, Bertini F, Losio S. Flexible polyurethane foams from epoxidized vegetable oils and a bio-based diisocyanate. Polymers. 2021;13(4):1-21.
70. Vieira FR, Gama NV, Evtuguin DV, Amorim CO, Amaral VS, Pinto PCOR, et al. Bio-Based Polyurethane Foams from Kraft Lignin with Improved Fire Resistance. Polymers. 2023;15(5).
71. Cabulis U, Ivdre A. Recent developments in the sustainability of the production of polyurethane foams from polyols based on the first-to the fourth-generation of biomass feedstock. Current Opinion in Green and Sustainable Chemistry. 2023:100866.
72. Polaczek K, Kurańska M, Auguścik-Królikowska M, Prociak A, Ryszkowska J. Open-cell polyurethane foams of very low density modified with various palm oil-based bio-polyols in accordance with cleaner production. Journal of Cleaner Production. 2021;290:125875.

73. Aydoğmuş E, Kamişli F. New commercial polyurethane synthesized with biopolyol obtained from canola oil: Optimization, characterization, and thermophysical properties. Journal of Molecular Structure. 2022;1256:132495.
74. Campanella A, Bonnaillie LM, Wool RP. Polyurethane foams from soyoil-based polyols. Journal of Applied Polymer Science. 2009;112(4):2567-78.
75. Wang C-S, Yang L-T, Ni B-L, Shi G. Polyurethane networks from different soy-based polyols by the ring opening of epoxidized soybean oil with methanol, glycol, and 1,2-propanediol. Journal of Applied Polymer Science. 2009;114(1):125-31.
76. Narine SS, Kong X, Bouzidi L, Sporns P. Physical Properties of Polyurethanes Produced from Polyols from Seed Oils: I. Elastomers. Journal of the American Oil Chemists' Society. 2007;84(1):55-63.
77. Silva MC, Takahashi JA, Chaussy D, Belgacem MN, Silva GG. Composites of rigid polyurethane foam and cellulose fiber residue. Journal of Applied Polymer Science. 2010;117(6):3665-72.
78. Stanzione M, Oliviero M, Cocca M, Errico ME, Gentile G, Avella M, et al. Tuning of polyurethane foam mechanical and thermal properties using ball-milled cellulose. Carbohydrate Polymers. 2020;231:115772-.
79. Yaakob Z, Min Min A, Satheesh Kumar MN, Kamarudin SSK, Hilmi MM, Khairul Zaman HM. Oleic acid-based polyurethane and its biocomposites with oil palm trunk fiber dust. Journal of Thermoplastic Composite Materials. 2010;23(4):447-58.
80. Ragauskas AJ, Li Y, Ren H. Rigid polyurethane foam reinforced with cellulose whiskers: Synthesis and characterization. Nano-Micro Letters. 2010;2(2).
81. Ferreira ES, Rezende CA, Cranston ED. Fundamentals of cellulose lightweight materials: bio-based assemblies with tailored properties. Green Chemistry: Royal Society of Chemistry; 2021. p. 3542-68.
82. Lavoine N, Bergström L. Nanocellulose-based foams and aerogels: processing, properties, and applications. Journal of Materials Chemistry A. 2017;5(31):16105-17.
83. Scherer GW. Drying gels. Journal of Non-Crystalline Solids. 1986;87(1-2):199 - 225.
84. Schwan M, Nefzger S, Zoghi B, Oligschleger C, Milow B. Improvement of Solvent Exchange for Supercritical Dried Aerogels. Frontiers in Materials. 2021;8.
85. Heath L, Thielemans W. Cellulose nanowhisker aerogels. Green Chemistry. 2010;12(8):1448.
86. Chen W, Yu H, Li Q, Liu Y, Li J. Ultralight and highly flexible aerogels with long cellulose i nanofibers. Soft Matter. 2011;7(21):10360-8.
87. Rostami J, Benselfelt T, Maddalena L, Avci C, Sellman FA, Cinar Ciftci G, et al. Shaping 90 wt% NanoMOFs into Robust Multifunctional Aerogels Using Tailored Bio-Based Nanofibrils. Adv Mater. 2022;34(38):e2204800.

88. Zhang M, Li M, Xu Q, Jiang W, Hou M, Guo L, et al. Nanocellulose-based aerogels with devisable structure and tunable properties via ice-template induced self-assembly. Industrial Crops and Products. 2022;179:114701.
89. Cervin NT, Andersson L, Ng JBS, Olin P, Bergström L, Waìšgberg L. Lightweight and strong cellulose materials made from aqueous foams stabilized by nanofibrillated cellulose. Biomacromolecules. 2013;14(2):503-11.
90. Li Q, McGinnis S, Sydnor C, Wong A, Renneckar S. Nanocellulose life cycle assessment. ACS Sustainable Chemistry and Engineering. 2013;1(8):919-28.
91. Ferreira ES, Rezende CA. Simple Preparation of Cellulosic Lightweight Materials from Eucalyptus Pulp. ACS Sustainable Chemistry and Engineering. 2018;6(11):14365-73.
92. Burke SR, Möbius ME, Hjelt T, Hutzler S. Properties of lightweight fibrous structures made by a novel foam forming technique. Cellulose. 2019;26(4):2529-39.
93. López Durán V, Erlandsson J, Wågberg L, Larsson PA. Novel, Cellulose-Based, Lightweight, Wet-Resilient Materials with Tunable Porosity, Density, and Strength. ACS Sustainable Chemistry and Engineering. 2018;6(8):9951-7.
94. Jianming Liao, Pengcheng Luan, Yuxiang Zhang, Li Chen LH, Lihuan Mo, Jun Li, et al. A lightweight, biodegradable, and recyclable cellulose-based bio-foam with good mechanical strength and water stability. Journal of Environmental Chemical Engineering. 2022;10(3):107788.
95. Morgan AB, Gilman JW. An overview of flame retardancy of polymeric materials: Application, technology, and future directions. Fire and Materials2013. p. 259-79.
96. statistics Cff. World fire statistic. 2023.
97. Thevega T, Jayasinghe JASC, Robert D, Bandara CS, Kandare E, Setunge S. Fire compliance of construction materials for building claddings: A critical review. Construction and Building Materials. 2022;361:129582.
98. Day M, Wiles DM. Combustibility of Loose Fiber Fill Cellulose Insulation: the Role of Borax and Boric Acid. Journal of Thermal Insulation. 1978;2(1):30-9.
99. Sprague RW, Shen KK. The Use of Boron Products in Cellulose Insulation. Journal of Thermal Insulation. 1979;2(4):161-74.
100. Lazar ST, Kolibaba TJ, Grunlan JC. Flame-retardant surface treatments. Nature Reviews Materials. 2020;5(4):259-75.
101. Kim Y, Lee S, Yoon H. Fire-Safe Polymer Composites: Flame-Retardant Effect of Nanofillers. Polymers [Internet]. 2021; 13(4).
102. Elbasuney S. Novel multi-component flame retardant system based on nanoscopic aluminium-trihydroxide (ATH). Powder Technology. 2017;305:538-45.
103. Ravadits I, Tóth A, Marosi G, Márton A, Szép A. Organosilicon surface layer on polyolefins to achieve improved flame retardancy through an oxygen barrier effect. Polymer Degradation and Stability. 2001;74(3):419-22.

104. Shen JA-O, Liang J, Lin X, Lin H, Yu J, Wang S. The Flame-Retardant Mechanisms and Preparation of Polymer Composites and Their Potential Application in Construction Engineering. LID - 10.3390/polym14010082 [doi] LID - 82. 2021(2073-4360 (Electronic)).
105. Laoutid F, Bonnaud L, Alexandre M, Lopez-Cuesta JM, Dubois P. New prospects in flame retardant polymer materials: From fundamentals to nanocomposites. Materials Science and Engineering: R: Reports. 2009;63(3):100-25.
106. Jimenez M, Duquesne S, Bourbigot S. Intumescent fire protective coating: Toward a better understanding of their mechanism of action. Thermochimica Acta. 2006;449(1):16-26.
107. Stieger G, Scheringer M, Ng CA, Hungerbühler K. Assessing the persistence, bioaccumulation potential and toxicity of brominated flame retardants: Data availability and quality for 36 alternative brominated flame retardants. Chemosphere. 2014;116:118-23.
108. Altarawneh M, Saeed A, Al-Harahsheh M, Dlugogorski BZ. Thermal decomposition of brominated flame retardants (BFRs): Products and mechanisms. Progress in Energy and Combustion Science. 2019;70:212-59.
109. Yao C, Yang H, Li Y. A review on organophosphate flame retardants in the environment: Occurrence, accumulation, metabolism and toxicity. Science of the Total Environment: Elsevier B.V.; 2021.
110. Final Report on the Safety Assessment of Sodium Metaphosphate, Sodium Trimetaphosphate, and Sodium Hexametaphosphate 1. International Journal of Toxicology. 2001;20(3):75-89.
111. Alongi J, Han Z, Bourbigot S. Intumescence: Tradition versus novelty. A comprehensive review. Progress in Polymer Science. 2015;51:28-73.
112. Hu C, Bourbigot S, Delaunay T, Collinet M, Marcille S, Fontaine G. Poly(isosorbide carbonate): A 'green' char forming agent in polybutylene succinate intumescent formulation. Composites Part B: Engineering. 2020;184:107675.
113. Kuan C-F, Kuan H-C, Ma C-CM, Chen C-H. Flame retardancy and nondripping properties of ammonium polyphosphate/poly(butylene succinate) composites enhanced by water crosslinking. Journal of Applied Polymer Science. 2006;102(3):2935-45.
114. Yangjuan Chen, Jing Zhan, Ping Zhang, Shibin Nie, Hongdian Lu, Lei Song, et al. Preparation of Intumescent Flame Retardant Poly(butylene succinate) Using Fumed Silica as Synergistic Agent. Industrial & Engineering Chemistry Research. 2010;49(17):8200-8.
115. Wang X, Song L, Yang H, Lu H, Hu Y. Synergistic Effect of Graphene on Antidripping and Fire Resistance of Intumescent Flame Retardant Poly(butylene succinate) Composites. Industrial & Engineering Chemistry Research. 2011;50(9):5376-83.

116. Zhang Y, Hu Y, Wang J, Tian W, Liew KM, Zhang Y, et al. Engineering carbon nanotubes wrapped ammonium polyphosphate for enhancing mechanical and flame retardant properties of poly(butylene succinate). Composites Part A: Applied Science and Manufacturing. 2018;115:215-27.
117. Beyer G. Nanocomposites: a new class of flame retardants for polymers. Plastics, Additives and Compounding 2002;4(10):22-8.
118. Dumazert L, Rasselet D, Pang B, Gallard B, Kennouche S, Lopez-Cuesta J-M. Thermal stability and fire reaction of poly(butylene succinate) nanocomposites using natural clays and FR additives. Polymers for Advanced Technologies. 2018;29(1):69-83.
119. Kandola BK, Mistik SI, Pornwannachai W, Anand SC. Natural fibre-reinforced thermoplastic composites from woven-nonwoven textile preforms: Mechanical and fire performance study. Composites Part B: Engineering. 2018;153:456-64.
120. Pornwannachai W, Ebdon JR, Kandola BK. Fire-resistant natural fibre-reinforced composites from flame retarded textiles. Polymer Degradation and Stability. 2018;154:115-23.
121. Yang Y, Wang X, Fei B, Li H, Gu X, Sun J, et al. Preparation of phytic acid-based green intumescent flame retardant and its application in PLA nonwovens. Polymers for Advanced Technologies. 2021;32(8):3039-49.
122. Battegazzore D, Frache A, Carosio F. Layer-by-Layer nanostructured interphase produces mechanically strong and flame retardant bio-composites. Composites Part B: Engineering. 2020;200.
123. Dorez G, Taguet A, Ferry L, Lopez Cuesta J-M. Phosphorous compounds as flame retardants for polybutylene succinate/flax biocomposite: Additive versus reactive route. Polymer Degradation and Stability. 2014;102:152-9.
124. Suwanniroj A, Suppakarn N. Water Hyacinth Fiber as a Bio-Based Carbon Source for Intumescent Flame-Retardant Poly (Butylene Succinate) Composites. Polymers [Internet]. 2023; 15(21).
125. Nie S, Liu X, Dai G, Yuan S, Cai F, Li B, et al. Investigation on flame retardancy and thermal degradation of flame retardant poly(butylene succinate)/bamboo fiber biocomposites. Journal of Applied Polymer Science. 2012;125(S2):E485-E9.
126. Yao W, Wang H, Guan D, Fu T, Zhang T, Dou Y. The Effect of Soluble Ammonium Polyphosphate on the Properties of Water Blown Semirigid Polyurethane Foams. Advances in Materials Science and Engineering. 2017;2017.
127. Li Q, Wang J, Chen L, Shi H, Hao J. Ammonium polyphosphate modified with β-cyclodextrin crosslinking rigid polyurethane foam: Enhancing thermal stability and suppressing flame spread. Polymer Degradation and Stability. 2019;161:166-74.
128. Jiang Q, Li P, Liu Y, Zhu P. Green flame-retardant flexible polyurethane foam based on polyphenol-iron-phytic acid network to improve the fire safety. Composites Part B: Engineering. 2022;239.

129. Lenz J, Pospiech D, Paven M, Albach RW, Günther M, Schartel B, et al. Improving the flame retardance of polyisocyanurate foams by dibenzo[d,f][1,3,2]dioxaphosphepine 6-oxide-containing additives. Polymers. 2019;11(8).
130. Tang G, Liu M, Deng D, Zhao R, Liu X, Yang Y, et al. Phosphorus-containing soybean oil-derived polyols for flame-retardant and smoke-suppressant rigid polyurethane foams. Polymer Degradation and Stability. 2021;191.
131. Cheng J, Wang H, Wang X, Li S, Zhou Y, Zhang F, et al. Effects of flame-retardant ramie fiber on enhancing performance of the rigid polyurethane foams. Polymers for Advanced Technologies. 2019;30(12):3091-8.
132. Liang J, Zhou T, Fu Y, Tian G, Zhang Y, Wang Z. Pretreated cellulose fiber for enhancing fire resistance of flexible polyurethane foam composites with reinforced properties. Industrial Crops and Products. 2023;205:117429.
133. Yun GW, Lee JH, Kim SH. Flame retardant and mechanical properties of expandable graphite/polyurethane foam composites containing iron phosphonate dopamine-coated cellulose. Polymer Composites. 2020;41(7):2816-28.
134. Guo W, Hu Y, Wang X, Zhang P, Song L, Xing W. Exceptional flame-retardant cellulosic foams modified with phosphorus-hybridized graphene nanosheets. Cellulose. 2018;26(2):1247-60.
135. Ghanadpour M, Carosio F, Larsson PT, Wågberg L. Phosphorylated Cellulose Nanofibrils: A Renewable Nanomaterial for the Preparation of Intrinsically Flame-Retardant Materials. Biomacromolecules. 2015;16(10):3399-410.
136. Ghanadpour M, Wicklein B, Carosio F, Wagberg L. All-natural and highly flame-resistant freeze-cast foams based on phosphorylated cellulose nanofibrils. Nanoscale. 2018;10(8):4085-95.
137. Zheng C, Li D, Ek M. Cellulose-fiber-based insulation materials with improved reaction-to-fire properties. Nordic Pulp & Paper Research Journal. 2017;32(3):466-72.
138. Zheng C, Li D, Ek M. Improving fire retardancy of cellulosic thermal insulating materials by coating with bio-based fire retardants. 2019;34(1):96-106.
139. He S, Liu C, Chi X, Zhang Y, Yu G, Wang H, et al. Bio-inspired lightweight pulp foams with improved mechanical property and flame retardancy via borate cross-linking. Chemical Engineering Journal. 2019;371:34-42.
140. Wu M, Huang Y, Zhang T, Kuga S, Ewulonu CM. Cellulose nanofibril-based flame retardant and its application to paper. ACS Sustainable Chemistry and Engineering. 2020;8(27):10222-9.
141. Liang S, Neisius NM, Gaan S. Recent developments in flame retardant polymeric coatings. Progress in Organic Coatings. 2013;76(11):1642-65.
142. Bifulco A, Imparato C, Aronne A, Malucelli G. Flame retarded polymer systems based on the sol-gel approach: recent advances and future perspectives. Journal of Sol-Gel Science and Technology. 2022.

143. Alongi J, Tata J, Carosio F, Rosace G, Frache A, Camino G. A comparative analysis of nanoparticle adsorption as fire-protection approach for fabrics. Polymers. 2015;7(1):47-68.
144. Carosio F, Alongi J, Malucelli G. Layer by Layer ammonium polyphosphate-based coatings for flame retardancy of polyester–cotton blends. Carbohydrate Polymers. 2012;88(4):1460-9.
145. Maddalena L, Carosio F, Gomez J, Saracco G, Fina A. Layer-by-Layer Assembly of Efficient Flame Retardant Coatings Based On High Aspect Ratio Graphene Oxide and Chitosan Capable of Preventing Ignition of PU Foam. Polymer Degradation and Stability. 2018;152:1-9.
146. Shi XH, Xu YJ, Long JW, Zhao Q, Ding XM, Chen L, et al. Layer-by-layer assembled flame-retardant architecture toward high-performance carbon fiber composite. Chemical Engineering Journal. 2018;353:550-8.
147. Iler RK. Multilayers of colloidal particles. Journal of Colloid and Interface Science. 1966;21:569-94.
148. Decher G, Hong J-D. BUILDUP OF ULTRATHIN MULTILAYER FILMS BY A SELF-ASSEMBLY PROCESS, 1 CONSECUTIVE ADSORPTION OF ANIONIC AND CATIONIC BIPOLAR AMPHIPHILES ON CHARGED SURFACES. Makromol Chem, Macromol Symp. 1991;46:321-7.
149. Decher G. Fuzzy Nanoassemblies: Toward Layered Polymeric Multicomposites. Science. 1997;277(5330):1232-7.
150. T. AFSHAR-RAD AIB, P.F. LUCKHAM, W. MACNAUGHTAN, D. CHAPMAN Forces between Poly-1-lysine of Molecular Weight Range 4,000-75,000 Adsorbed on Mica Surfaces Colloids and Surfaces. 1987;25:263-77.
151. Veronika Kozlovskaya SO, Alioscka Sousa,Matthew Libera, and Svetlana A. Sukhishvili. Hydrogen-Bonded Polymer Capsules Formedby Layer-by-Layer Self-Assembly. Macromolecules. 2003(36):8590-2.
152. Kotov NA. LAYER-BY-LAYER SELF-ASSEMBLY: THE CONTRIBUTION OF HYDROPHOBIC INTERACTIONS. NanoStructured Materials. 1999;12:789-96.
153. Hazel L. Tan MJM, Guiquan Pan, P. Gregory Van Patten. Temperature Dependence of Polyelectrolyte Multilayer Assembly. Langmuir. 2003;19:9311-4.
154. J. D. Mendelsohn CJB, V. V. Chan, A. J. Pal, A. M. Mayes, M. F. Rubner. Fabrication of Microporous Thin Films fromPolyelectrolyte Multilayers. Langmuir. 2000;16:5017-23.
155. Antipov AA, Sukhorukov GB. Polyelectrolyte multilayer capsules as vehicles with tunable permeability. Adv Colloid Interface Sci. 2004;111(1-2):49-61.
156. Mauser T, Déjugnat C, Sukhorukov GB. Reversible pH-Dependent Properties of Multilayer Microcapsules Made of Weak Polyelectrolytes. Macromolecular Rapid Communications. 2004;25(20):1781-5.
157. Richard A. McAloney MS, Vyacheslav Dudnik, M. Cynthia Goh. Atomic Force Microscopy Studies of Salt Effects on Polyelectrolyte Multilayer Film Morphology. Langmuir. 2000;17:6655-63.

158. Joao M. C. Lourenco PAR, Ana Maria Botelho do Rego, Francisco M. Braz Fernandes, Augusto M. C. Moutinho, Maria Raposo. Counterions in Poly(allylamine hydrochloride) and Poly(styrene sulfonate) Layer-by-Layer Films. Langmuir. 2004;20:8103-9.
159. Lars Wågberg RH. Kinetics of Polyelectrolyte Adsorption on Cellulosic Fibers. Langmuir. 2001;17:1096-103.
160. Marais A, Utsel S, Gustafsson E, Wågberg L. Towards a super-strainable paper using the Layer-by-Layer technique. Carbohydrate Polymers. 2014;100:218-24.
161. Yuri M. Lvov GAG, Sandeep Eadula, Zhiguo Zheng, Zonghuan Lu. Dry and wet strength of paper. Layer-by-layer nanocoating of mill broken fibers for improved paper. Nordic Pulp & Paper Research Journal. 2006;21:552-7.
162. Magovac E, Vončina B, Jordanov I, Grunlan JC, Bischof S. Layer-by-Layer Deposition: A Promising Environmentally Benign Flame-Retardant Treatment for Cotton, Polyester, Polyamide and Blended Textiles. Materials [Internet]. 2022; 15(2).
163. Yu-Chin Li, Jessica Schulz, Sarah Mannen, Chris Delhom, Brian Condon, SeChin Chang, et al. Flame Retardant Behavior of Polyelectrolyte-Clay Thin Film Assemblies on Cotton Fabric. ACS Nano. 2010;4(6):3325-37.
164. Li YC, Schulz J, Grunlan JC. Polyelectrolyte/nanosilicate thin-film assemblies: influence of pH on growth, mechanical behavior, and flammability. ACS Appl Mater Interfaces. 2009;1(10):2338-47.
165. Köklükaya O, Carosio F, Wågberg L. Superior Flame-Resistant Cellulose Nanofibril Aerogels Modified with Hybrid Layer-by-Layer Coatings. ACS Applied Materials & Interfaces. 2017;9(34):29082-92.
166. Bourbigot S, Le Bras M, Delobel R. Fire Degradation of an Intumescent Flame Retardant Polypropylene Using the Cone Calorimeter. Journal of Fire Sciences. 1994;13(1):3-22.
167. Kandola BK, Horrocks AR. Complex char formation in flame-retarded fibre-intumescent combinations ? IV. Mass loss and thermal barrier properties. Fire and Materials. 2000;24(6):265-75.
168. Li YC, Mannen S, Morgan AB, Chang S, Yang YH, Condon B, et al. Intumescent all-polymer multilayer nanocoating capable of extinguishing flame on fabric. Adv Mater. 2011;23(34):3926-31.
169. Carosio F, Di Blasio A, Alongi J, Malucelli G. Green DNA-based flame retardant coatings assembled through Layer by Layer. Polymer. 2013;54(19):5148-53.
170. Fang F, Zhang X, Meng Y, Gu Z, Bao C, Ding X, et al. Intumescent flame retardant coatings on cotton fabric of chitosan and ammonium polyphosphate via layer-by-layer assembly. Surface and Coatings Technology. 2015;262:9-14.

171. Li S, Ding F, Lin X, Li Z, Ren X. Layer-by-Layer Self-assembly of Organic-inorganic Hybrid Intumescent Flame Retardant on Cotton Fabrics. Fibers and Polymers. 2019;20(3):538-44.
172. Malucelli G. Sol-Gel and Layer-by-Layer Coatings for Flame-Retardant Cotton Fabrics: Recent Advances. Coatings. 2020;10(4):333.
173. Köklükaya O, Carosio F, Grunlan JC, Wågberg L. Flame-Retardant Paper from Wood Fibers Functionalized via Layer-by-Layer Assembly. ACS Applied Materials and Interfaces. 2015;7(42):23750-9.
174. Pan Y, Liu L, Zhao H. Recyclable flame retardant paper made from layer-by-layer assembly of zinc coordinated multi-layered coatings. Cellulose. 2018;25(9):5309-21.
175. Lisuzzo L, Cavallaro G, Parisi F, Milioto S, Lazzara G. Colloidal stability of halloysite clay nanotubes. Ceramics International. 2019;45(2):2858-65.
176. Maddalena L, Gomez J, Fina A, Carosio F. Effects of graphite oxide nanoparticle size on the functional properties of layer-by-layer coated flexible foams. Nanomaterials. 2021;11(2):1-15.
177. Negrell-Guirao C, Carosio F, Boutevin B, Cottet H, Loubat C. Phosphonated oligoallylamine: Synthesis, characterization in water, and development of layer by layer assembly. Journal of Polymer Science, Part B: Polymer Physics. 2013;51(16):1244-51.
178. Cain AA, Plummer MGB, Murray SE, Bolling L, Regev O, Grunlan JC. Iron-containing, high aspect ratio clay as nanoarmor that imparts substantial thermal/flame protection to polyurethane with a single electrostatically-deposited bilayer. Journal of Materials Chemistry A. 2014;2(41):17609-17.
179. Celi L, Lamacchia S, Ajmone Marsan F, Barberis E. Interaction of Inositol Hexaphosphate on Clays: Adsorption and Charging Phenomena. Soil Science. 1999;164:574-85.
180. Socrates G. Infrared and Raman characteristic group frequencies. Tables and charts. 3rd Edition ed: Wiley; 2001.
181. Carosio F, Maddalena L, Gomez J, Saracco G, Fina A. Graphene Oxide Exoskeleton to Produce Self-Extinguishing, Nonignitable, and Flame Resistant Flexible Foams: A Mechanically Tough Alternative to Inorganic Aerogels. Advanced Materials Interfaces. 2018;5(23):1801288-.
182. Zhang Y, Li Y, Zhang Y. Preparation and intercalation structure model of halloysite-stearic acid intercalation compound. Applied Clay Science. 2020;187:105451.
183. Drevelle C, Lefebvre J, Duquesne S, Le Bras M, Poutch F, Vouters M, et al. Thermal and fire behaviour of ammonium polyphosphate/acrylic coated cotton/PESFR fabric. Polymer Degradation and Stability. 2005;88(1):130-7.
184. Schmitt J, Gruenewald T, Decher G, Pershan PS, Kjaer K, Loesche M. Internal structure of layer-by-layer adsorbed polyelectrolyte films: a neutron and x-ray reflectivity study. Macromolecules. 1993;26(25):7058-63.

185. Ladam G, Schaad P, Voegel JC, Schaaf P, Decher G, Cuisinier F. In Situ Determination of the Structural Properties of Initially Deposited Polyelectrolyte Multilayers. Langmuir. 2000;16(3):1249-55.
186. Krogman KC, Zacharia NS, Schroeder S, Hammond PT. Automated Process for Improved Uniformity and Versatility of Layer-by-Layer Deposition. Langmuir. 2007;23(6):3137-41.
187. Pandey KK. A study of chemical structure of soft and hardwood and wood polymers by FTIR spectroscopy. Journal of Applied Polymer Science. 1999;71(12):1969-75.
188. J.M. Fang, R.C. Sun, J.Tomkinson. Isolation and characterization of hemicelluloses and cellulose from rye straw by alkaline peroxide extraction. Cellulose. 2000;7:87 - 107.
189. Yang S-s, Chen Z-b. The Study on Aging and Degradation Mechanism of Ammonium Polyphosphate in Artificial Accelerated Aging. Procedia Engineering. 2018;211:906-10.
190. Levanič J, Šenk VP, Nadrah P, Poljanšek I, Oven P, Haapala A. Analyzing TEMPO-Oxidized Cellulose Fiber Morphology: New Insights into Optimization of the Oxidation Process and Nanocellulose Dispersion Quality. ACS Sustainable Chemistry & Engineering. 2020;8(48):17752-62.
191. Stana-Kleinschek K, Strnad S, Ribitsch V. Surface characterization and adsorption abilities of cellulose fibers. Polymer Engineering & Science. 2004;39(8):1412-24.
192. Marcioni M, Zhao M, Maddalena L, Pettersson T, Avolio R, Castaldo R, et al. Layer-by-Layer-Coated Cellulose Fibers Enable the Production of Porous, Flame-Retardant, and Lightweight Materials. ACS Appl Mater Interfaces. 2023;15(30):36811-21.
193. Shafizadeh F, Fu YL. Pyrolysis of cellulose. Carbohydrate Research. 1973;29(1):113-22.
194. Davies PJ, Horrocks AR, Alderson A. The sensitisation of thermal decomposition of ammonium polyphosphate by selected metal ions and their potential for improved cotton fabric flame retardancy. Polymer Degradation and Stability. 2009;88(1):114-22.
195. Du M, Guo B, Jia D. Thermal stability and flame retardant effects of halloysite nanotubes on poly(propylene). European Polymer Journal. 2006;42(6):1362-9.
196. Zhao J, Deng C-L, Du S-L, Chen L, Deng C, Wang Y-Z. Synergistic flame-retardant effect of halloysite nanotubes on intumescent flame retardant in LDPE. Journal of Applied Polymer Science. 2014;131(7).
197. Ibrahim EE, Chipara DM, Thapa R, Lozano K, Chipara M. Raman Spectroscopy of Isotactic Polypropylene-Halloysite Nanocomposites. Journal of Nanomaterials. 2012;2012:793084.

198. Vuluga Z, Corobea MC, Elizetxea C, Ordonez M, Ghiurea M, Raditoiu V, et al. Morphological and Tribological Properties of PMMA/Halloysite Nanocomposites. Polymers [Internet]. 2018; 10(8).
199. Liang Z, Pan P, Zhu B, Dong T, Inoue Y. Mechanical and thermal properties of poly(butylene succinate)/plant fiber biodegradable composite. Journal of Applied Polymer Science. 2009;115(6):3559-67.
200. Wu W, Cao X, Luo J, He G, Zhang Y. Morphology, thermal, and mechanical properties of poly(butylene succinate) reinforced with halloysite nanotube. Polymer Composites. 2013;35(5):847-55.
201. Gonghua Hong, Yang Meng, Zexun Yang, Haitao Cheng, Shuangbao Zhang, Song W. Mussel-Inspired Polydopamine Modification of Bamboo Fiber and Its Effect on the Properties of Bamboo Fiber/Polybutylene Succinate Composites. BioResources. 2017;12(4):8419 - 42.
202. Battegazzore D, Frache A, Carosio F. Sustainable and High Performing Biocomposites with Chitosan/Sepiolite Layer-by-Layer Nanoengineered Interphases. ACS Sustainable Chemistry & Engineering. 2018;6(8):9601-5.
203. Ray SS. Clay-containing polymer nanocomposites : from fundamentals to real applications: Elsevier; 2013.
204. Schartel B, Hull TR. Development of fire-retarded materials—Interpretation of cone calorimeter data. Fire and Materials. 2007;31(5):327-54.
205. Marney DCO, Russell LJ, Wu DY, Nguyen T, Cramm D, Rigopoulos N, et al. The suitability of halloysite nanotubes as a fire retardant for nylon 6. Polymer Degradation and Stability. 2008;93(10):1971-8.
206. Green J. A Review of Phosphorus-Containing Flame Retardants. Journal of Fire Sciences. 1992;10(6):470-87.
207. Cullis CF, Hirschler MM, Tao QM. Studies of the effects of phosphorus-nitrogen-bromine systems on the combustion of some thermoplastic polymers. European Polymer Journal. 1991;27(3):281-9.
208. Doley PM, Yuen AC, Kabir I, Liu L, Wang C, Chen TB, et al. Thermal Hazard and Smoke Toxicity Assessment of Building Polymers Incorporating TGA and FTIR—Integrated Cone Calorimeter Arrangement. Fire [Internet]. 2022; 5(5).
209. Hull TR, Stec AA, Lebek K, Price D. Factors affecting the combustion toxicity of polymeric materials. Polymer Degradation and Stability. 2007;92(12):2239-46.
210. Alongi J, Carosio F, Malucelli G. Layer by layer complex architectures based on ammonium polyphosphate, chitosan and silica on polyester-cotton blends: flammability and combustion behaviour. Cellulose. 2012;19(3):1041-50.
211. Avolio R, Bonadies I, Capitani D, Errico ME, Gentile G, Avella M. A multitechnique approach to assess the effect of ball milling on cellulose. Carbohydr Polym. 2012;87(1):265-73.
212. Carosio F, Ghanadpour M, Alongi J, Wågberg L. Layer-by-layer-assembled chitosan/phosphorylated cellulose nanofibrils as a bio-based and flame protecting nano-exoskeleton on PU foams. Carbohydrate Polymers. 2018;202:479-87.

213. Corazzari I, Nisticò R, Turci F, Faga MG, Franzoso F, Tabasso S, et al. Advanced physico-chemical characterization of chitosan by means of TGA coupled on-line with FTIR and GCMS: Thermal degradation and water adsorption capacity. Polymer Degradation and Stability. 2015;112:1-9.
214. Zheng Z, Qiang L, Yang T, Wang B, Cui X, Wang H. Preparation of microencapsulated ammonium polyphosphate with carbon source- and blowing agent-containing shell and its flame retardance in polypropylene. Journal of Polymer Research. 2014;21(5):443.
215. Stana-Kleinschek K, Strnad S, Ribitsch V. Surface characterization and adsorption abilities of cellulose fibers. Polymer Engineering & Science. 1999;39(8):1412-24.
216. Avella M, Avolio R, Bonadies I, Carfagna C, Errico ME, Gentile G. Effect of compatibilization on thermal degradation kinetics of HDPE-based composites containing cellulose reinforcements. Journal of thermal analysis and calorimetry. 2010;102(3):975-82.
217. Köklükaya O, Karlsson RMP, Carosio F, Wågberg L. The use of model cellulose gel beads to clarify flame-retardant characteristics of layer-by-layer nanocoatings. Carbohydrate Polymers. 2021;255:117468-.
218. Mondal P, Khakhar DV. Rigid polyurethane–clay nanocomposite foams: Preparation and properties. Journal of Applied Polymer Science. 2006;103(5):2802-9.
219. Sandberg PI. Determination of the effects of moisture on the thermal transmissivity of cellulose fiber loose-fill insulation. 1992.
220. Cervin NT, Aulin C, Larsson PT, Wågberg L. Ultra porous nanocellulose aerogels as separation medium for mixtures of oil/water liquids. Cellulose. 2012;19(2):401-10.
221. Li Y, Tanna VA, Zhou Y, Winter HH, Watkins JJ, Carter KR. Nanocellulose Aerogels Inspired by Frozen Tofu. ACS Sustainable Chemistry and Engineering. 2017;5(8):6387-91.
222. Alam MK, He M, Chen W, Wang L, Li X, Qin X. Stable and Salt-Resistant Janus Evaporator Based on Cellulose Composite Aerogels from Waste Cotton Fabric. ACS Applied Materials and Interfaces. 2022;14(36):41114-21.
223. Wu T, Farnood R. Cellulose fibre networks reinforced with carboxymethyl cellulose/chitosan complex layer-by-layer. Carbohydrate Polymers. 2014;114:500-5.
224. Wågberg L, Forsberg S, Johansson A, Juntti P. Engineering of fibre surface properties by application of the polyelectrolyte multilayer concept. Part I : Modification of paper strength. Journal of Pulp and Paper Science (JPPS). 2002;28(7):222-8.
225. Bloot APM, Kalschne DL, Amaral JAS, Baraldi IJ, Canan C. A Review of Phytic Acid Sources, Obtention, and Applications. Food Reviews International. 2023;39(1):73-92.

226. Terayama H. Method of Colloid Titration (A New Titration between Polymer Ions). J Polym Sci. 1952;8(2):243-53.
227. Wang L, Sánchez-Soto M. Green Bio-based Aerogels Prepared from Recycled Cellulose Fiber Suspensions.
228. Celzard A, Zhao W, Pizzi A, Fierro V. Mechanical properties of tannin-based rigid foams undergoing compression. Materials Science and Engineering: A. 2010;527(16-17):4438-46.
229. Sehaqui H, Salajková M, Zhou Q, Berglund LA. Mechanical performance tailoring of tough ultra-high porosity foams prepared from cellulose i nanofiber suspensions. Soft Matter. 2010;6(8):1824-32.
230. Ates M, Karadag S, Eker AA, Eker B. Polyurethane foam materials and their industrial applications. Polymer International. 2022;71(10):1157-63.
231. Apte V. Flammability Testing of Materials Used in Construction, Transport, and Mining: Woodhead Publishing; 2021.
232. Hidalgo JP, Torero JL, Welch S. Fire performance of charring closed-cell polymeric insulation materials: Polyisocyanurate and phenolic foam. Fire and Materials , 42 (4) pp 358-373 (2018). 2018;42(4):358-73.
233. Giebułtowicz J, Rużycka M, Wroczyński P, Purser DA, Stec AA. Analysis of fire deaths in Poland and influence of smoke toxicity. Forensic Science International. 2017;277:77-87.
234. Liu DY, Zhao B, Wang JS, Liu PW, Liu YQ. Flame retardation and thermal stability of novel phosphoramide/expandable graphite in rigid polyurethane foam. Journal of Applied Polymer Science. 2018;135(27).
235. Carosio F, Cuttica F, Di Blasio A, Alongi J, Malucelli G. Layer by layer assembly of flame retardant thin films on closed cell PET foams: Efficiency of ammonium polyphosphate versus DNA. Polymer Degradation and Stability. 2015;113:189-96.
236. Liu X, Salmeia KA, Rentsch D, Hao J, Gaan S. Thermal decomposition and flammability of rigid PU foams containing some DOPO derivatives and other phosphorus compounds. Journal of Analytical and Applied Pyrolysis. 2017;124:219-29.
237. Członka S, Strąkowska A, Strzelec K, Kairytė A, Kremensas A. Melamine, silica, and ionic liquid as a novel flame retardant for rigid polyurethane foams with enhanced flame retardancy and mechanical properties. Polymer Testing. 2020;87.
238. Wu N, Niu F, Lang W, Yu J, Fu G. Synthesis of reactive phenylphosphoryl glycol ether oligomer and improved flame retardancy and mechanical property of modified rigid polyurethane foams. Materials and Design. 2019;181.
239. Wang L, Wang C, Liu P, Jing Z, Ge X, Jiang Y. The flame resistance properties of expandable polystyrene foams coated with a cheap and effective barrier layer. Construction and Building Materials. 2018;176:403-14.
240. Gao L, Zheng G, Zhou Y, Hu L, Feng G. Improved mechanical property, thermal performance, flame retardancy and fire behavior of lignin-based rigid

polyurethane foam nanocomposite. Journal of Thermal Analysis and Calorimetry. 2015;120(2):1311-25.
241. Ferrari AC, Basko DM. Raman spectroscopy as a versatile tool for studying the properties of graphene. Nature Nanotechnology 2013 8:4. 2013;8(4):235-46.
242. Ayiania M, Weiss-Hortala E, Smith M, McEwen JS, Garcia-Perez M. Microstructural analysis of nitrogen-doped char by Raman spectroscopy: Raman shift analysis from first principles. Carbon. 2020;167:559-74.
243. Alongi J, Camino G, Malucelli G. Heating rate effect on char yield from cotton, poly(ethylene terephthalate) and blend fabrics. Carbohydrate Polymers. 2013;92(2):1327-34.
244. Guin T, Krecker M, Milhorn A, Grunlan JC. Maintaining hand and improving fire resistance of cotton fabric through ultrasonication rinsing of multilayer nanocoating. Cellulose. 2014;21(4):3023-30.
245. Qin L, Zhang Y, Fan Y, Li L. Cellulose nanofibril reinforced functional chitosan biocomposite films. Polymer Testing. 2023;120:107964.
246. Kawasaki T, Nakaji-Hirabayashi T, Masuyama K, Fujita S, Kitano H. Complex film of chitosan and carboxymethyl cellulose nanofibers. Colloids and Surfaces B: Biointerfaces. 2016;139:95-9.
247. Grexa O, Lübke H. Flammability parameters of wood tested on a cone calorimeter. Polymer Degradation and Stability. 2001;74(3):427-32.